

QC869  
.C65  
1985  
ATSL

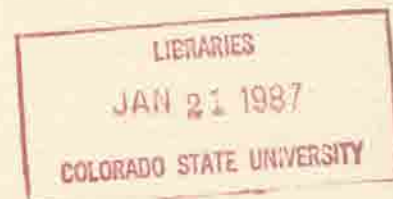
# CIRA



Cooperative Institute for Research in the Atmosphere

Colorado State University  
Foothills Campus  
Fort Collins, Colorado 80523

Colorado State University  
National Oceanic and Atmospheric Administration



SUMMARY REPORT

Pingree Park Research Retreat

June 19-21, 1985



QC  
869  
-C65  
1985  
ATSL

TABLE OF CONTENTS

	<u>Page</u>
Abstract . . . . .	1
Agenda . . . . .	2
List of Attendees . . . . .	6
Presentations . . . . .	7
Small Group Summaries . . . . .	113

\* \* \*

ABSTRACT

On June 19-21, 1985 a retreat was held at the CSU Mountain Campus of Pingree Park for students and faculty involved with current research projects. The following is a compilation of attendees, presentations, and summary reports of the small group sessions.

1985 Research Retreat  
Pingree Park  
June 19-22, 1985

Agenda

Wednesday, June 19, 1985

- 3:00 p.m. Depart Ft. Collins (From Atmospheric Science Building)
- 4:30 p.m. Check-in at Main Conference Center - Hotchkiss Lodge
- 6:00 p.m. Dinner
- 7:00 p.m. Open/Recreation
- 8:00 p.m. Large Group Session L1  
(prefaced by 15-minute organizational session  
with Pingree Staff) - Hotchkiss Lodge Lounge
- R. Pielke, Chairperson: "Applications of Near-Real  
Time Modeling with Supercomputer" (25 minutes)
- R. Green: "Use of Micro-computers in Pre-STORM  
Field Studies - 1985" (20 minutes)
- 9:00 p.m. Adjourn

Thursday, June 20, 1985

- 7:00 a.m. Breakfast
- 8:00 a.m. Large Group Session L2 - Hotchkiss Lodge Lounge
- T. Brubaker, Chairperson: "New Concepts in  
Microprocessors" (20 minutes)
- N. Allen: "New Satellites E/S & LAN" (20 minutes)
- M. Wetzel: "Theory and Observations of Spectral  
Radiance for Cloud Studies" (20 minutes)
- G. Campbell/D. Randel: "El Nino Discovered in  
Radiation Budget Measurements" (20 minutes)
- 10:30 a.m. Open/Recreation/Lunch  
Cafeteria Lunch Noon - 1:00 p.m.

1:30 p.m.

Small Groups Session S1

"Computer Systems for Research"  
(Location: Lounge N. Allen's cabin)

Leader: N. Allen  
Recorder: D. Lubich  
T. Brubaker  
G. Burton  
W. Davis  
R. Green  
D. Randel  
M. Wetzel

"VAS"

(Location: Lounge A. Lipton's cabin)

Leader: A. Lipton  
Recorder: P. Laybe  
J. Behunek  
V. Bringi  
D. Hillger  
J. Purdom  
E. Steiner

"Atmospheric Modeling"

(Location: Lounge R. Pielke's cabin)

Leader: R. Pielke  
Recorder: L. Smith  
D. Abbs  
G. Campbell  
H-C. Kuo  
C-F. Shih

3:30 p.m.

Open

4:30 p.m.

Large Group Session L3 - Hotchkiss Lodge Lounge

T. Vonder Haar, Chairperson:

D. Hillger: "Satellite Sounding Near Severe Storms"  
(20 minutes)

J. Purdom: "Mesoscale Forecasting Research" (25 minutes)

6:00 p.m.

Dinner and Open

7:30 p.m. Informal Large Group Session L4 - Hotchkiss Lodge Lounge  
T. Vonder Haar, Chairperson  
Reports from all Small Group Chairmen on items they are/will be addressing (5 minutes each)

Friday, June 21, 1985

7:00 a.m. Breakfast

8:00 a.m. Small Groups Presentations S2

10:30 a.m. Open/Recreation/Lunch  
Cafeteria lunch Noon - 1:00 p.m.

1:30 p.m. Small Group Session S3

"Shortrange Forecasting Including Severe Storms"  
(Location: Lounge in J. Purdom's cabin)

Leader: J. Purdom  
Recorder: J. Behunek  
D. Abbs  
T. Brubaker  
G. Burton  
R. Green  
D. Lubich  
R. Pielke

"Climate Studies"  
(Location: Lounge in D. Randel's cabin)

Leader: D. Randel  
Recorder: C-F. Shih  
G. Campbell  
W. Davis  
P. Laybe  
L. Smith  
E. Steiner

"Radiation Theory and Observations"  
(Location: Lounge of M. Wetzel's cabin)

Leader: M. Wetzel  
Recorder: H-C. Kuo  
D. Hillger  
A. Lipton

3:30 p.m. Open

4:30 p.m.            Large Group Session L5 Wrap-up session and summary reports;  
Action items (Classroom)

6:00 p.m.            Steak Cookout

Saturday, June 22, 1985

7:00 a.m.            Breakfast

NOTE: The small group sessions are purposefully small to enhance discussion and participation. Since all, other than the leaders and recorders, are encouraged to meet with two small groups, it is important that scheduled meeting times and locations not be rearranged.

\* \* \*

ATTENDEES

CIRA

D. Abbs, Visiting Fellow  
N. Allen, Research Associate  
G. Burton, Research Associate  
G. Campbell, Visiting Scientist  
W. Davis, Research Associate  
D. Hillger, Visiting Fellow  
D. Lubich, Research Associate  
T. Vonder Haar, Director

CSU

J. Behunek, Research Associate  
T. Brubaker, Electrical Engineering  
P. Laybe, Research Associate  
R. Pielke, Atmospheric Science (Deputy Director, CIRA)

NOAA/NESDIS/RAMM Branch

R. Green, Meteorologist/CIRA Research Associate  
J. Purdom, Branch Chief/CIRA Fellow

Students

H-C. Kuo  
A. Lipton  
D. Randel  
C-F. Shih  
L. Smith  
M. Wetzel

CIRES (Cooperative Institute for Research in Environmental Sciences)

E. Steiner

Staff

R. Garcia, Department Manager  
B. Schwinger  
J. Williams

PRESENTATIONS

"Applications of Near-Real Time Modeling With Supercomputer"  
R. Pielke

"Use of Micro-computers in Pre-STORM Field Studies - 1985"  
R. Green

"New Concepts in Microprocessors"  
T. Brubaker

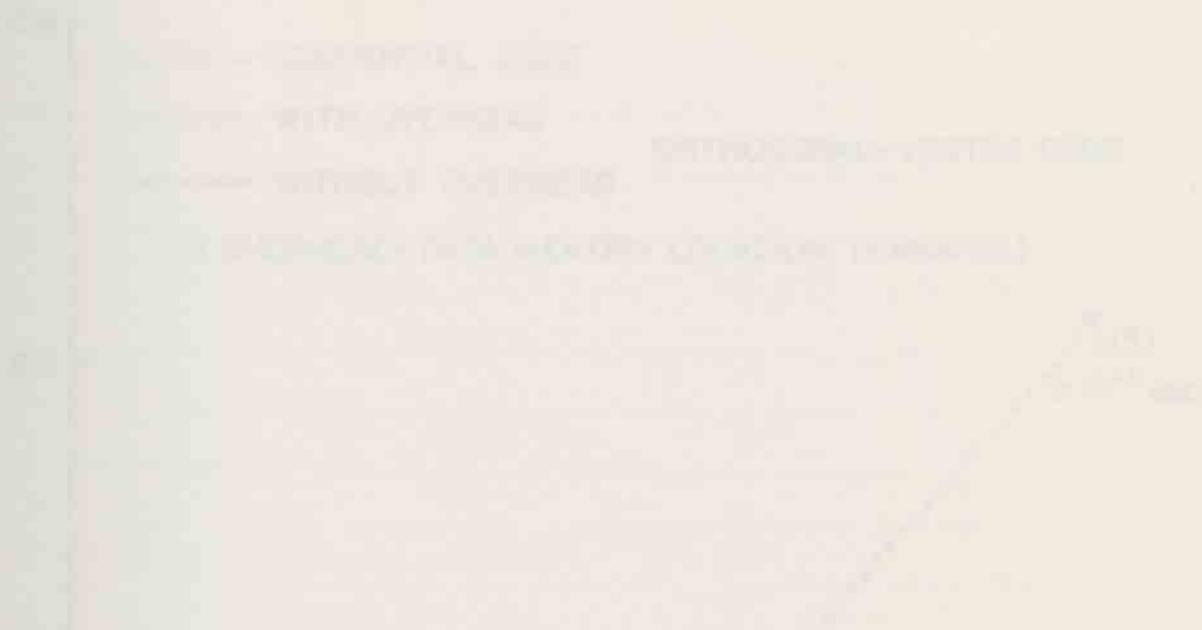
"New Satellites E/S & LAN"  
N. Allen

"Theory and Observations of Spectral Radiance for Cloud Studies"  
M. Wetzel

"El Nino Discovered in Radiation Budget Measurements"  
G. Campbell/D. Randel

"Satellite Sounding Near Severe Storms"  
D. Hillger

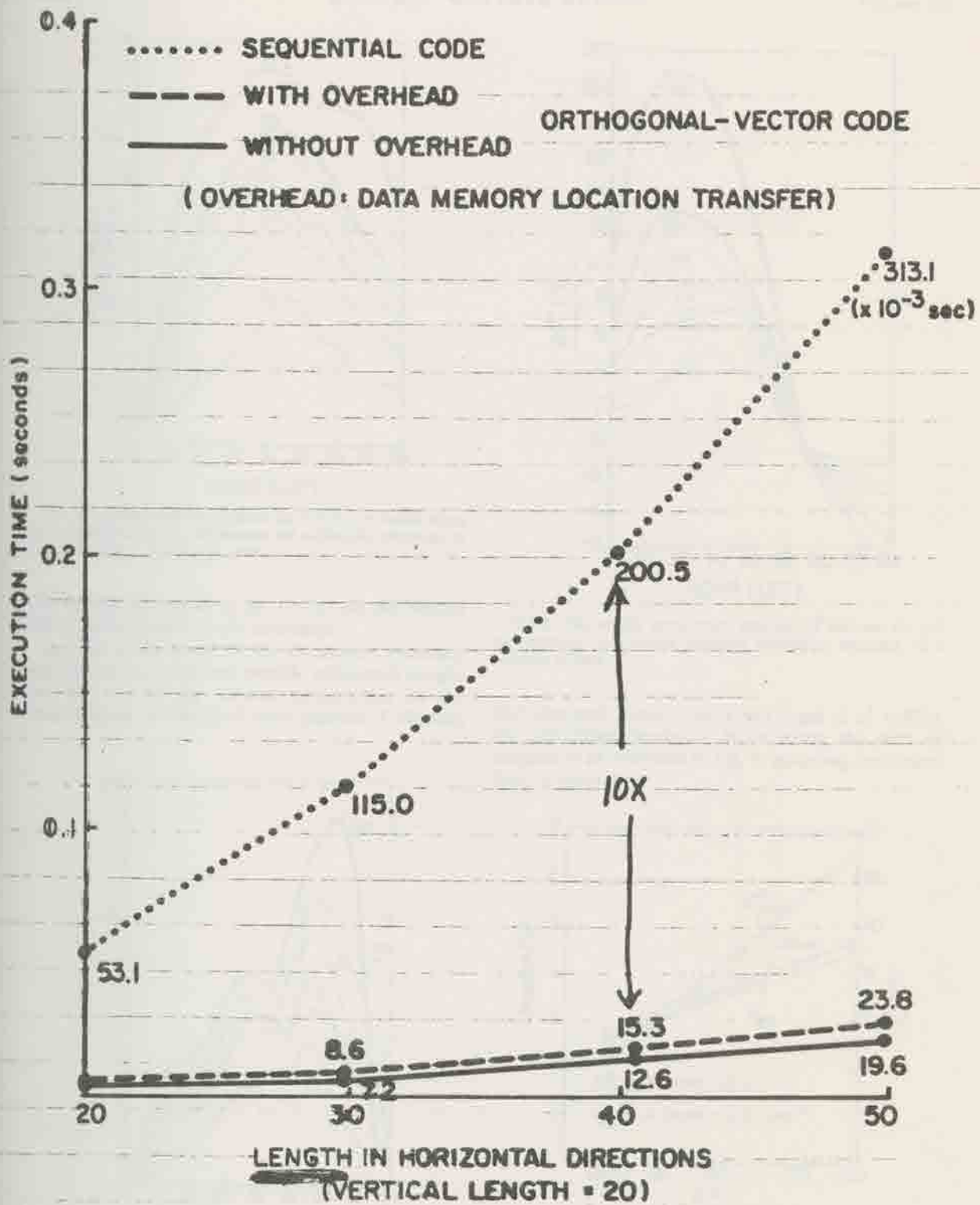
"Mesoscale Forecasting Research"  
J. Purdom



R. Pielke

"Applications of Near-Real Time Modeling With Supercomputer"





\* F1 0.1 → 0.05  
 \* F5 1.0 0.05

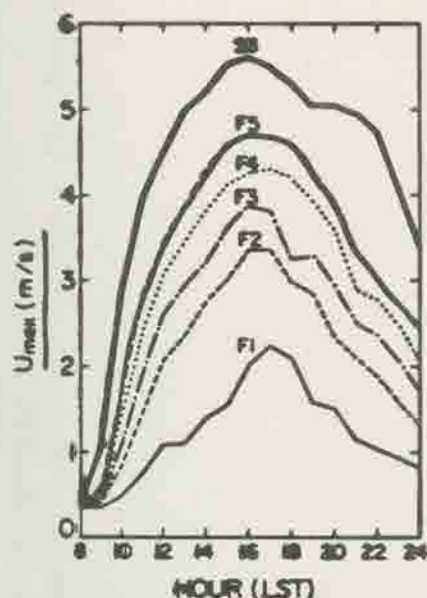


FIG. 4. The maximum wind speed ( $m s^{-1}$ ) at 5 m height along the domain cross section, for various soil availability contrasts, as a function of time. Flat terrain cases.

(1977b) and Ookouchi *et al.* (1978) on the inland side of the mountain in the afternoon.

Analysis of the terms in the circulation tendency equation for case M3 can provide additional insight into the role of the various components in the determination of the final flow pattern. Following

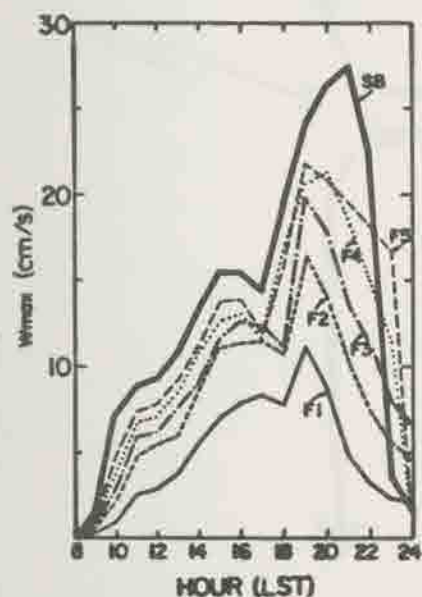


FIG. 5. The maximum vertical wind speed ( $cm s^{-1}$ ) in the simulated domain cross section, for various soil availability contrasts, as a function of time. Flat terrain cases.

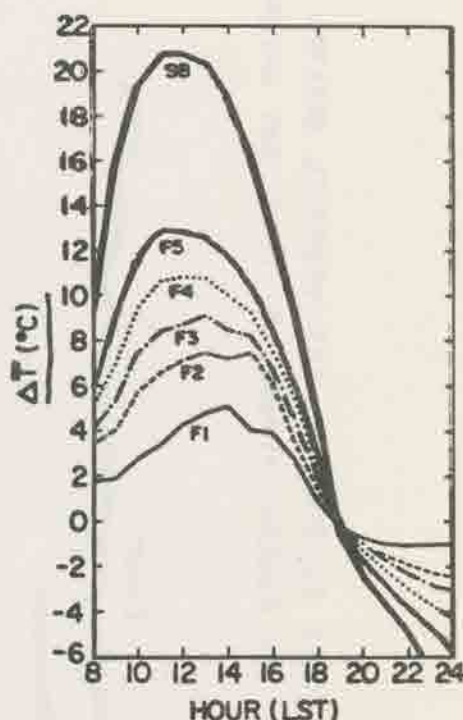


FIG. 6. The surface temperature contrast  $\Delta T$  between dry and wet domains, for various moisture availability contrasts, as a function of time.

McNider and Pielke (1981) and Segal *et al.* (1983), the circulation tendency  $\partial C/\partial t$  along the path of integration as indicated in Fig. 9, assuming frictionless flow, is given by

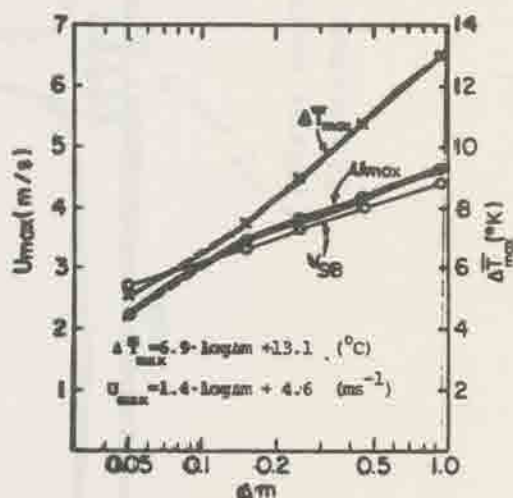
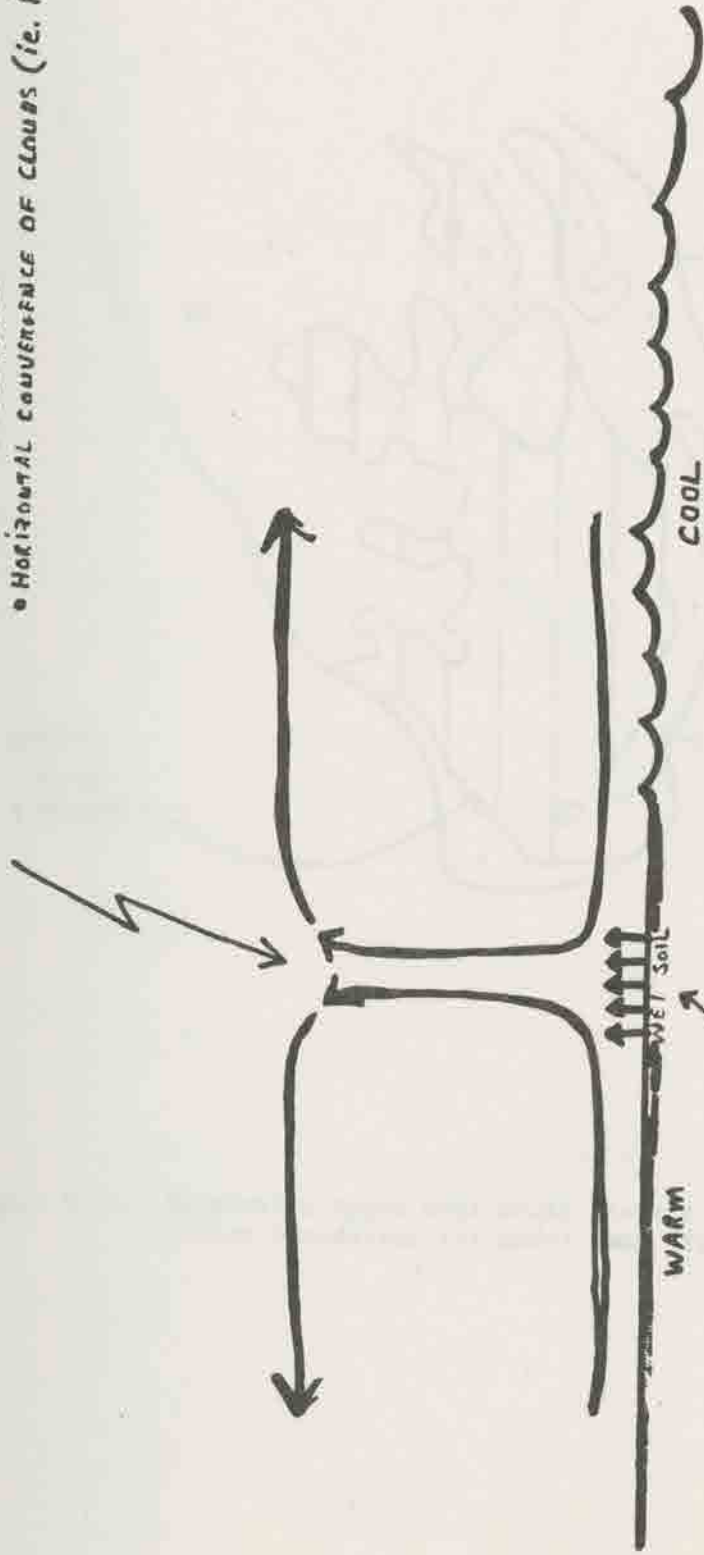


FIG. 7. Log-linear dependence of  $U_{max}$  (the maximum  $U$  at the surface along the domain cross section) and  $\Delta T_{max}$  as a function of the difference in the soil moisture availability  $\Delta m$  ( $\Delta m = m - m_0$ , where  $m_0 = 0.05$ ). The open circles indicate wind speed values obtained from Fig. (7).

SEA BREEZE PRECONDITIONS THE LOW LEVEL ATMOSPHERE BY

- MOISTURE CONVERGENCE
- HEAT CONVERGENCE
- HORIZONTAL CONVERGENCE OF CLOUDS (i.e. PROMOTES MIXERS)



GREATER MOISTURE FLUX WEAKENS SEA BREEZE CONVERGENCE SINCE THE HORIZONTAL TEMPERATURE GRADIENT IS LESS, BUT IT ENRICHES THE AVAILABLE BUOYANT ENERGY

ENRICHMENT OF THE LOW-LEVEL ENVIRONMENT

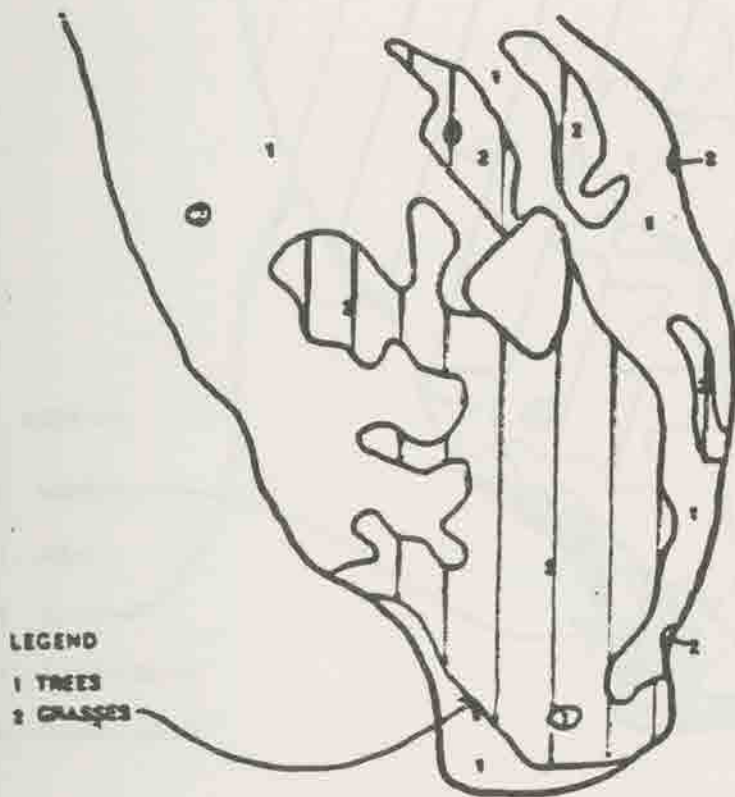


Figure 5.14. Vegetation types over South Florida used to define the bottom boundaries for model runs (from McCumber, 1980).

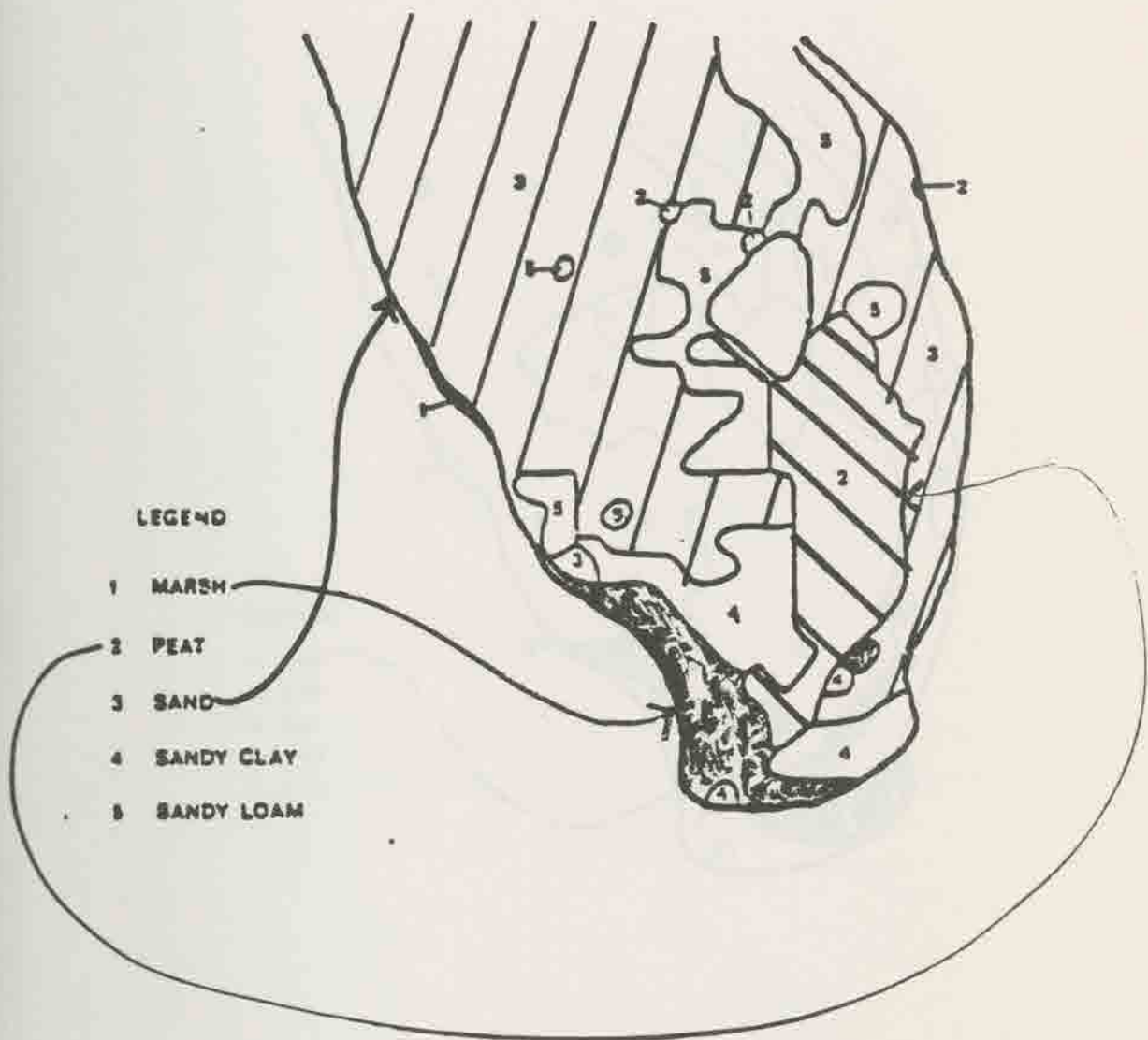


Figure 5.13. Soil types over South Florida used to define the bottom boundary for model runs (from McCumber, 1980).

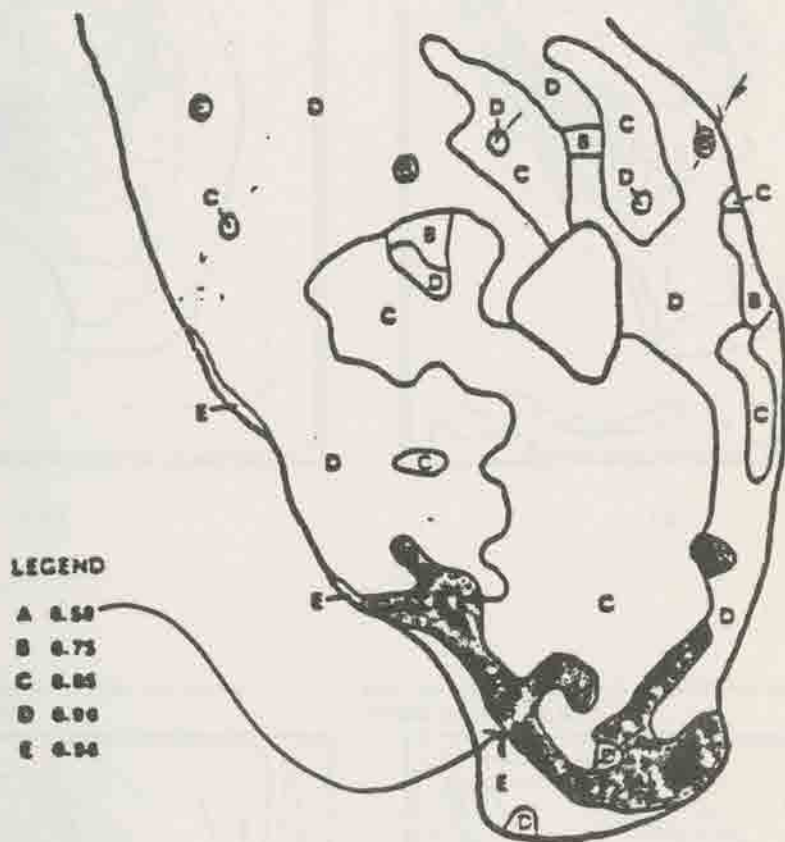
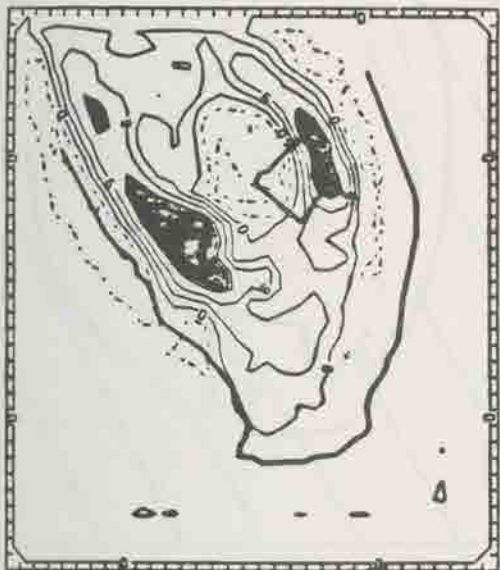


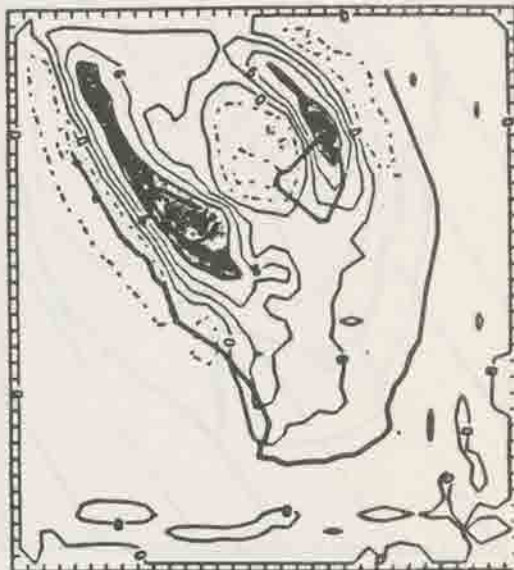
Figure 5.15. Vegetation shielding coverage ( $\sigma$ ) over South Florida used to define the bottom boundaries for model runs (from McCumber, 1980).

HR = 14.3 GEOSTROPHIC WIND IS 2.0M/SEC FROM 150. DEG  
VERTICAL VELOCITY @ LEVEL



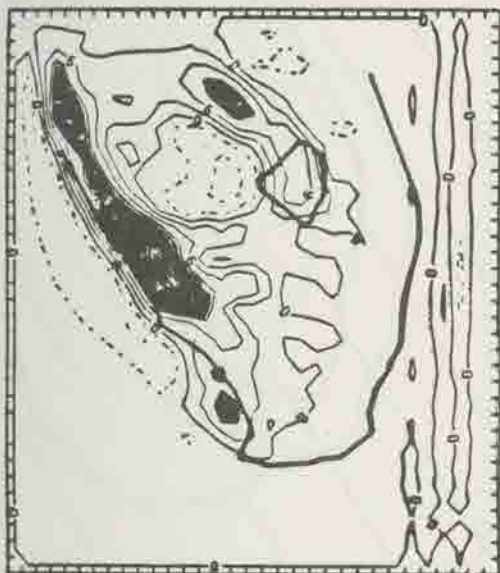
(a)

HR = 14.3 GEOSTROPHIC WIND IS 5.7M/SEC FROM 160. DEG  
VERTICAL VELOCITY @ LEVEL



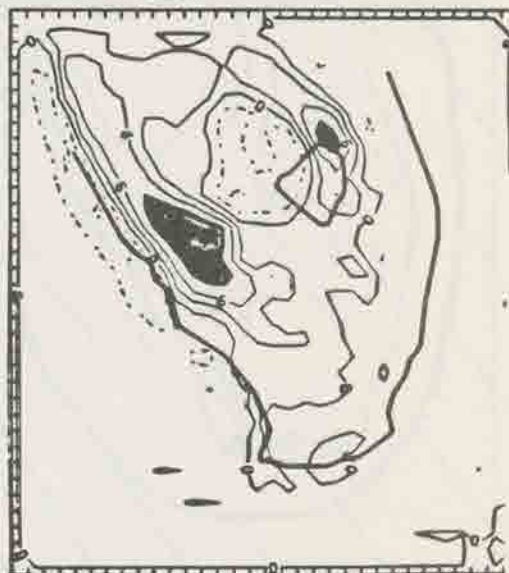
(b)

HR = 14.3 GEOSTROPHIC WIND IS 5.0M/SEC FROM 160. DEG  
VERTICAL VELOCITY @ LEVEL



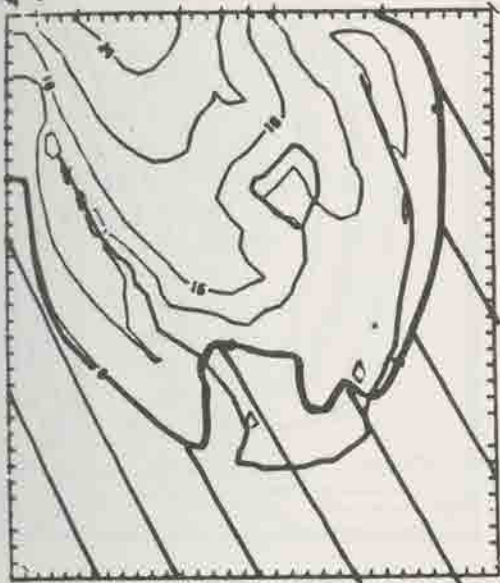
(c)

HR = 14.3 GEOSTROPHIC WIND IS .3M/SEC FROM 150. DEG  
VERTICAL VELOCITY @ LEVEL



(d)

HOUR = 14.3 GEOSTROPHIC WIND IS 2.0M/SEC FROM 150. DEG  
 $\theta_s - \theta_0$   
S LEVEL



(a)

HOUR = 14.3 GEOSTROPHIC WIND IS 5.7M/SEC FROM 150. DEG  
 $\theta_s - \theta_0$   
S LEVEL



(b)

HOUR = 14.3 GEOSTROPHIC WIND IS 5.0M/SEC FROM 150. DEG  
 $\theta_s - \theta_0$   
S LEVEL



(c)

HOUR = 14.3 GEOSTROPHIC WIND IS 5.0M/SEC FROM 150. DEG  
 $\theta_s - \theta_0$   
S LEVEL



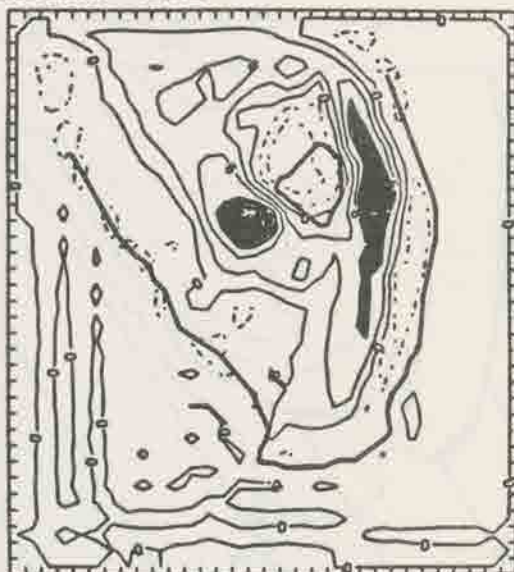
(d)

• 12.3 GEOSTROPHIC WIND IS 4.2M/SEC FROM 225. DEG  
OIL VELOCITY @ LEVEL



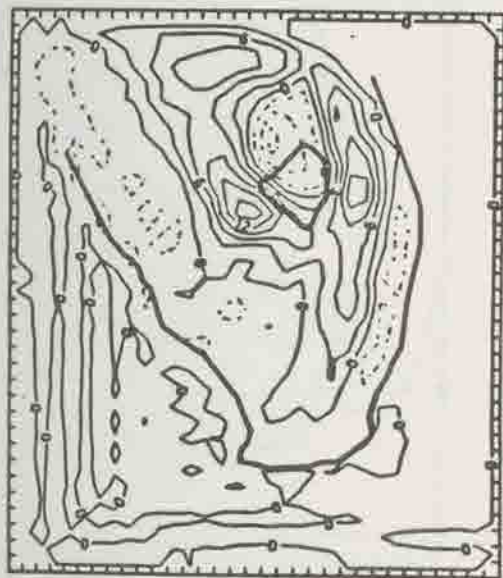
(a)

• 14.3 GEOSTROPHIC WIND IS 4.2M/SEC FROM 225. DEG  
VERTICAL VELOCITY @ LEVEL



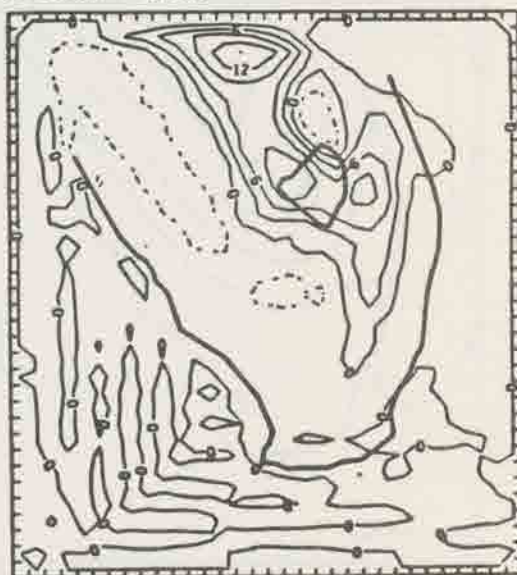
(b)

• 16.3 GEOSTROPHIC WIND IS 4.2M/SEC FROM 225. DEG  
OIL VELOCITY @ LEVEL



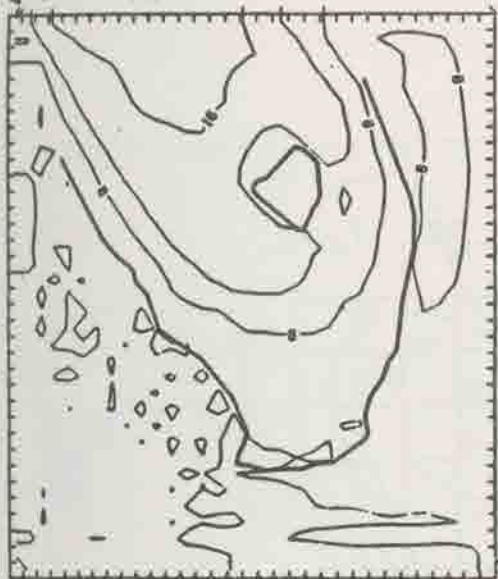
(c)

• 18.3 GEOSTROPHIC WIND IS 4.2M/SEC FROM 225. DEG  
VERTICAL VELOCITY @ LEVEL



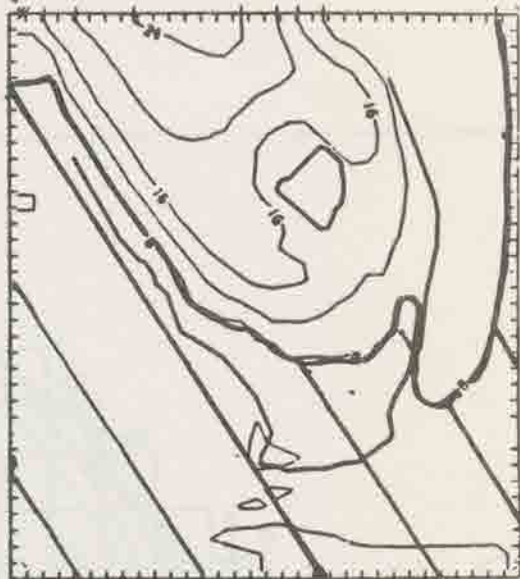
(d)

$H = 12.3$  GEOSTROPHIC WIND IS 4.2M/SEC FROM 225. DEG.  
 $\theta_a - \theta_s$   
5 LEVEL



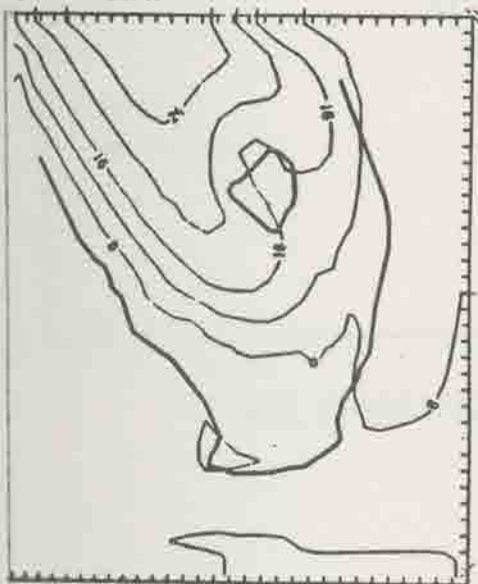
(a)

$H = 14.3$  GEOSTROPHIC WIND IS 4.2M/SEC FROM 225. DEG.  
 $\theta_a - \theta_s$   
5 LEVEL



(b)

$H = 16.3$  GEOSTROPHIC WIND IS 4.2M/SEC FROM 225. DEG.  
 $\theta_a - \theta_s$   
5 LEVEL



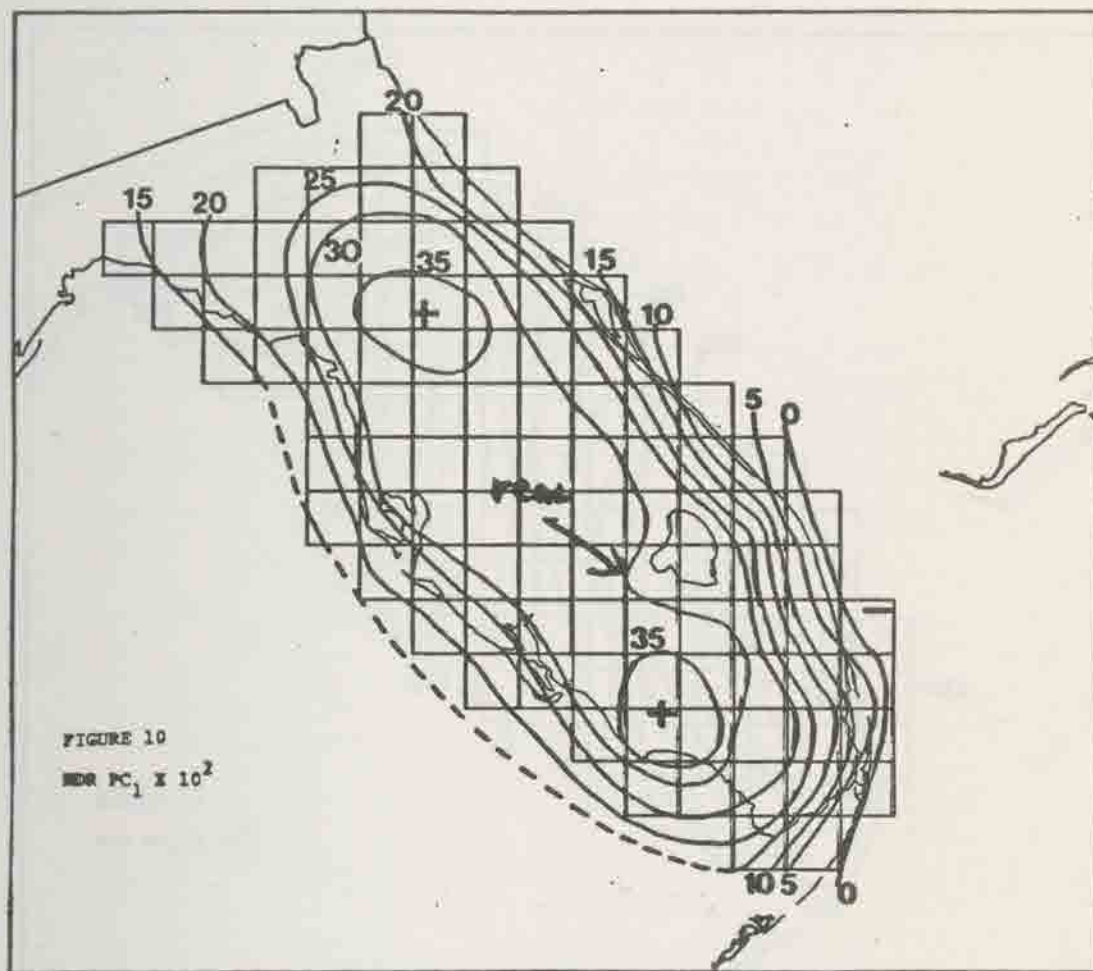
(c)

$H = 18.3$  GEOSTROPHIC WIND IS 4.2M/SEC FROM 225. DEG.  
 $\theta_a - \theta_s$   
5 LEVEL



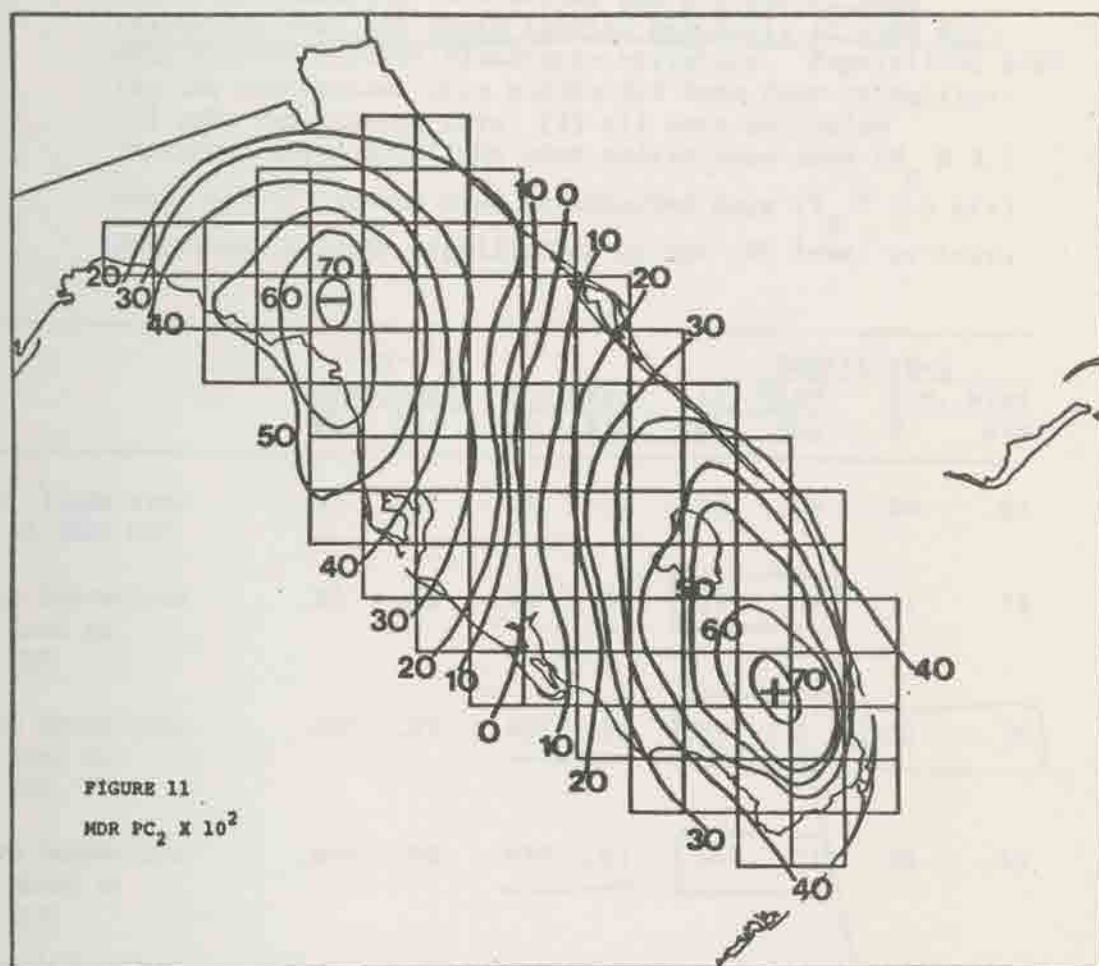
(d)

OBJECTIVE #3 DETERMINATION OF DAILY PATTERNS



FIRST PRINCIPAL COMPONENT OF THE MDR DATA

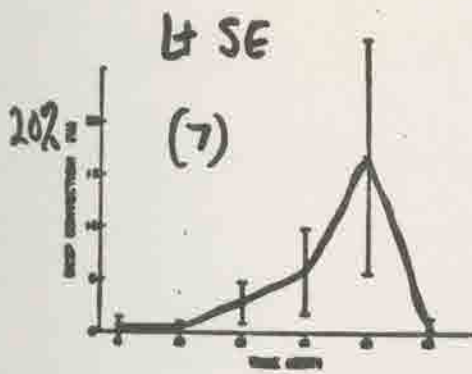
OBJECTIVE #3: DETERMINATION OF DAILY PATTERNS



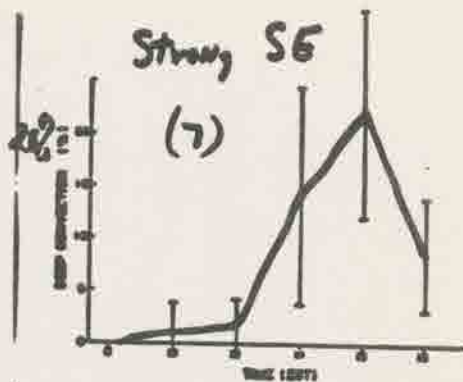
SECOND PRINCIPAL COMPONENT OF THE MDR DATA

Table 4.4. Correlation coefficients and significance from a bivariate regression analysis correlating the percent of deep convection over the South Florida peninsula at 1400 EST with several percent cloudiness variables. Populations used for the regressions were subdivided into four categories: (1) only undisturbed days, (2) all days including disturbed days, (3) light wind undisturbed days ( $V_g \leq 3.5$  m/s), and (4) strong wind undisturbed days ( $V_g > 3.5$  m/s). Asterisks indicate significance at the .05 level or less.

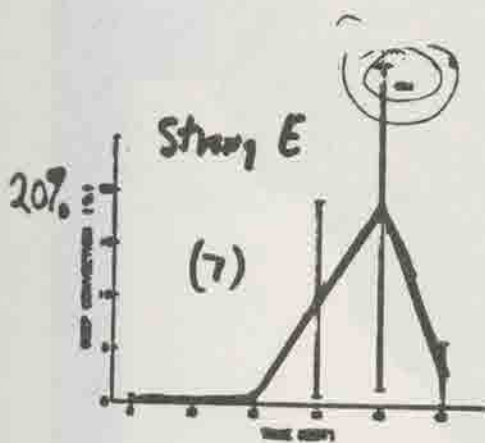
	Un- disturbed		All Days		Undisturbed			
	$\bar{V}$	Sig	$\bar{V}$	Sig	Lt. Wind $\bar{V}$	Sig	Str. Wind $\bar{V}$	Sig
% All Clouds over Land at 0800 EST	.10	.68	.29	.16	.34	.28	.20	.61
% Deep Convection over Land at 0800 EST	.26	.25	.40*	.05	.61*	.04	.11	.78
% Deep Convection over Land at 1000 EST	.59*	.01	.46*	.03	.81*	0	.55	.16
% Deep Convection over Water at 0800 EST	.44*	.05	.43*	.03	.74*	.01	.30	.43



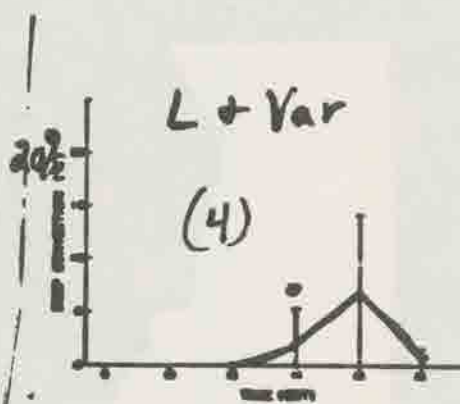
(a)



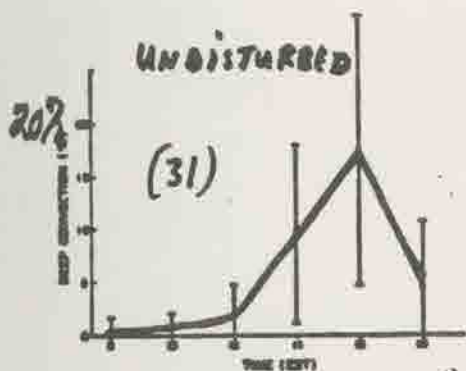
(b)



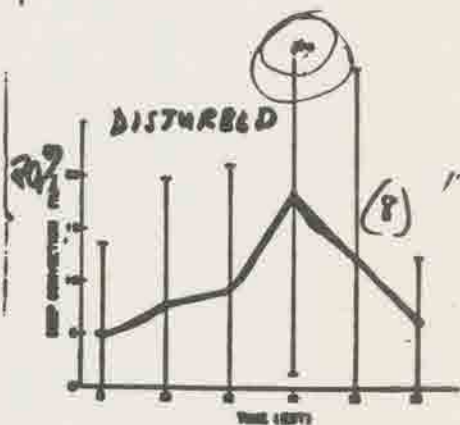
(c)



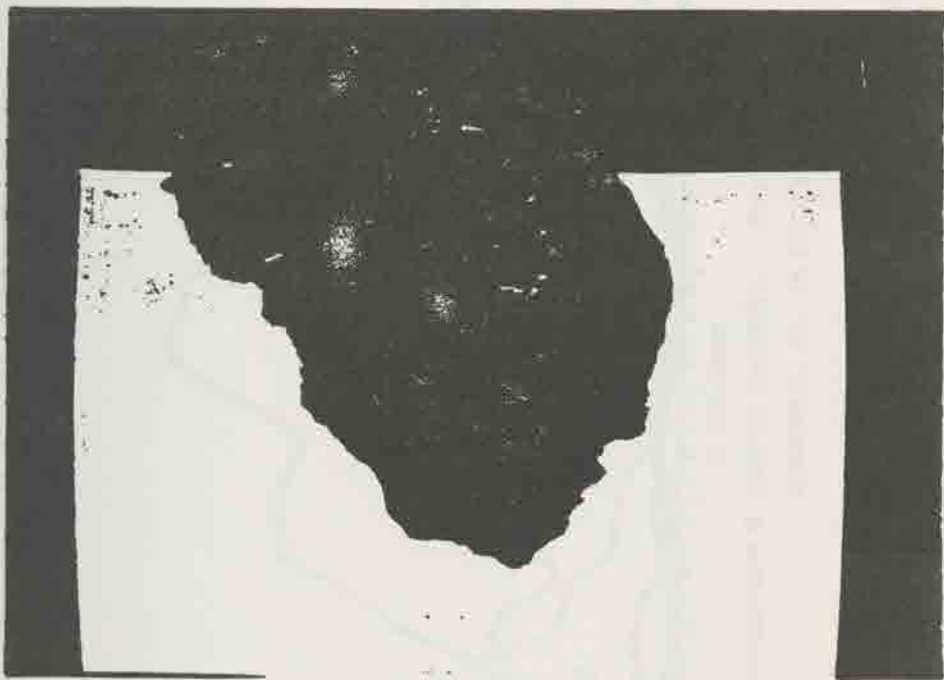
(d)



(e)



(f)



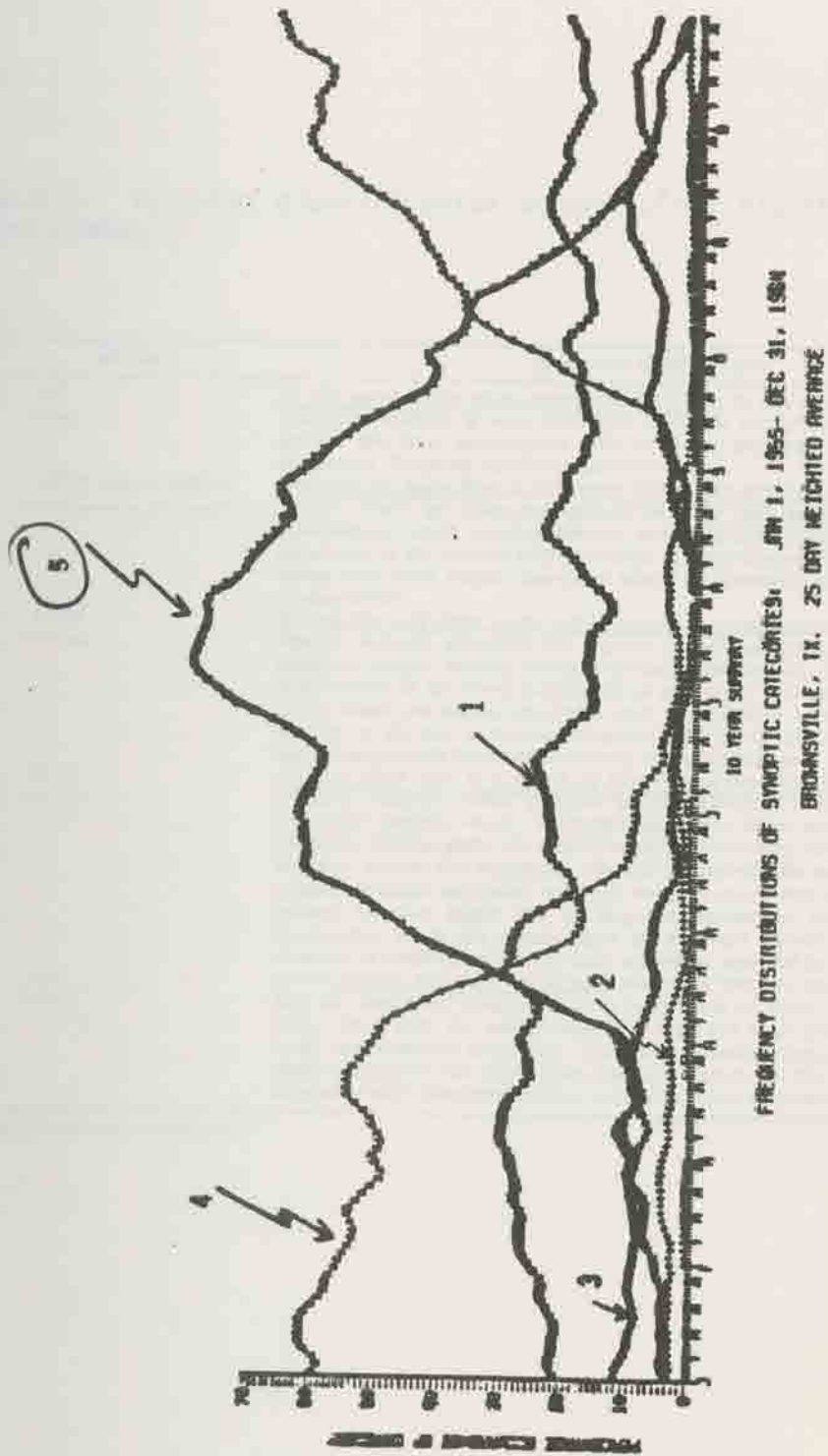


Figure 4a. 25 day average occurrence of synoptic categories for Brownsville, Texas. (From Lindsey, 1980; and Garstang *et al.*, 1980).

Table 1. Synoptic classification scheme (from Pielke, 1982; modified from Lindsey<sup>1</sup>).

Category	Air mass	Reason for categorization <sup>a</sup>
1	<u>mT</u>	<u>In the warm sector of an extratropical cyclone.</u> In this region the thickness and vorticity advection is weak with little curvature to the surface isobars. There is limited low level convergence with an upper level ridge leading to produce subsidence. Southerly low-level winds are typical.
2	<u>mT/cP, mT/cA, mP/cA</u>	<u>Ahead of the warm front in the region of cyclonic curvature to the surface isobars.</u> Warm air advecting uplope over the cold air stabilizes the thermal stratification, while positive vorticity advection and low-level frictional convergence add to the vertical lifting. Because of the warm advection, the geostrophic winds veer with height. Low-level winds are generally north-easterly through south-easterly.
3	<u>cP, cA</u>	<u>Behind the cold front in the region of cyclonic curvature to the surface isobars.</u> Positive vorticity advection and negative thermal advection dominate, with the resultant cooling causing strong boundary layer mixing. The resulting thermal stratification in the lower troposphere is neutral, or even slightly, superadiabatic. Gusty winds are usually associated with this sector of an extratropical cyclone. Because of the cold advection, the geostrophic winds back with height. Low-level winds are generally from the north-west through south-west.
4	<u>cP, cA</u>	<u>Under a polar high in a region of anticyclonic curvature to the surface isobars.</u> Negative vorticity, weak negative thermal advection and low-level frictional divergence usually occur, producing boundary layer subsidence. Because of relatively cool air aloft, the thermal stratification is only slightly stabilized during the day, despite the subsidence. At night, however, the relatively weak surface pressure gradient associated with this category causes very stable layers near the ground on clear nights due to long-wave radiational cooling. The low-level geostrophic winds are usually light to moderate varying slowly from north-westerly to south-easterly as the ridge progresses eastward past a fixed location.
5	<u>mT</u>	<u>In the vicinity of a subtropical ridge</u> where the vorticity and thickness advection, and the horizontal pressure gradient at all levels are weak. The large upper-level ridge, along with the anticyclonically curved low level pressure field, produces weak but persistent subsidence. This sinking causes a stabilization of the atmosphere throughout the troposphere. Low-level winds over the eastern United States associated with these systems tend to blow from the south-east through south-west.

<sup>a</sup>The discussion applies to northern hemisphere.

Table 2. Overview of air quality related aspects of the 5 synoptic categories illustrated in Figure 2 and described in Table 1 (northern hemisphere). (Modified from Pielke *et al.*, 1985)

FLORIDA SUMMER

GROUP / Characteristics	CATEGORY 1	2	3	4	5
surface winds	brisk SW surface winds	light to moderate SE to SW surface winds	strong NE to W surface winds	light and variable winds	light SE to SW winds
vertical motion	ascending synoptic descent at the cold front approach	synoptic ascent due to warm advection and positive vorticity advection aloft	synoptic ascent due to positive vorticity advection aloft (in this region this ascent more than compensates for the descent due to cold advection)	synoptic descent (due to warm advection and/or negative vorticity advection aloft)	synoptic subsidence (descending branch of the Hadley cell). Becomes stronger as you approach the ridge axis.
temperature advection	little temperature advection at the surface	warm advection above the frontal inversion	cold advection at the surface	warm temperature advection at the surface	warm temperature advection at the surface
inversion	weak synoptic subsidence inversion caps planetary boundary layer	boundary layer capped by frontal inversion	deep planetary boundary layer	synoptic subsidence inversion and/or warm advection aloft create an inversion which caps the planetary boundary layer	synoptic subsidence inversion
diurnal variation in boundary layer stability	Moderate diurnal variability in the boundary layer stability	little diurnal variability in boundary layer stability because of cloud cover	little diurnal variability in the boundary layer stability because of strong winds and destabilizing of boundary layer by cold advection	In the absence of snow cover because of clear skies and light winds, large diurnal variability in boundary layer stability	moderate diurnal variability in boundary layer stability
diurnal variation in surface layer stability	Moderately unstable surface layer during the day moderately stable surface layer during the night	stably stratified surface layer day and night	near neutral surface layer day and night	mostly to moderately unstable surface layer during the day unless snow cover present or low sun angle in which case surface layer tends to be stably stratified. Very stable surface layer at night	moderately to strong unstable surface layer during the day moderate to strong stable surface layer during the night.
humidity	often humid in relative and absolute sense	often dry in absolute sense but humid in relative sense	dry in the absolute sense, usually dry in the relative sense	dry in the absolute sense humid in the relative sense at night/dry in relative sense during the day except when ground is snow-covered	humid in relative and absolute sense
cloud cover	clear to partly cloudy skies except near small lakes	mostly cloudy to cloudy	clear to scattered or broken shallow convective clouds	clear except tendency for fog at night	day: scattered fair weather cumulus night: clear (except near the mesoscale systems listed below)
diurnal mesoscale systems	small lakes	embedded lines of convection	forced airflow over rough terrain systems, lake effect storms	mountain-valley flows land-sea breezes urban circulations (thermally-forced systems)	mountain-valley flows land-sea breezes urban circulations (thermally-forced system)
precipitation type	organized lines of convective precipitation	often stable cloud types and precipitation. Overcast in general	medium to shallow depth convective clouds, showery precipitation	no precipitation	shallow convective clouds with deeper convective clouds and precipitation organized by thermally forced mesoscale systems such as listed above
ventilation	moderate to good ventilation	poor ventilation of low level (i.e., below frontal inversion) emissions	excellent ventilation	night or snow-covered ground: poor ventilation day: poor to moderate ventilation	day: moderate to good ventilation night: moderate to poor ventilation
deposition	dry deposition except wet deposition in showers	dominated by wet deposition	dry deposition except in showers	dry deposition	dry deposition except wet deposition in showers and thunderstorms
transport	long range	long range above inversion	long range	more local as you approach the center of the polar high	more local as you approach the center of the subtropical high

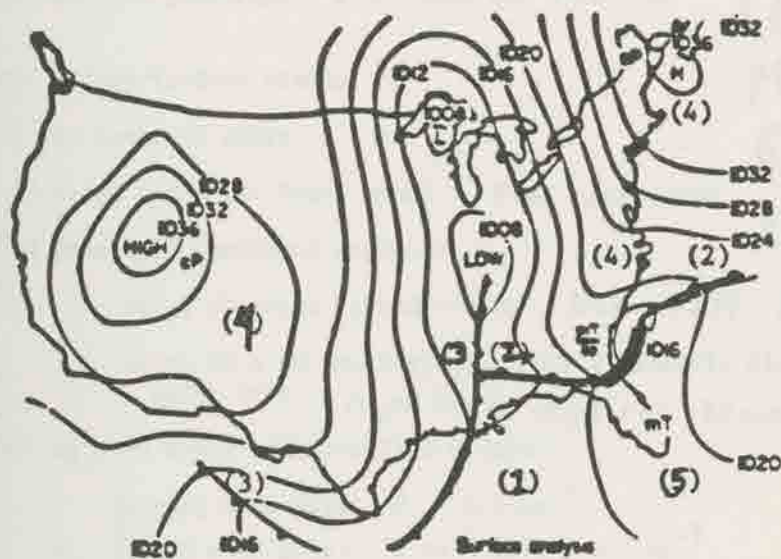


Figure 2. Example of a surface analysis chart (for January 9, 1964) showing the application of the synoptic climatological model for the five synoptic classes listed in Table 1 (reproduced from Pielke, 1982).

• Relation between large scale environment and percent coverage of deep cumulus convection (trigger  $\rightleftharpoons$  preconditioning)

- i) magnitude of convective instability:  $\Delta\theta_e$
- ii) depth of convective instability:  $\Delta p$
- \* iii) magnitude of moisture deficiency:  $\theta_{es} - \theta_e$
- iv) lifted index at 500 mb
- v) 200 mb wind speed
- vi) surface geostrophic wind speed and direction

P. Michaels/UVA  
 J. McQueen/CSU  
 J.L. Song/CSU  
 M. Segal/CSU  
 R. Kessler/CSU  
 Y. Oochouchi/JRRI

• synoptic categorization scheme

- i) by synoptic class
  - a) using the polar front model **FIVE CATEGORIES**
  - b) principal component analyses

P. MICHAELS



using observed "thunder-days" **NCC 1948-1978 SEASONAL AUA.**  
 using 20 x 20 nautical mile hourly manually digitized radar data **10,800 hours high res. 20 n.mi. 450 days**

- ii) by wind speed and direction groups
  - a {
    - strong wind days:  $V_g > 3.5 \text{ ms}^{-1}$
    - light wind days:  $1 \text{ ms}^{-1} \leq V_g \leq 3.5 \text{ ms}^{-1}$
    - very light and variable days:  $V_g < 1 \text{ ms}^{-1}$
  - b {
    - northeast:  $1^\circ - 60^\circ$
    - east:  $61^\circ - 120^\circ$
    - southeast:  $121^\circ - 180^\circ$
    - southwest:  $181^\circ - 240^\circ$
    - west:  $241^\circ - 300^\circ$

iii) disturbed/undisturbed

• Relation between deep convection and antecedent deep convection

- i) % all clouds over land at 0800 EST
- ii) % deep convection over land at 0800 EST
- \* iii) % deep convection over land at 1000 EST
- \* iv) % deep convection over water at 0800 EST

• Patterning of deep convection for each class

- i) satellite composite imagery
- ii) mesoscale model simulations
  - mass convergence in lower troposphere
  - moisture deficit in lower troposphere

# Use of a Personal Computer Workstation for 0-1 Range Forecasting

## « PRE-STORM »

R. Green

"Use of Micro-computers in Pre-STORM Field Studies - 1985"

1. To evaluate the feasibility and  
utility of using a Personal Computer as a  
operational meteorological workstation.

2. To assess the information on 0-1  
interval information re forecasting RFS's.

## **Use of a Personal Computer Workstation for Short Range Forecasting**

### **● PRE-STORM ●**

#### **Objectives:**

- 1. To evaluate the feasibility and utility of using a Personal Computer as an operational meteorological workstation.**
- 2. To assess the usefulness of VAS retrieval information in forecasting MCS's.**

## **Personal Computer Workstation Hardware Configuration**

- **IBM PC/XT with 8087 Math Processor**
- **640K RAM Memory**
- **10 Meg Hard Disk**
- **Twin Displays – Monochrome and Color**
- **Modem – 1200 Baud**
- **Dot-matrix Graphics Printer**

## **Personal Computer Workstation Software Features**

- **DOS 2.1**
- **FORTRAN, Pascal and Assembler Code**
- **RAM Storage of 24 Graphics Frames**
- **Image Animation Rate of up to 15 fps**
- **Compressed Data Transfer**
- **Menu-driven User Interface**
- **Data Archive to Diskettes**

**Major Problem Areas with the  
Personal Computer Workstation  
at PRE-STORM**

- Slow transmission of products over telephone line – even at 1200 baud.
- Lengthy processing times to create retrieval data base.
- Crude resolution of image display – especially for visible data.

## **Imminent Solutions to the Major Problem Areas with the Personal Computer Workstation**

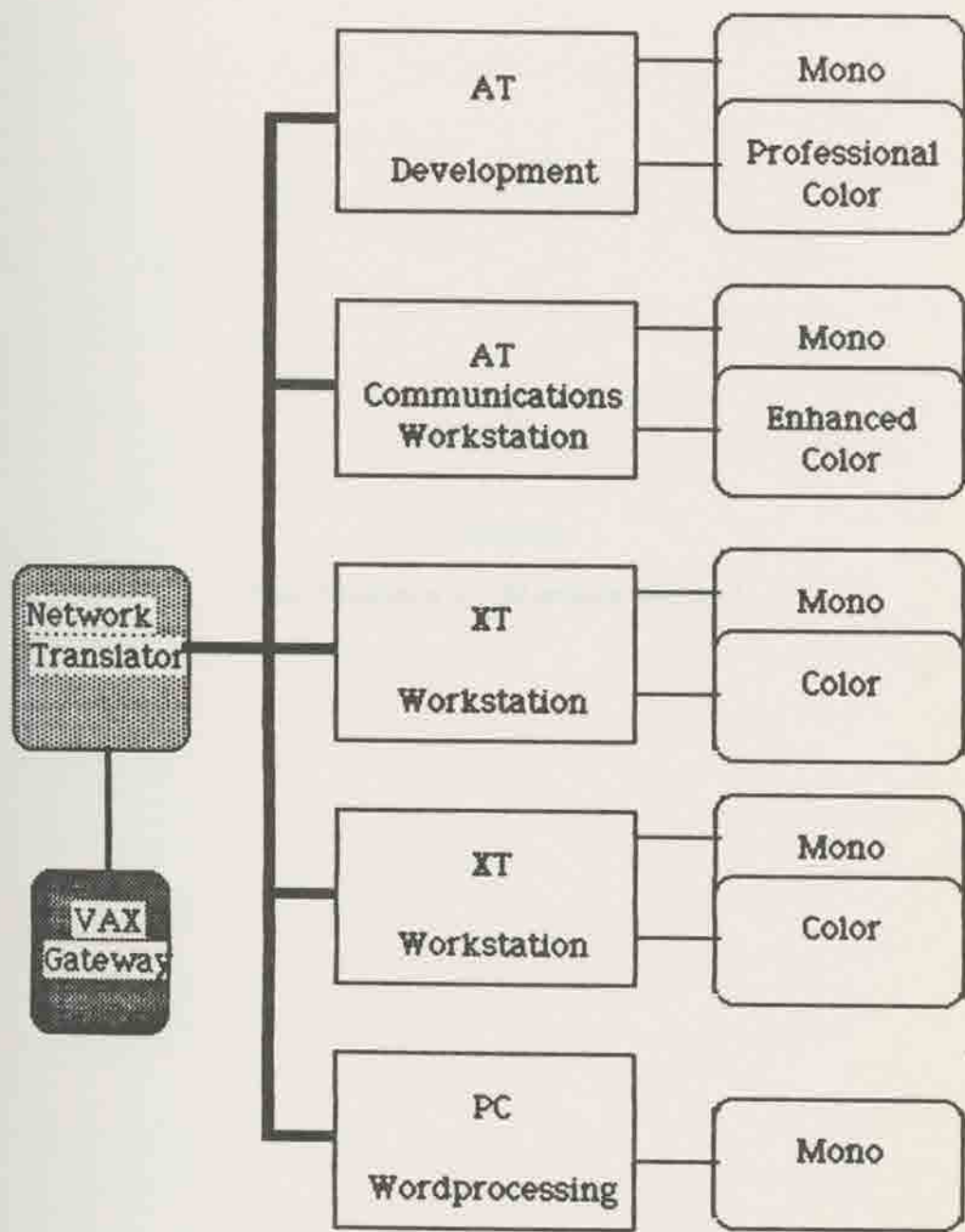
- **2400 baud modem technology available for use on voice-grade lines.**
- **PC/AT processing speed three times faster than XT (processor and I/O).**
- **Two new displays available:**
  - **640 X 350 X 16 colors**
  - **640 X 480 X 256 colors.**

## Requirements for a Host Computer to Support an Operational Personal Computer Workstation

- A product processing schedule which will consistently meet workstation access times.
- A dedicated modem port for each operational workstation.
- Full-time operator support and on-call technical support.
- Well thought-out down times or a back-up system.

**Future Ideas  
for  
Personal Computer Workstations**

- **Laser/Optical Storage Disks --  
100 Megabytes on \$30 Disk**
- **Laser Printers -- Fast and Quiet**
- **Networks -- File and Device Sharing**
- **Satellite Communications**
- **NCAR Unidata Plans**
- **NESDIS VDUC Workstations**
- **STORM-Central Support**



T. Brubaker

"New Concepts in Microprocessors"

## BRIEF HISTORY

The four-bit microprocessor was developed in 1970.

The eight-bit microprocessor followed several years later.

Currently 16-bit microprocessors are integrated into products.

The 32-bit microprocessor race is warming up. The estimated market is tens of billions of dollars.

## THE MARKET SEGMENTS

Business applications and office automation

Engineering work stations

Numerical control

Expert Systems

Robotics

Video graphics

Signal processing

GENERAL CHARACTERISTICS OF  
32-BIT MICROPROCESSORS

Clock speeds in the 12-16 MHz range with a goal of 25 MHz.

Due to their density fewer peripheral chips will be required and probably most peripheral functions will be handled by slave 8- and 16-bit microprocessors.

CMOS implementation for minimal power consumption.

Sophisticated memory addressing including virtual memory.

THE NATIONAL SEMICONDUCTOR 32032

A VAX-type pipelined microcomputer architecture with virtual memory support and a highly regular (orthogonal) instruction designed for high level language support.

Up to 16 megabytes of random access memory.

A 25 MHz clock rate for the CMOS version.

MOTOROLA 68020

16.67 MHz

On-chip instruction cache

8-gigabytes of virtual memory

Concurrent instruction execution

Internal barrel shifter to speed execution

ZILOG Z80,000

Cache memory for both data and instructions

25 MHz CPU clock

Sophisticated six level pipeline architecture

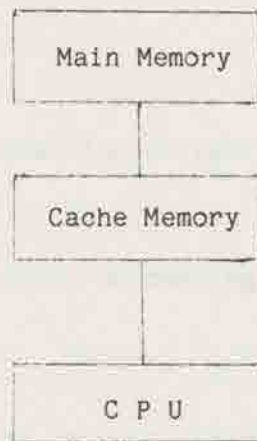
On-chip memory management

The CPU can generate physical addresses directly

## THE REDUCED INSTRUCTION SET

### MICROCOMPUTERS (RISC)

The concept utilized fewer instructions with most memory access instructions eliminated.



The arithmetic instructions are performed using register-to-register operations giving one machine cycle time execution.

Implementations require good compilers to minimize main memory access, i.e., we want data that is required stored in the Cache Memory.

COLORADO STATE UNIVERSITY LIBRARIES

PROSPECTS IN OUR ATMOSPHERIC SCIENCE WORK

Vastly improved work stations each having color graphics. We will see the stand-alone graphics probably disappear.

Sophisticated graphics processing done largely in hardware under microprocessor control.

The ability to integrate processing directly into sensors.

The capability for sophisticated processing and display at remote sites with minimal cost.

Vastly improved communication between distributed computer systems allowing data and information to be shared at high speed.

THE USE OF SPECIAL PURPOSE VLSI  
CHIP DESIGNS TO ENHANCE MICROCOMPUTER  
PERFORMANCE IN PROCESSING SATELLITE DATA

By carefully designing our systems, the processes of

- a. Data Ingest
- b. Display
- c. Information extraction

will be integrated resulting in improved system performance.

We will carefully optimize software and peripheral VLSI hardware.

As an example, consider level comparisons with IR data. With a hardware comparator we can generate cloud size above a certain level directly in the data stream.

UNIVERSITY MICROFILMS

## MICROCOMPUTER CONTROL OF THE OPTICAL DISK

The optical disk provides a media to archive large amounts of image data and/or information

A still picture system exists that stores 24,000 individual color frames with about one second access time.

I believe these systems have great potential for allowing rapid information comparisons of current data-information with data-information from past events.

# History

MID 1970's

1981 THIRD GENERATION

VAX II/780 - COMTEL

N. Allen

"New Satellites E/S & LAN"

Weather Laboratory -

Real Time Weather Data

WMO STATIONS -

Local Area Network

Increased Computer

Resources

UNIVERSITY MICROFILMS

# HISTORY . . . .

MID 1970's

1981 THIRD GENERATION

- VAX 11/780 - COMTAL

—  
1985 FOURTH GENERATION

- WEATHER LABORATORY —  
REAL TIME WEATHER DATA
- WORK STATIONS —  
LOCAL AREA NETWORK
- INCREASED COMPUTER  
RESOURCES

NEW ....

SATELLITE EARTH STATION  
AND  
LOCAL AREA NETWORKS  
for  
WORK STATIONS AND WX LAB

---

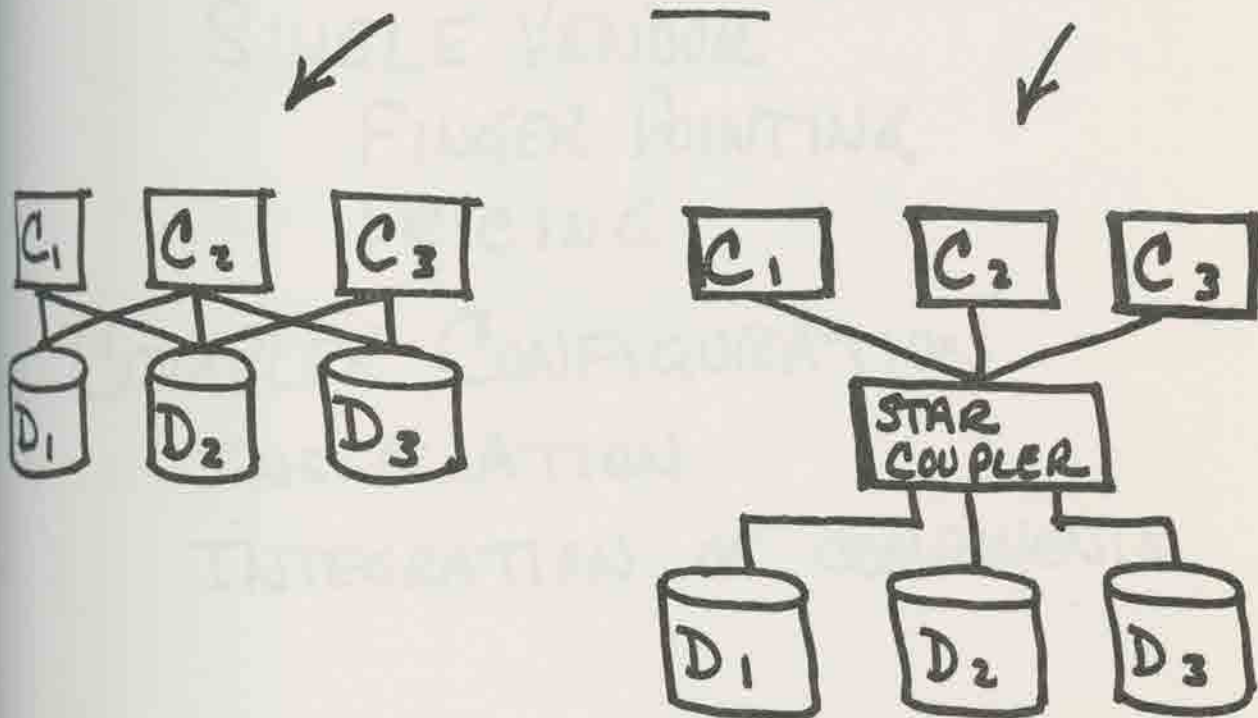
BACKGROUND ...

1984 GOES AAA CONFERENCE  
WEATHER LABORATORY  
WORKSTATIONS  
• IBM PC, XT, AT  
• APPLE

## CRITERIA...

- FRAME SYNCHRONIZER - AA
- PROCESSOR/STORAGE REDUNDANCY
- INTEGRATE WITH VAX 780
- COMTAL, OPTRONICS, ZETA-8
- IRIS SOFTWARE
- DATA ACCESS - NO TRANSFER

### DUAL PORTING - VS. CLUSTER



## SOFTWARE

OPERATING SYSTEM - VMS

LAYERED PRODUCTS

. FORTRAN

. PASCAL

. C

## MAINTENANCE

SINGLE VENDOR

FINGER POINTING

PRICING

## COMPLEX CONFIGURATION

INSTALLATION

INTEGRATION OF COMPONENTS

RESEARCH AND EDUCATIONAL  
NEEDS FOR  
CIRA AND THE DEPARTMENT

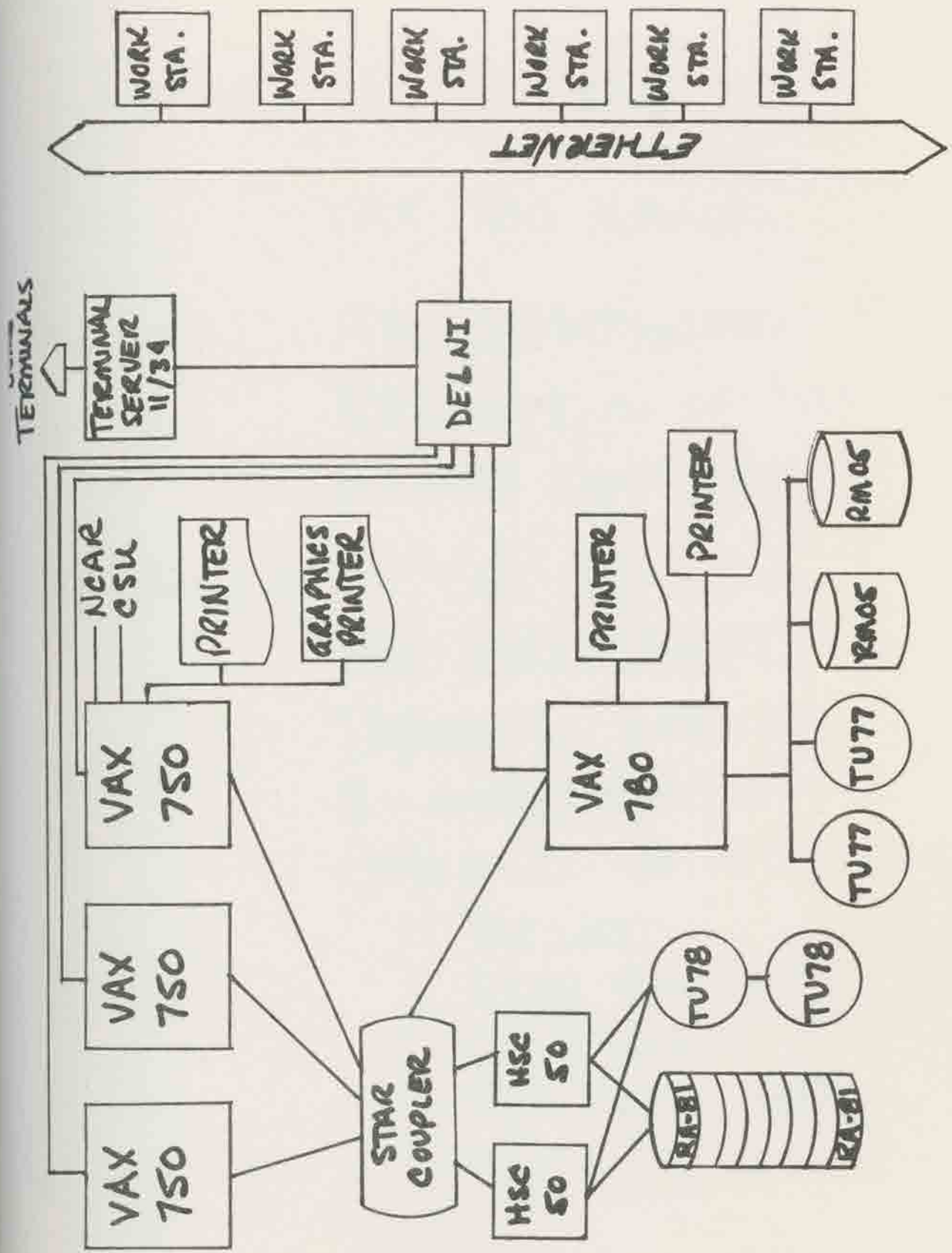
---

DIGITAL EQUIPMENT CORPORATION  
WORK STATION GRANT PROPOSAL

---

PROPOSAL TO DEC — MARCH  
ACCEPTED BY DEC — APRIL  
FUNDING CIRA/CSU — MAY  
PURCHASE ORDER — JUNE

---



# INSTALLATION SCHEDULE

JULY - VAX 780 MEMORY

AUGUST - AIR CONDITIONER  
RELOCATION OF VAX 780  
ETHER NET (CABLE)

SEPTEMBER -

VAX 750 -DEPT  
TERMINAL SERVER  
2- WORK STATIONS  
PHASE I OF CLUSTER

- DELNI
- STAR COUPLER
- (1) HSC50
- VAX 780 — 750

OCTOBER - PHASE II - CLUSTER

(2) VAX 750 - EARTH STATION

(2) TU-78 TAPE DRIVES

(5) RA-81 DISKS - 456 M/R ea.

(4) WORK STATIONS.

VAX C COMPILER

NOVEMBER

FINISH TRAINING

BEGIN CLUSTER OPERATION

START AAA DEVELOPMENT

DECEMBER - OPERATIONAL

CLUSTER

ETHERNET

WORKSTATIONS.

M. Wetzel

"Theory and Observations of Spectral Radiance for Cloud Studies"

THEORY AND OBSERVATION  
OF  
SPECTRAL RADIANCES  
FOR CLOUD STUDIES

1. Importance of spectral representation in cloud radiation models.
2. Physical radiative behavior of water species.
3. Effects of the spectral characteristics of water on remote sensing by passive means.
4. Discrimination of cloud parameters :
  - (a) phase
  - (b) particle size
  - (c) single-scatter albedo
  - (d) optical depth/reflectance ..... absorptance
  - (e) dispersion of particle size spectrum
  - (f) cloud top altitude



STRATIFORM WATER CLOUD

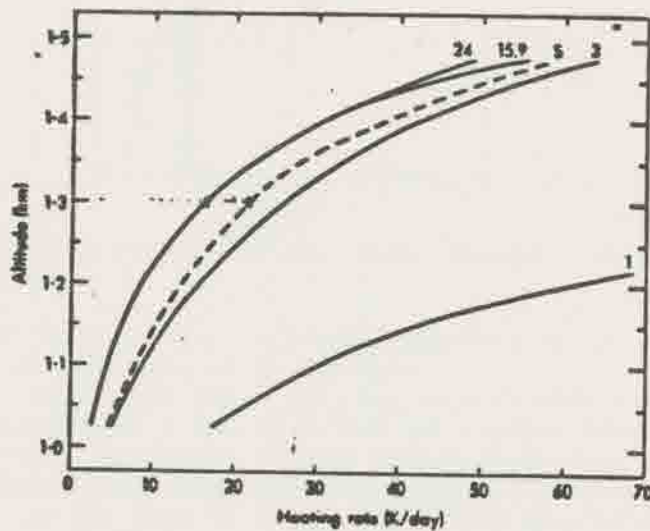


Figure 7. Comparison of the heating rate profiles in a cloud layer for all 5 versions of the scheme with the work of Stephens (1978a).

1, 3, 9, 15, 24: NUMBER OF SPECTRAL BANDS WITHIN  
0.25 - 4.0  $\mu\text{m}$ , FOR TWO-STREAM  
MODEL

S: MATRIX OPERATOR / DOUBLING + ADDING, 15 BANDS

DIFFERENCES: MULTIPLE SCATTERING  
GASEOUS ABSORPTION

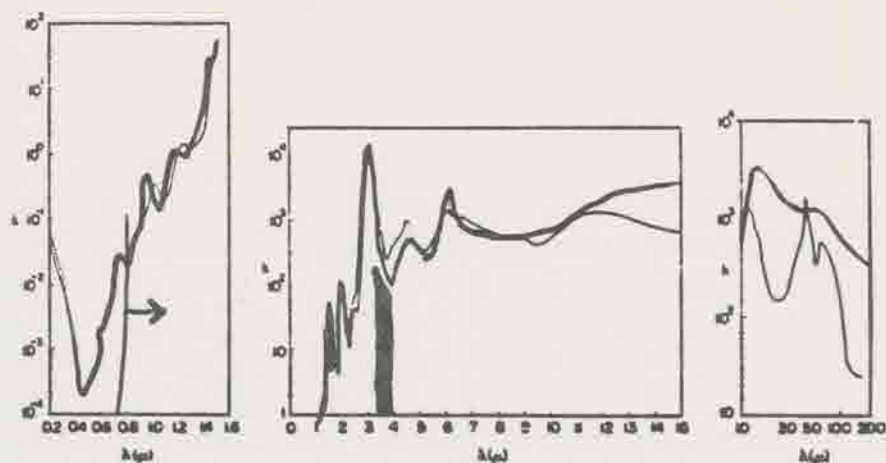


FIG. 1a,b,c. Absorption coefficient  $k = 4\pi n_2/\lambda$  in  $(\text{cm})^{-1}$  versus wavelength in microns for water (dashed curve) and ice (full curve).

$1.0 \leq \lambda \leq 2.45 \mu$  and  $3.3 \leq \lambda \leq 11 \mu$ : Centeno (1941). Agrees with McAlister to about 1.5% except near the  $3\text{-}\mu$  and the  $6\text{-}\mu$  bands, where the steep slope of the curve makes values at a given wavelength difficult to determine. The minimum value given by McAlister in the  $3\text{-}\mu$  band is about 4% less than that given by Centeno; the difference is less in the  $6\text{-}\mu$  band. Kislovskii's values are generally within

5% (often much closer) of those of Centeno in this region.

$2.5 \leq \lambda \leq 3.2 \mu$ : McAlister (1964). When these data are combined with the values of  $k$  for water in the  $3\text{-}\mu$  band, the resulting curve of  $n_r$  vs.  $\lambda$  is smoother than when Centeno's reflectivity data are used.

$11.5 \leq \lambda \leq 17.5 \mu$ : Kislovskii (1959). In this region the absorption coefficient is such that it is very difficult to determine  $n_r$  accurately from the reflection measurements. Our computed data showed considerable scatter. The values given by Kislovskii provide a smooth curve, which is an approximate mean of the values that would be obtained by using our selection of  $k$  (previous section) and the reflectivity measurements of Centeno or McAlister.

$18 \leq \lambda \leq 50 \mu$ : In this region we have only the pre-1920 data summarized by Dorsey (1940) and the mathematical model of Kislovskii (1959), which utilizes the data of Dorsey and the absorption values from Plyler and Acquista (1954). We have drawn a smooth curve through the values computed from Dorsey's data, interpolating on the basis of the shape of the curve given by Kislovskii. Two of the points given by Dorsey were rejected (at  $21$  and  $23 \mu$ ) since they differed significantly from such a curve. Our resulting values are slightly higher than those given by Kislovskii, as is to be expected on the basis of the lower

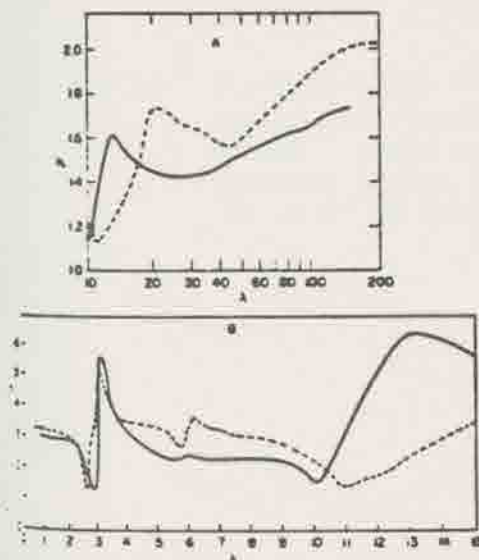


FIG. 2a,b. Index of refraction  $n_r$  versus wavelength in microns for water (dashed curve) and ice (full curve).

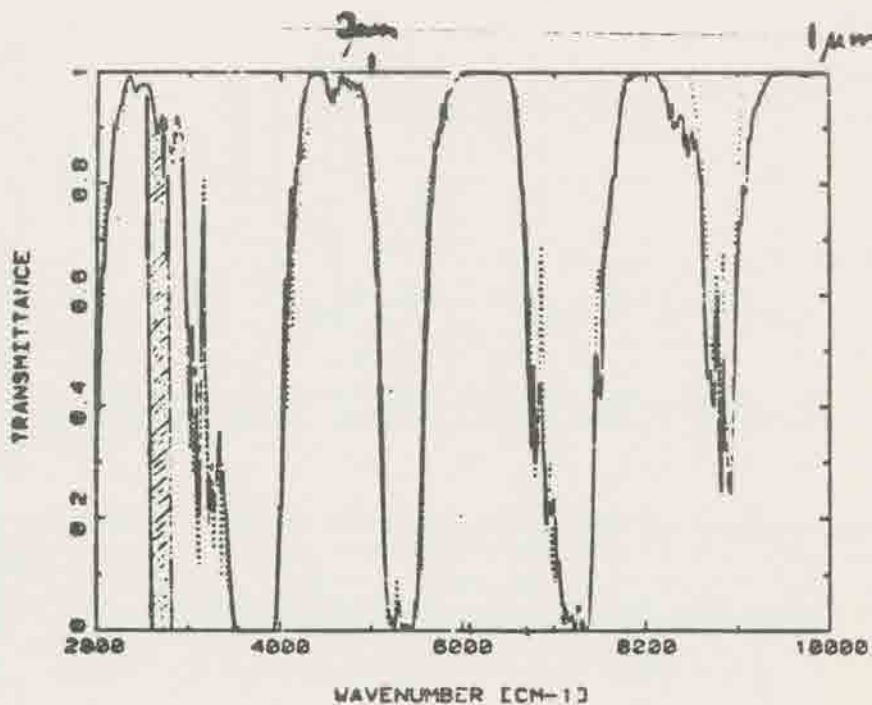


Figure 11: Spectral water vapor transmission at  $20 \text{ cm}^{-1}$  resolution through a 1 cm path of water vapor (sea level). Shown by hatching is the 3.55-3.93 micron channel, giving high transmittance through vapor for the image in Figure 7 (from Davies, et al., 1984).

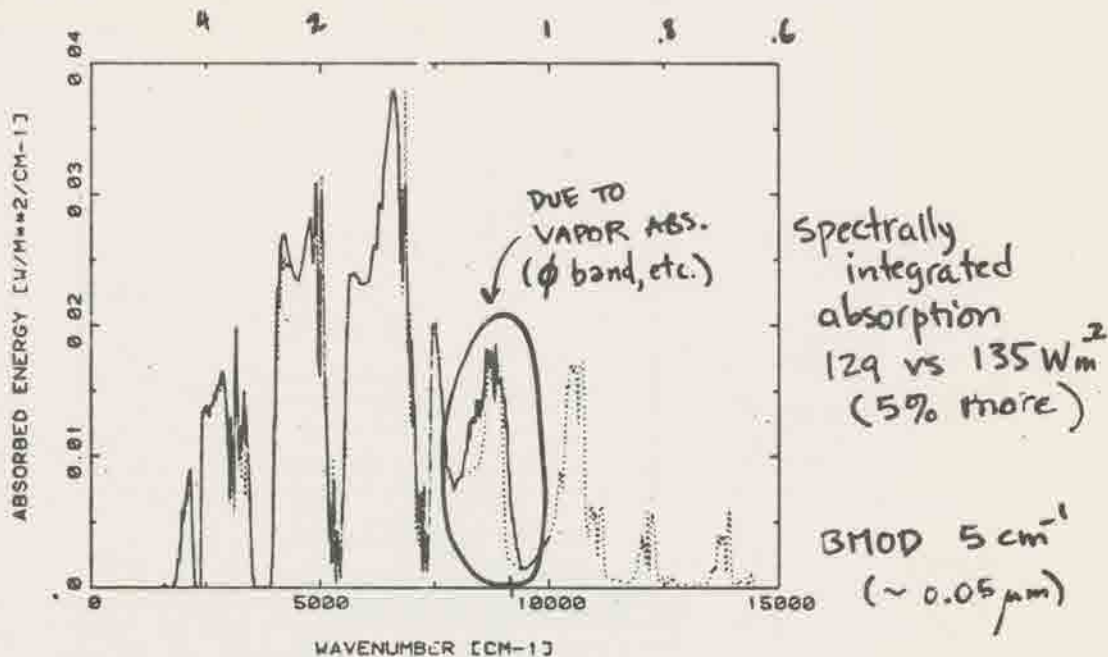


FIG. 3. Spectral absorption at  $20 \text{ cm}^{-1}$  resolution, typical of a 1 km thick cloud with cloud top altitude of 2 km in a standard atmosphere with overhead sun, using BMOD (solid) and LOWTRAN 5 (dotted).

lar intensity. Vapor absorption within the cloud, depicted by the solid curve of Fig. 4, is seen to be negligible at low wavenumbers, due to strong vapor absorption above the cloud. At larger wavenumbers,

however, where the vapor bands are weaker, allowing more radiation to reach the cloud top, and where the droplet absorption is also reduced, the vapor absorption within the cloud may be significant and becomes

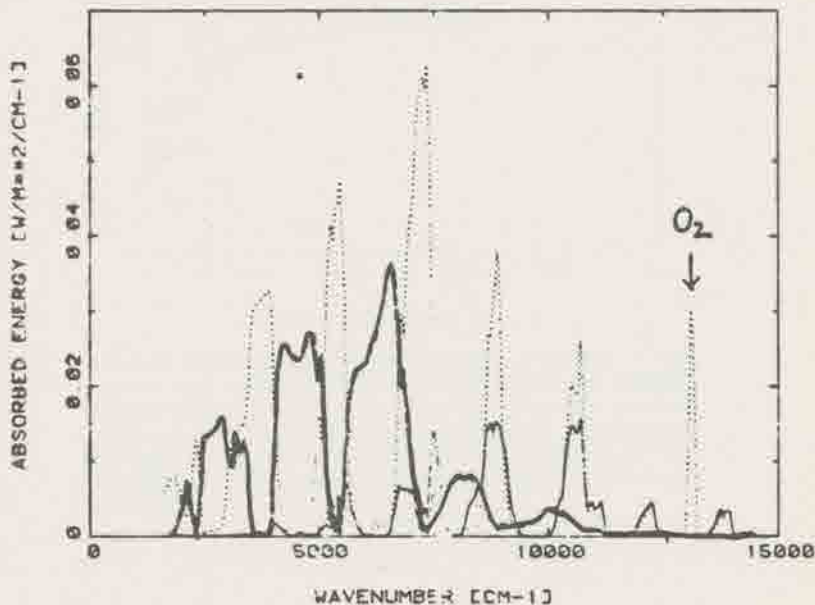
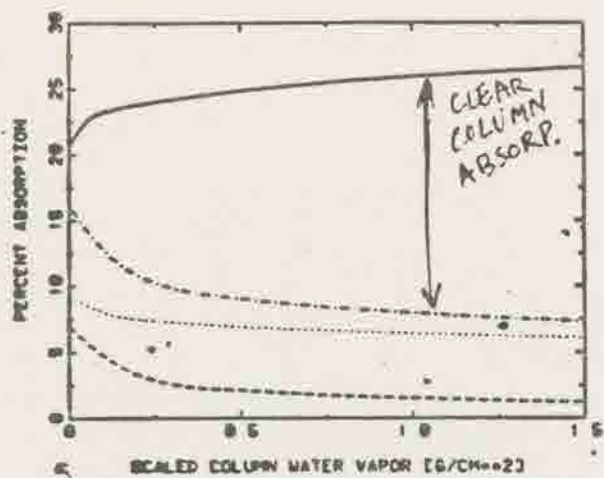
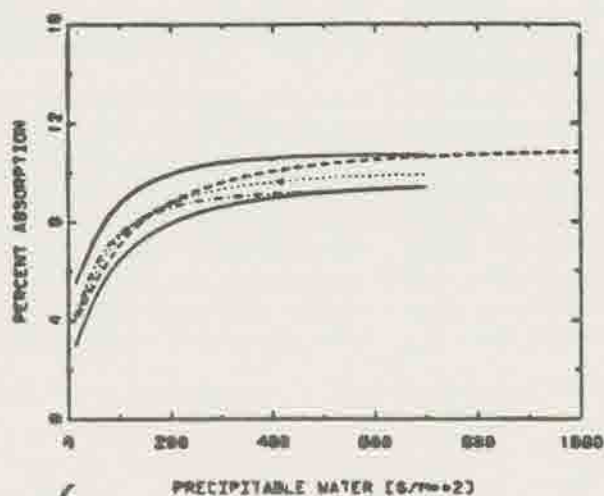


FIG. 4. Spectral absorption at  $50 \text{ cm}^{-1}$  resolution, by cloud water vapor (solid), cloud droplets (dashed) and column vapor (dotted), typical of a 1 km thick stratus cloud with cloud top altitude of 2 km in a standard atmosphere with overhead sun.



BUT OCCURS ONLY  
IN VAPOR ABSORP.  
REGIONS; MUCH  
STRONGER THERE

5  
FIG. 5. Integrated absorption, as a percentage of the extraterrestrial insolation, versus scaled water vapor amount above the top of a typical 1 km thick stratus with cloud top altitude of 2 km and overhead sun: Cloud plus above-cloud absorption (solid); total cloud absorption (dot-dash); cloud droplet absorption (dots); cloud vapor absorption (dashed).



IN-CLOUD VAPOR  
CAN BE MORE  
SIGNIFICANT THAN  
CLOUD TYPE

6  
FIG. 6. Integrated cloud absorption, as a percentage of the extraterrestrial insolation, versus liquid water content, for overhead sun and different cloud types between 1 and 2 km in a standard atmosphere. Stratus (dotted); nimbostratus (dashed); stratocumulus (dot-dash); stratus with twice the standard water vapor within the cloud (upper solid); stratus with half the standard water vapor (lower solid).

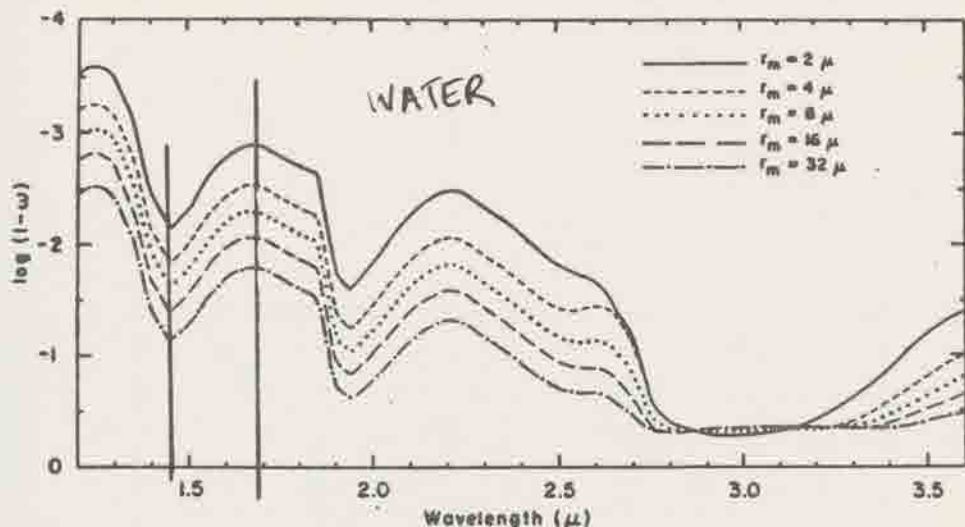


FIG. 4. Single-scattering albedo for a cloud of spherical water particles for five different particle size distributions.

a. General single-scattering results

Fig. 1 shows the dependence of the normalized phase function  $p(\theta)$  (Deirmendjian, 1964, 1969) upon the particle size parameter  $x_m$  in the case of no absorption ( $k_s=0$ ) with the real refractive index equal to 1.33, the value for liquid water in the visible. The variable  $\theta$  is the angle of scatter.

The individual curves have been vertically displaced from one another. The short horizontal line intersecting a given phase curve denotes the position at which the phase function has a value of unity. For the largest values of  $x_m$ , the very precipitous decline in the value of  $p$  near  $0^\circ$  corresponds to the diffraction peak (Deirmendjian, 1964; Dave, 1969c); the strong maximum at a scattering angle of  $142^\circ$  is the main rainbow (caused by rays undergoing a single internal reflection)

with its first supernumery bow (van de Hulst, 1957, p. 241) located at  $147^\circ$ ; the second rainbow (two internal reflections) is located at  $123^\circ$  while its first supernumery bow lies at  $114^\circ$ ; and finally, the glory corresponds to the overall increase and oscillatory behavior near  $180^\circ$ . As  $x_m$  decreases, all these features become less pronounced and broader; in addition, the rainbow shifts in location toward larger scattering angles and the slope of the phase function decreases until near  $x_m=1/2$  it is very similar to the Rayleigh phase function.

The effect of introducing absorption within the particles is investigated in Fig. 2. For  $x_m=32$ , the glory and rainbow have been effectively suppressed when  $w_s \geq 0.03$ . This effect can be understood using concepts from geometrical optics. A ray traversing a path equal to the particle radius will be diminished in strength by  $\exp(-kr) = \exp(-2x_m k_s)$ , where  $k$  is the linear absorp-

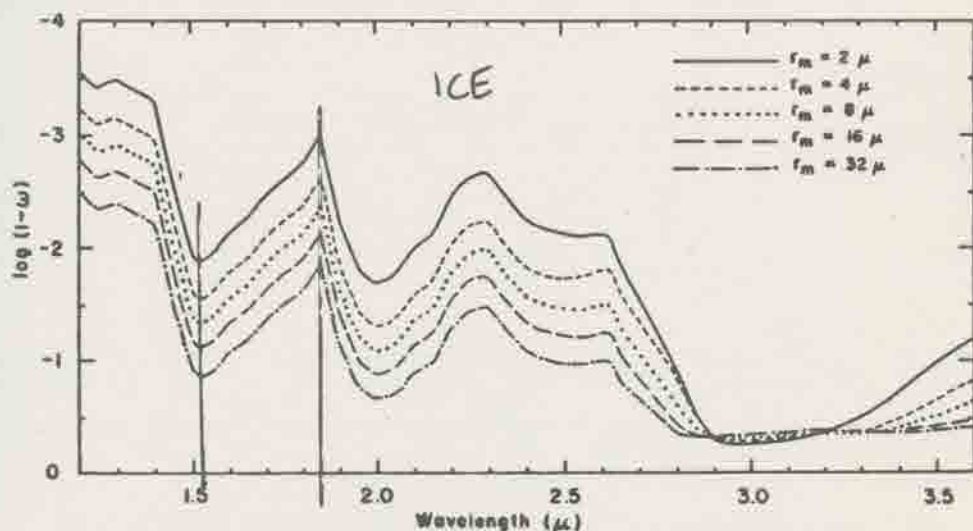


FIG. 5. Same as Fig. 4 except for spherical ice particles.

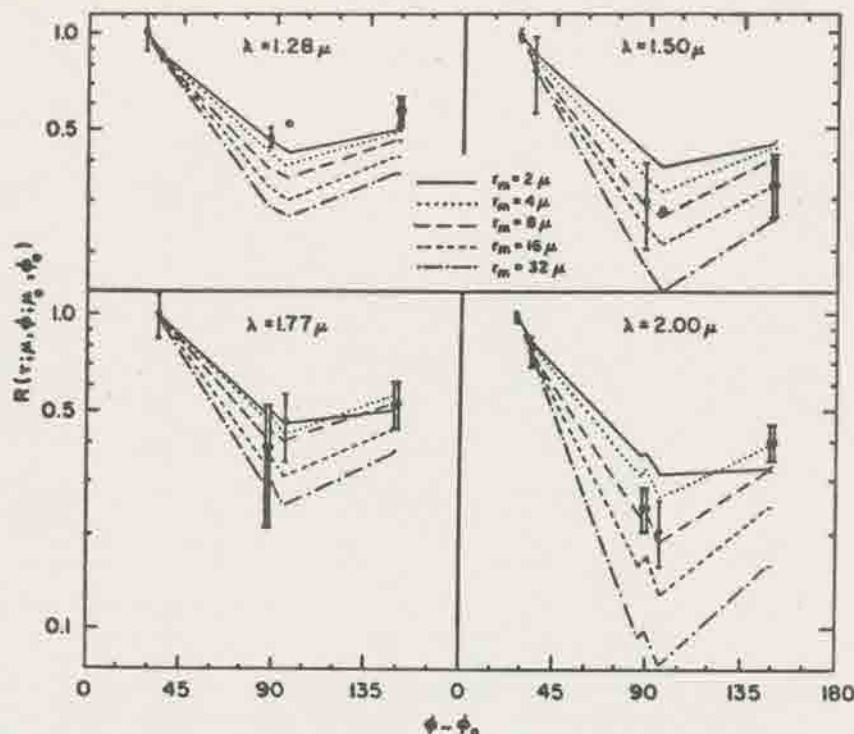


FIG. 14. Theoretical and observed cloud reflectivities for  $\theta = 80^\circ$  and  $56 \leq \theta_0 \leq 64$  normalized to unity at the smallest observed value of  $\phi - \phi_0$ . The theoretical calculations are for water particles at values of  $\theta$ ,  $\theta_0$  and  $\phi - \phi_0$ , correct for each observed point and connected by straight lines. The computations were made for  $\tau = 32$ , but are approximately valid for  $\tau \geq 10$ . The observations by Blau *et al.* were made on cumulus clouds at 4000 ft above hurricane Gladys.

and  $64^\circ$ . The theoretical computations were performed for spherical water particles at the angles appropriate for each observation, and the theoretical points were joined together by straight lines. As mentioned above, no correction for gas absorption was made.

All the theoretical spectra are normalized to fit the data point at the lowest value of  $(\phi - \phi_0)$ . A particle size of  $8 \mu$  appears to yield the best fit to the measurements, a result compatible with typical direct sampling measurements of cumulus clouds. Unfortunately, the ab-

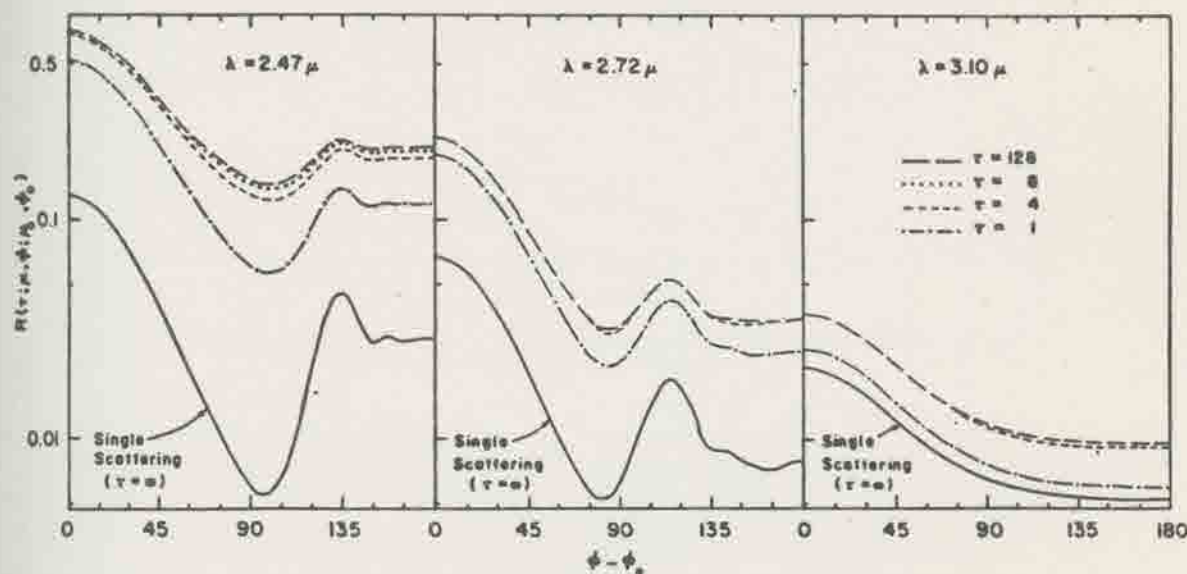


FIG. 15. Theoretical cloud reflectivities as a function of azimuth angle for  $\theta = 80^\circ$  and  $\theta_0 = 50^\circ$  for a size distribution of spherical ice particles having  $r_m = 16 \mu$ .

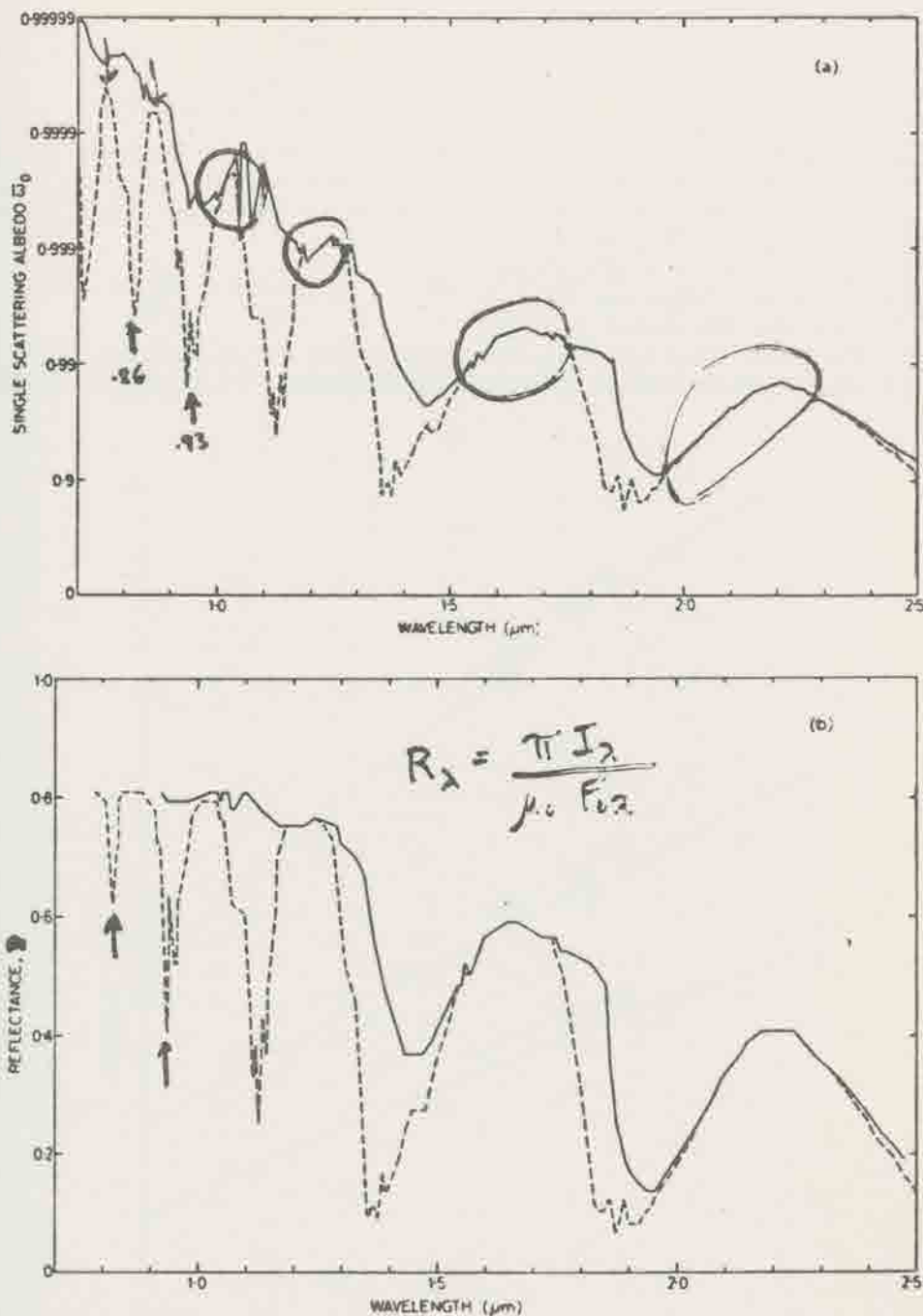


FIG. 1. (a) Single-scattering albedo  $\omega_0$  vs  $\lambda$  and (b) reflectance  $R$  vs  $\lambda$  for  $\tau = 64$  drops alone (solid line) and drops plus vapor (dotted line).

this dependence is that with increasing drop size, absorption in the liquid increases relative to scattering, as shown by the size dependence of  $\omega_0$ .

*Influence of optical thickness*

Fig. 3 shows for a fixed drop radius (6  $\mu\text{m}$ ) the variation with optical thickness of reflectance at 1.65

and 2.2  $\mu\text{m}$ . As optical depth  $\tau$  is increased the spectral reflectance increases at a monotonic but steadily decreasing rate. With decreasing  $\omega_0$  (increasing absorption) a given increase in  $\tau$  produces a smaller increase in reflectance. This is simply because an increase in reflectance when  $\tau$  is increased by  $\Delta\tau$  is produced by photons which have traveled

obtained implies

$$Q_{\text{obs}} = 4sakm^2[1 - (1 - m^2)^{2.7}] \quad (5)$$

or

$$Q_{\text{obs}} = 1.7ak \quad \text{if } m = 1.33.$$

In the geometric optics limit, the extinction efficiency  $Q_{\text{ext}}$  takes the value 2, and hence the single-scattering albedo for a weakly absorbing water droplet is given by

$$1 - \bar{\omega}_0 = \frac{Q_{\text{obs}}}{Q_{\text{ext}}} = 0.85ak, \quad (6)$$

which is the last approximation that we introduce to obtain a simple relationship for absorption in deep

clouds. By inserting (6) into (3) we obtain the final result.

$$\alpha = H(\mu_0) \left[ \frac{0.85ak}{1 - g(1 - 0.85ak)} \right]^{1.7}. \quad (7)$$

a formula which contains only bulk absorption coefficient  $k$ , drop radius  $a$ , incident direction  $\mu_0$  (note that  $H(\mu_0)$  depends weakly on  $\bar{\omega}_0$  even though the dependence is not written explicitly) and the asymmetry factor  $g$ . For terrestrial water clouds at solar wavelengths,  $g$  is only weakly dependent on size and will remain within the approximate range 0.8-0.85 (see Hansen and Travis, 1974); furthermore, over the spectral region 1-2  $\mu\text{m}$ , where most absorption of solar energy takes place,  $1 - \bar{\omega}_0$  is

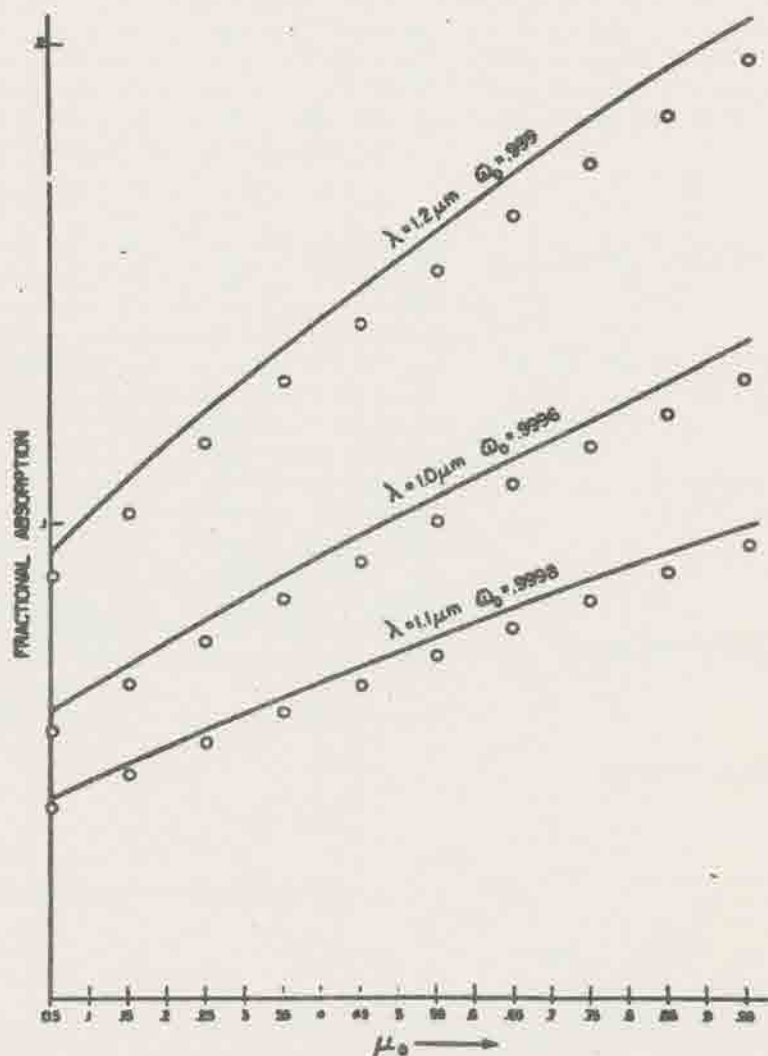


FIG. 4. The solid curves represent fractional absorption at specified wavelengths versus  $\mu_0$  (cosine of solar zenith angle) according to Eq. (8); the circles represent fractional absorption from detailed Mie doubling calculations; mean drop radius 10  $\mu\text{m}$ .

in conventional radiative transfer treatments, and may pose an additional problem.

In the following sections, we will discuss primarily (but not exclusively) data for this Dec. 19 cloud layer. There was, however, nothing special about that cloud; other sets of data for cloud measurements on other days show all the essential features which we will discuss in the context of this particular cloud, which was a stratocumulus cloud layer over northwestern Tasmania, with base 4,300 ft (1,310 m) and top 5,400 ft (1,645 m). We will also often restrict our discussion to the four wavelengths of Figure 3, but data from the circular variable-filter device (notably 1.66  $\mu\text{m}$  wavelength) were also used. Inclusion of further wavelengths did not modify the result or the conclusions; it is only for the sake of simplicity that we have restricted our discussion to those four or five wavelengths.

#### a. Direct comparison of computed and measured spectral reflectance

Since the microphysical measurements in this cloud indicated an optical thickness  $\tau$  of 18 and a mean radius  $\bar{r}$  of 8  $\mu\text{m}$ , these numbers were used to obtain reflectance at the four reference wavelengths (0.75, 1.0, 1.2, and 2.25  $\mu\text{m}$ ), and the values thus obtained are plotted (horizontal lines) on Figure 4, superimposed on the (time-varying) values for the corresponding measured reflectances. Neither the absolute nor the relative magnitudes of the reflectances agreed very well: the computed reflectances at the three shorter wavelengths fall distinctly below the measured values, while the reduction or spread in the reflectances (from the shortest to the longest wavelength) was seriously underestimated by the computations.

It is also possible to ignore the microphysical

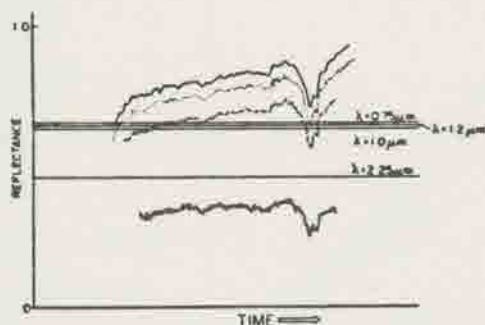


Fig. 4. Portion of the data of Fig. 3, superimposed with theoretical values for  $\tau$ ,  $\bar{r}$  given by the measured cloud microphysics (horizontal lines).

measurements and, by a numerical search technique, to determine those values for  $\tau$  and  $\bar{r}$  which agree best (in a least-squares sense) with the spectral measurements. In this case (and in most of our data), the search procedure tended to find two regions of optimum agreement, each with similar values for  $\tau$ , but with widely different values for  $\bar{r}$ , one very large (12-20  $\mu\text{m}$ ) and one very small ( $\sim 0.5 \mu\text{m}$ ). We believe that this may reflect the behavior shown in Figure 2, where it is seen that a single value of  $\omega_0$  can usually be produced by two values of radius, giving a kind of ambiguity (not total ambiguity because two values of  $\bar{r}$  giving the same  $\omega_0$  at one wavelength do not give the same  $\omega_0$  at all wavelengths). We have used both pairs of values from the search procedure in Figure 5, these being denoted (a) and (b).

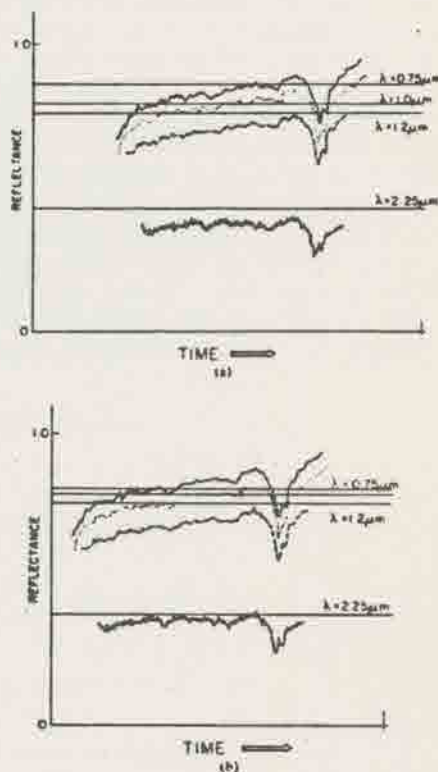


Fig. 5. Similar to Fig. 4, but the theoretical values were obtained for values of  $\tau$ ,  $\bar{r}$  which a search algorithm selected for optimum agreement between measured and calculated data (i.e., values which a remote-sensing procedure might provide). The search algorithm gave to almost equally preferable values: one ( $\tau=32$ ,  $\bar{r}=0.5 \mu\text{m}$ ) was used in (a); the other ( $\tau=32$ ,  $\bar{r}=12 \mu\text{m}$ ) in (b).

330 pm thick

F. H. C. x 1.1

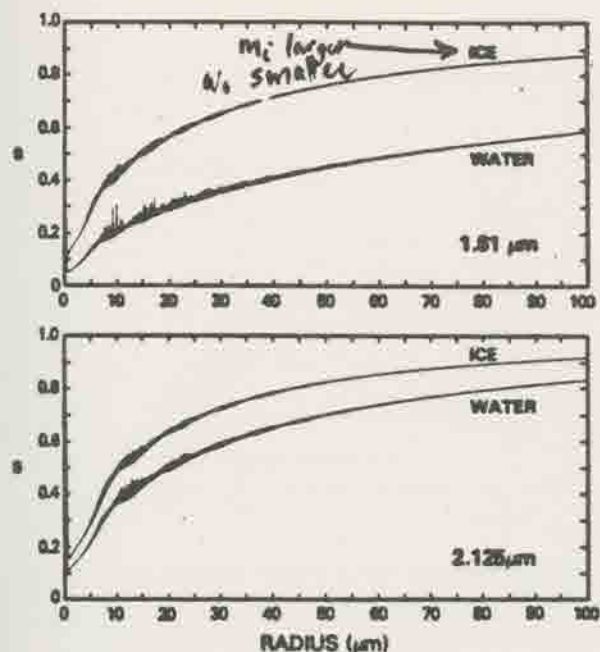


FIG. 4. Similarity parameter for ice and water as a function of particle size.

The second radiation parameter is the scaled optical thickness  $\tau^*$  which is related to the cloud optical thickness  $\tau$  by

$$\tau^* = (1 - g)\tau. \quad (4)$$

The spherical albedo of a semi-infinite cloud layer was found by van de Hulst (1974) to be described

by  $s$ . In that numerical study, arbitrary combinations of  $g$  and  $\omega_0$  which formed the same values of  $s$  were found to give the same spherical albedo. For the observational problem, numerical calculations were performed to determine if the reflection function was invariant in  $s$  and  $\tau^*$ . Fig. 5 shows the calculated reflection function of a cloud as a function of  $\tau^*$  for several different values of  $s$ . The values given in Fig. 5 are for  $\mu = 1$  and  $\mu_0 = 0.474$  to agree with the geometry of the Skylab observations. The reflection function was calculated using the doubling algorithm described by Hansen (1971a). The calculations used the Henyey-Greenstein phase function for a number of values of  $\omega_0$ ,  $g$  and  $\tau$  to span the range of  $s$  and  $\tau^*$  shown. The variance in the points defining the curves of Fig. 5 was appreciable for values of  $\tau^* \leq 1.0$ . For larger values of  $\tau^*$ , the similarity parameter was found to be a suitable parameter in predicting the reflection function.

An interesting point noted in forming Fig. 5 was that the figure could also have been based on phase functions derived from Mie calculations for particle size distributions. By following such a procedure it would be more difficult to span the range of  $s$  in a uniform manner because of the difficulty in choosing reasonable values of the refractive index and size. However, doubling calculations were made using the phase function generated by Mie calculations for two particle size distributions and the four sets of refractive indices given in Table 1. These were compared with similar calculations based on Henyey-Greenstein phase functions with the same  $\omega_0$ ,  $g$ , and  $\tau^*$ . For no absorption ( $\omega_0 = 1.0$ ) the intensities cal-

$$s = \left( \frac{1 - \omega_0}{1 - g\omega_0} \right)^{1/2},$$

a function of particle size at any given wavelength

$s \rightarrow 0$  for strong scattering

$s \rightarrow 1$  for strong absorption

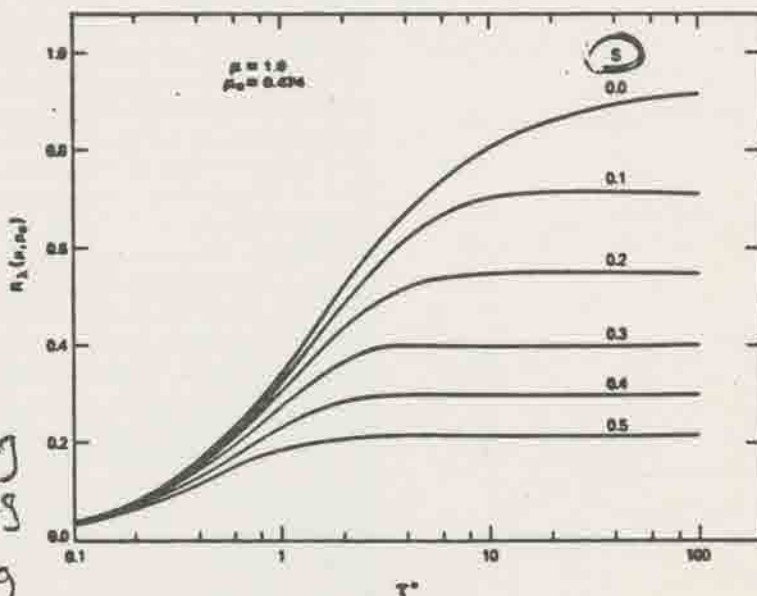


FIG. 5. Cloud reflection function as a function of scaled optical thickness. Six different values of the similarity parameter are shown.

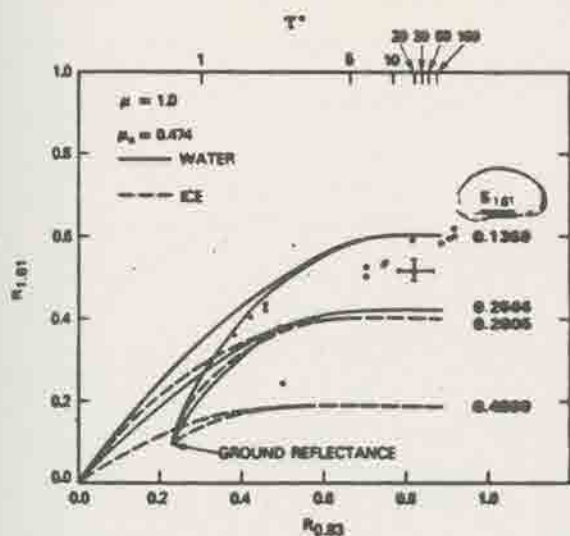


FIG. 10. Cloud reflection function at  $0.83 \mu\text{m}$  versus  $1.61 \mu\text{m}$ . The data points from Table 2 are shown as black dots whose radii are approximately equal to the root mean square of the variance for the picture elements sampled. The absolute error is drawn on one sample point and is representative of each of the sample points.

absorption and re-emission influencing the  $11.4 \mu\text{m}$  observations.

The remaining observations listed in Table 2 are for clouds. In the case of clouds the sounding temperatures were found by using the stereographically determined heights together with the 0500 MST sounding shown in Fig. 8. For  $0.83 \mu\text{m}$  reflection functions  $> 0.6$  the cloud optical thickness is sufficiently large to assume that the  $11.4 \mu\text{m}$  emissivity of the cloud was unity. For all cloud cases with a reflection function at  $0.83 \mu\text{m} > 0.6$ , the sample standard deviation between the  $11.4 \mu\text{m}$  blackbody temperature and the sounding temperature was  $3.2^\circ\text{C}$ . The stated accuracy for the cloud-top altitude determination is  $\sim 0.5 \text{ km}$ . Thus, the sample standard deviation in temperature is less than the error limit of the altitude determination. The difficulty in finding cloud features on which to apply stereography was a source of error in this temperature comparison. The large temperature differences between  $11.4 \mu\text{m}$  observations and the soundings for areas G and H are difficult to explain without additional information. Detailed radiative transfer calculations were performed for  $11.4 \mu\text{m}$ , in which water dimer absorption was included. These calculations indicated the  $11.4 \mu\text{m}$  intensity and consequently the equivalent brightness temperatures are sensitive to the single scattering albedo and the asymmetry factor at this wavelength. Due to these two parameters a one to two degree uncertainty in the equivalent brightness temperature is expected. It is felt that a combination of the above effects causes the discrepancies between the equivalent  $11.4 \mu\text{m}$  blackbody temper-

atures and the sounding temperatures noted in Table 2. As a result of this comparison, it appears that with the exception of locations G and H the  $11.4 \mu\text{m}$  observations are representative of the temperature of the cloud top when  $R_{0.83}$  is  $> 0.6$ . For  $R_{0.83} < 0.6$ , the cloud optical thickness is small enough that transmission of the  $11.4 \mu\text{m}$  radiation from the ground becomes appreciable. In this latter case, the blackbody temperature at  $11.4 \mu\text{m}$  is somewhat greater than the sounding temperature as seen in Table 2.

To resolve the disagreement in the  $11.4 \mu\text{m}$  brightness temperatures and the sounding temperatures, the S-190A photographs were visually inspected using adjacent frames in a stereographic viewer to determine the structure of the cloud which included locations G and H. This cloud feature was found to have a more complex geometric structure than was evident in the altitude contour analysis. The contour analysis shows two layers,  $\sim 1 \text{ km}$  apart. Visual inspection shows at least part of this upper layer to be optically thin for that part over land. Locations G and H were chosen where the two layers overlap. In this overlap region it is not possible to establish the optical thickness of the upper layer. If the upper layer is optically thin then the emission from the lower cloud transmitted through the upper cloud may explain the temperature disparity for these locations.

Fig. 10 illustrates the 16 cloud pairs of observations of  $R_{0.83}$  and  $R_{1.61}$  presented in Table 2, while Fig. 11 shows corresponding results for  $R_{0.83}$  and  $R_{2.125}$ . The curves shown in Figs. 10 and 11 are theoretical calculations relating the reflection functions to one another for the noted values of  $s$ . In both Figs. 10 and 11 curves are shown for zero ground albedo and for the wavelength-dependent ground albedos

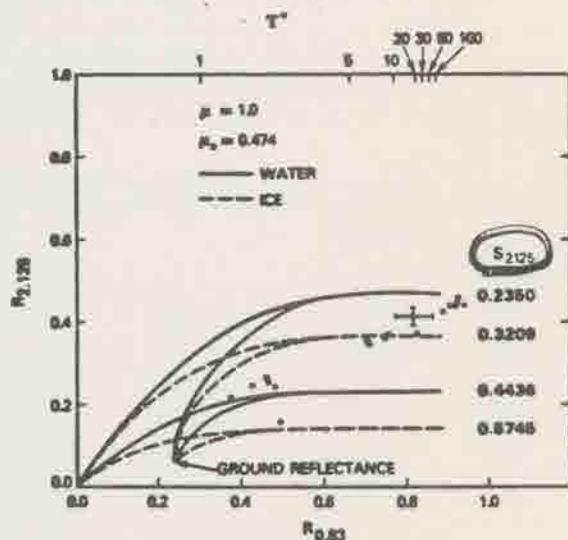


FIG. 11. As in Fig. 10 except for the reflection function of  $0.83 \mu\text{m}$  versus  $2.125 \mu\text{m}$ .

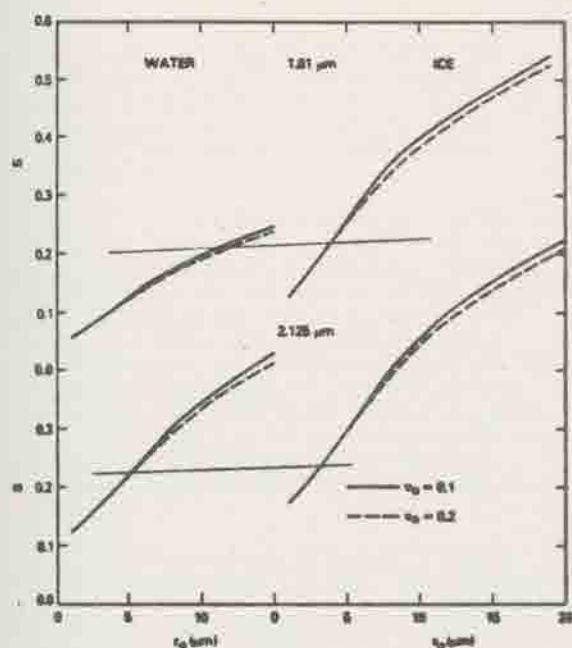


FIG. 12. Similarity parameter for distributions of ice and water particles as a function of effective radius  $r_e$ , effective variance  $v_e$ , and wavelength.

found at location Q. The theoretical curves were generated from doubling calculations for two particle size distributions. The distribution function for the particles was the modified gamma distribution in the form discussed by Hansen (1971b). The parameters used in the distribution are the effective radius  $r_e$  and a dimensionless effective variance  $v_e$ . These quantities are radius-squared weighted means and variances of the size distribution. The parameters ( $r_e$ ,  $v_e$ ) for the distributions used in Figs. 10 and 11 are (5.56  $\mu\text{m}$ , 0.111) for the upper curve in each phase and (16.2  $\mu\text{m}$ , 0.128) for the lower curves. The mode radii for each case were 3.7 and 10.0  $\mu\text{m}$ , respectively. The corresponding values of the similarity

parameter are noted on the right in Figs. 10 and 11. Because the similarity parameter is assumed to be unity at 0.83  $\mu\text{m}$ , the reflection function in this channel is directly related to the effective optical thickness as indicated by the upper scale in Figs. 10 and 11. The values for the similarity parameter noted on the right-hand sides of Figs. 10 and 11 indicate that for a given  $\tau^*$ , the reflection function at 1.61 and 2.125  $\mu\text{m}$  can assume a number of different values depending upon  $s$ . Thus, any measured value shown in either Fig. 10 or Fig. 11 could be used to empirically determine the parameter pair  $s$  and  $\tau^*$ . Further, as was shown in Fig. 4 the similarity parameter has a one-to-one correspondence with particle size for each phase.

Using the modified gamma distribution of particle sizes, the relationship between the similarity parameter and the effective radius was calculated and is displayed in Fig. 12. The measurements which are used to infer  $s$  can then be used to determine the particle size for each phase. In terms of the cloud microphysics, a possibly more significant parameter set for the particle size distribution is the mode radius  $r_0$  and the dispersion  $\delta$ . In terms of the distribution parameters these are given by:

$$r_0 = r_e(1 - 3v_e),$$

$$\delta = \left( \frac{v_e}{1 - 2v_e} \right)^{1/2}.$$

The procedure outlined above was applied to the data listed in Table 2. Because the ground reflectance in the scene was variable and because the cloud shadows were appreciably separated from the clouds due to their finite size and large solar zenith angle, only  $R_{0.83} \geq 0.7$  were considered. Thus, samples were for clouds of scaled optical thicknesses  $\sim 5$  or larger. The results of applying the reflection function analyses discussed are given in terms of the experimentally derived scaled optical thickness, similarity parameters and effective particle sizes as shown in Table 3. The first four regions of Table 3 are for

TABLE 3. Scaled optical thickness, similarity parameters and effective radii ( $\mu\text{m}$ ) for ice and water.

Location	$\tau^*$	1.61 $\mu\text{m}$			2.125 $\mu\text{m}$		
		$s \times 10^2$	$r_e$ (water)	$r_e$ (ice)	$s \times 10^2$	$r_e$ (water)	$r_e$ (ice)
A*	>30	135 $\pm$ 18	5.7 $\pm$ 1.1	1.4 $\pm$ 0.6	262 $\pm$ 15	6.6 $\pm$ 0.6	3.8 $\pm$ 0.5
B*	>30	137 $\pm$ 18	5.8 $\pm$ 1.1	1.4 $\pm$ 0.6	262 $\pm$ 15	6.6 $\pm$ 0.6	3.8 $\pm$ 0.5
C*	>30	151 $\pm$ 18	6.4 $\pm$ 1.1	1.8 $\pm$ 0.6	263 $\pm$ 15	6.6 $\pm$ 0.6	3.8 $\pm$ 0.5
D	>30	144 $\pm$ 18	6.1 $\pm$ 1.1	1.6 $\pm$ 0.6	248 $\pm$ 16	6.1 $\pm$ 0.6	3.4 $\pm$ 0.5
E	12.2	194 $\pm$ 17	9.6 $\pm$ 1.0	3.4 $\pm$ 0.5	305 $\pm$ 14	8.1 $\pm$ 0.6	5.2 $\pm$ 0.4
F	11.1	146 $\pm$ 18	6.1 $\pm$ 1.1	1.7 $\pm$ 0.6	269 $\pm$ 15	6.8 $\pm$ 0.6	4.2 $\pm$ 0.5
G	6.7	181 $\pm$ 17	8.5 $\pm$ 1.0	2.8 $\pm$ 0.5	308 $\pm$ 14	8.3 $\pm$ 0.6	5.3 $\pm$ 0.4
H	6.4	186 $\pm$ 17	9.3 $\pm$ 1.0	3.0 $\pm$ 0.5	316 $\pm$ 13	8.5 $\pm$ 0.6	5.6 $\pm$ 0.4
I	5.1	205 $\pm$ 17	10.6 $\pm$ 1.0	3.5 $\pm$ 0.5	327 $\pm$ 13	9.1 $\pm$ 0.6	5.8 $\pm$ 0.4
J	5.0	192 $\pm$ 17	9.5 $\pm$ 1.0	3.2 $\pm$ 0.5	322 $\pm$ 13	8.8 $\pm$ 0.6	5.7 $\pm$ 0.4

\*  $R_{0.83}$  greater than reflection function of semi-infinite cloud. Sloping cloud surface assumed and slope factor applied to 1.61 and 2.125  $\mu\text{m}$  reflection functions.

Kyle et al, 1984

The overall dimensions of the CPR box is approximately 77 x 25 cm and the weight 35 Kg. The scanner requires 25 watts of 115 v 60 hz power and about 1000 watts of 28 v DC power for heaters.

In normal operation data from all channels is recorded simultaneously. The data is recorded on a tape recorder in analog form and simultaneously run through 10 bit digital A/D converters and recorded in digital form. Timing, scan count and other information is merged with the scanner signal as it is recorded.

The initial CPR flights in the summer of 1976 suffered from at least the normal number of misfortunes. The  $1\mu\text{m}$  channel detector failed after the first few days. Channels 2 and 3 each drifted about 10A to the blue and the filter on the  $14\mu\text{m}$  water vapor channel seems to have been defective. A University of Missouri (Rolla) laser radar (lidar) system, supported by Goddard funding, was also on these flights. It was hoped to intercompare the CPR and lidar cloud data, however the lidar suffered even more misfortunes (technical and other) than the CPR. Thus to date it has not been possible to compare the two data sets. Despite these and other difficulties much interesting radiometer data was obtained and analysis is proceeding.

There were two major differences between the 1976 CPR and the present version. First the  $2.165\mu\text{m}$  channel was not on the earlier version. Secondly uncoated silicon detectors were used for channels 1, 2 and 3. These had a signal to noise ratio of between 200 and 300.

The ice-cloud, water cloud, snow discriminator detector worked quite well in general. As indicated in Table 2 the algorithm ratios the reflectance of the  $1.64\mu\text{m}$  channel to that of the clear  $0.754\mu\text{m}$  channel and compares the results with theoretical calculations. At  $1.64\mu\text{m}$  ice absorbs an appreciable amount of the incident radiation but water does not. At  $0.754\mu\text{m}$  neither pure ice nor water absorb radiation. For a given reflectance in the  $0.754\mu\text{m}$  channel ice clouds will appear brighter than water clouds at  $1.64\mu\text{m}$  while snow will be very dark. Figures 2a and b and 3a and b are two examples of the theme.

Figure 2 shows water clouds over Crater Lake, Oregon on July 1, 1976. The left hand picture shows the scene viewed by the clear channel at  $0.754\mu\text{m}$ . On the right is the same scene with the pixels identified as water clouds (light gray), ice clouds (dark gray), snow (white) or clear surface (black). Very thin clouds or haze are identified as surface thus the clouds appear more lacy in the phase picture than they

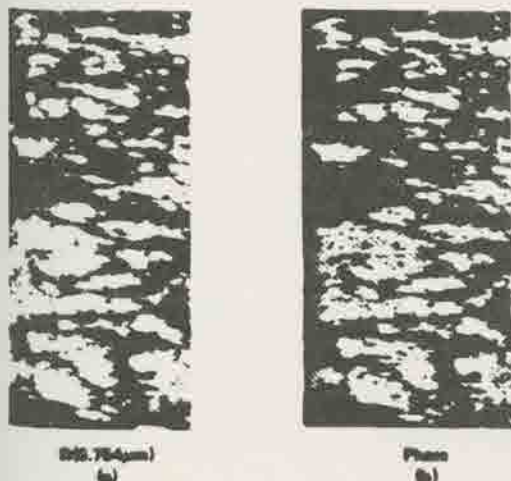


Figure 2. Water Clouds over Oregon

actually are. Figure 3 shows a mixed scene over Boulder, Colorado on July 6, 1976. Here building cumulus clouds are shown to be ice capped in the phase picture on the right. The small white patches at top of the phase picture indicate snow fields in the mountains. Colors are arbitrary in the phase picture hence we have made snow white as that is the color normally associated with it. Other things besides ice and snow can appear bright at  $0.754\mu\text{m}$  and dark at  $1.64\mu\text{m}$  thus aliasing can occur. Examples of this are seen in the bottom left hand corner of the phase picture where a number of bright areas inside Boulder are falsely identified as snow. Cross referencing to the black body temperatures measured by the  $11\mu\text{m}$  channel will permit the elimination of most of these cases.

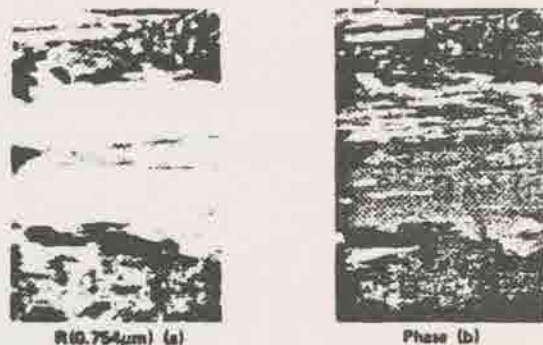


Figure 3. Ice Capped Cumulus over Boulder

Cloud top altitudes are obtained by comparing the reflectance ratios  $R(0.761)/R(0.754)$  and  $R(0.763)/R(0.754)$  with theory and with empirical data. They can also be estimated from black body temperatures calculated from the  $11\mu\text{m}$  channel. Figure 4 shows the clear atmosphere transmission in the oxygen A-band calculated for a Gaussian filter whose full width at half maximum transmission is  $20\text{ cm}^{-1}$ . The sun is at the zenith and the observer is looking to the nadir giving a total air mass of two for the sea level case and one for the 500 mb case. Cloud altitudes are obtained by comparing the measured reflectances with calculated values under the assumption that the radiation follows straight line paths from sun to cloud to observer.

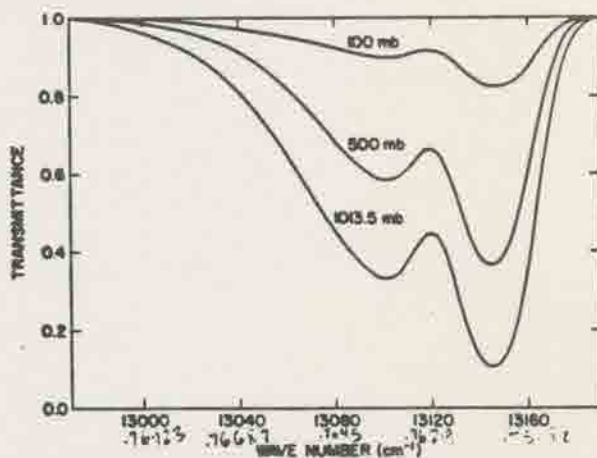


Figure 4. Calculated Oxygen A-band Transmissions for a Typical Filter and Several Path Lengths. See Text.

Figure 5 is a graph of data taken at a fixed nadir angle of  $33^\circ$  over northwestern Missouri in the early afternoon of July 6, 1976. The aircraft was traveling from west to east and patchy cumulus are scattered over the field of view. In the lower half of the figure are shown the  $0.754\mu\text{m}$  reflectance curve and the  $11\mu\text{m}$  black body temperature curve. The

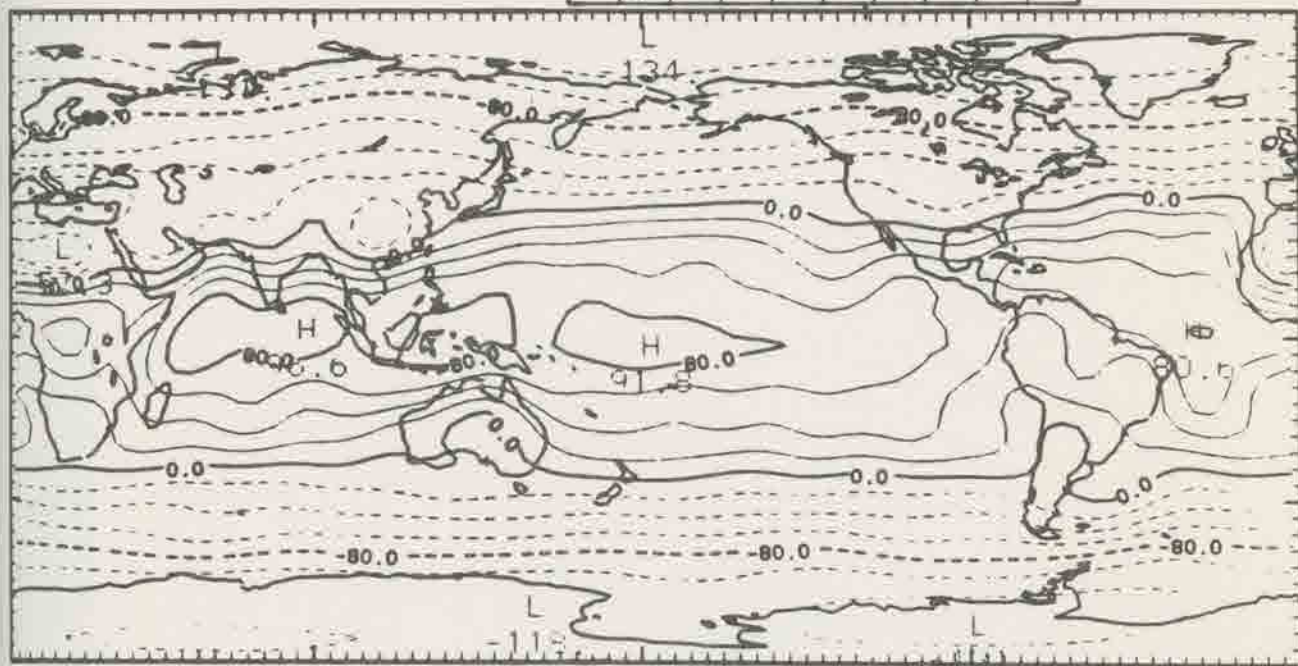
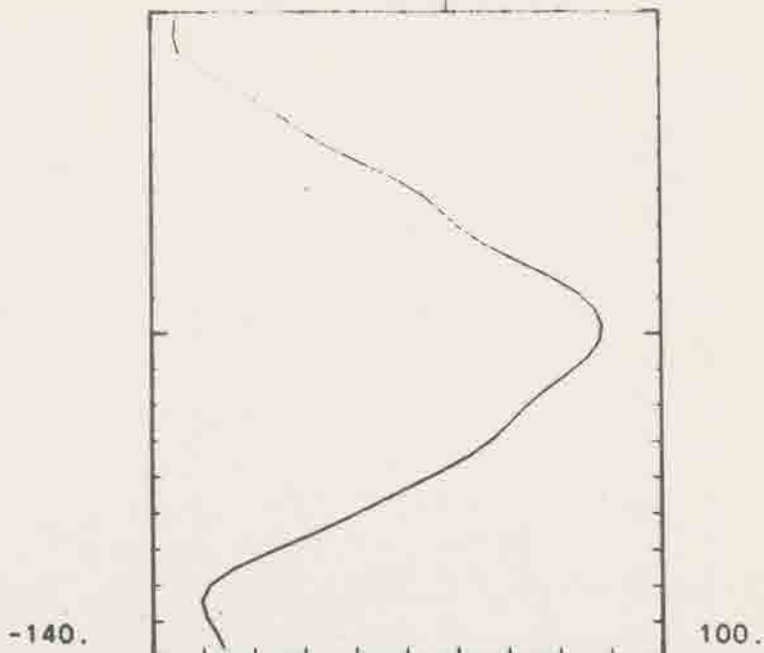
## SUMMARY

- NARROW WAVELENGTH BANDS ARE USED TO ISOLATE ABSORPTION & SCATTERING BEHAVIOR OF INDIVIDUAL SPECIES
- SHORT WAVELENGTH ARE USED TO AVOID ABSORPTION ENTIRELY
- MULTIPLE SPECTRAL BANDS CAN BE USED TO IDENTIFY CLOUD MICROPHYSICAL PARAMETERS

G. Campbell/D. Randel

"El Nino Discovered in Radiation Budget Measurements"

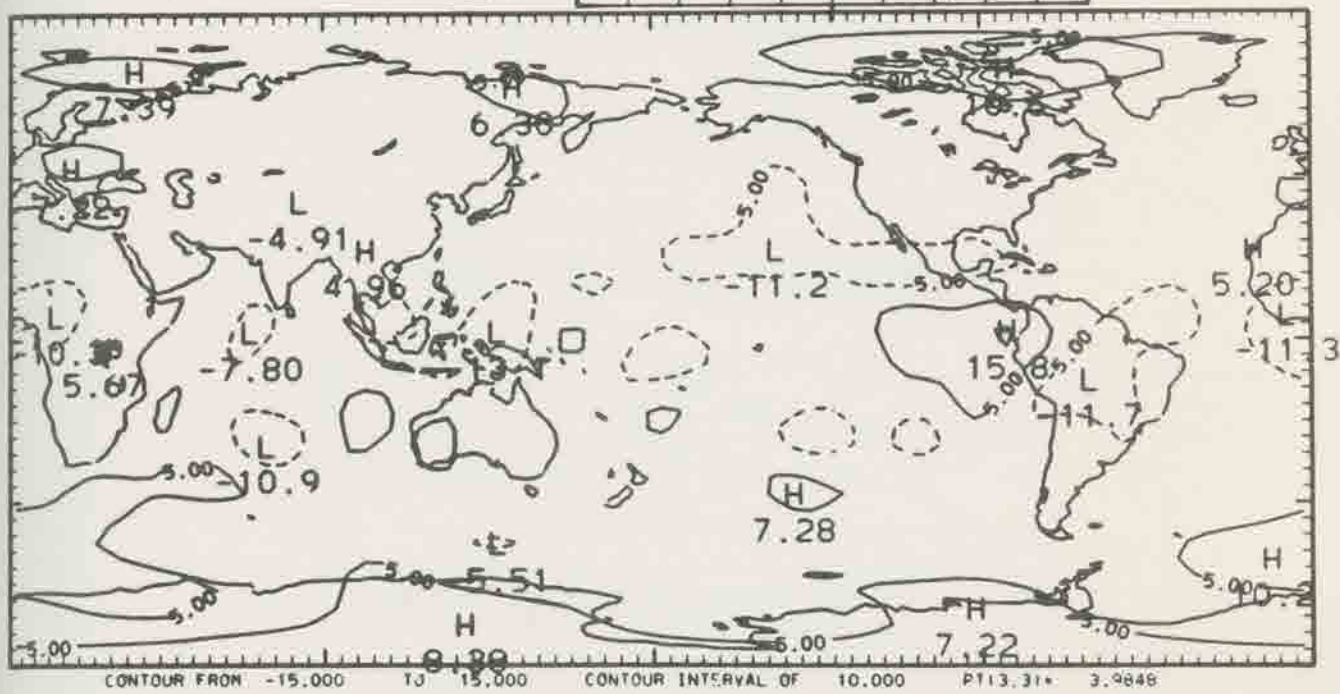
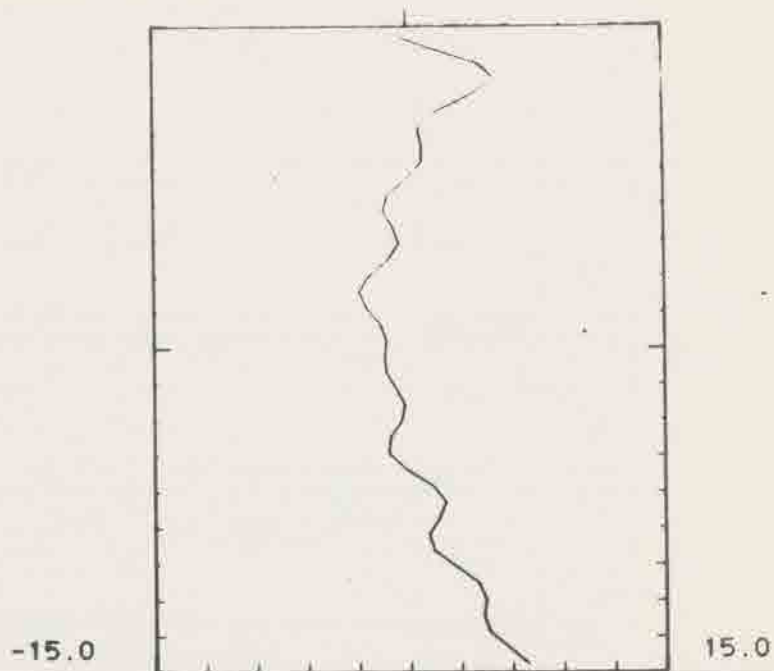
WIMBUS 7 ERB CSU  
182 M O NET D  
W/m2 FOURYNET



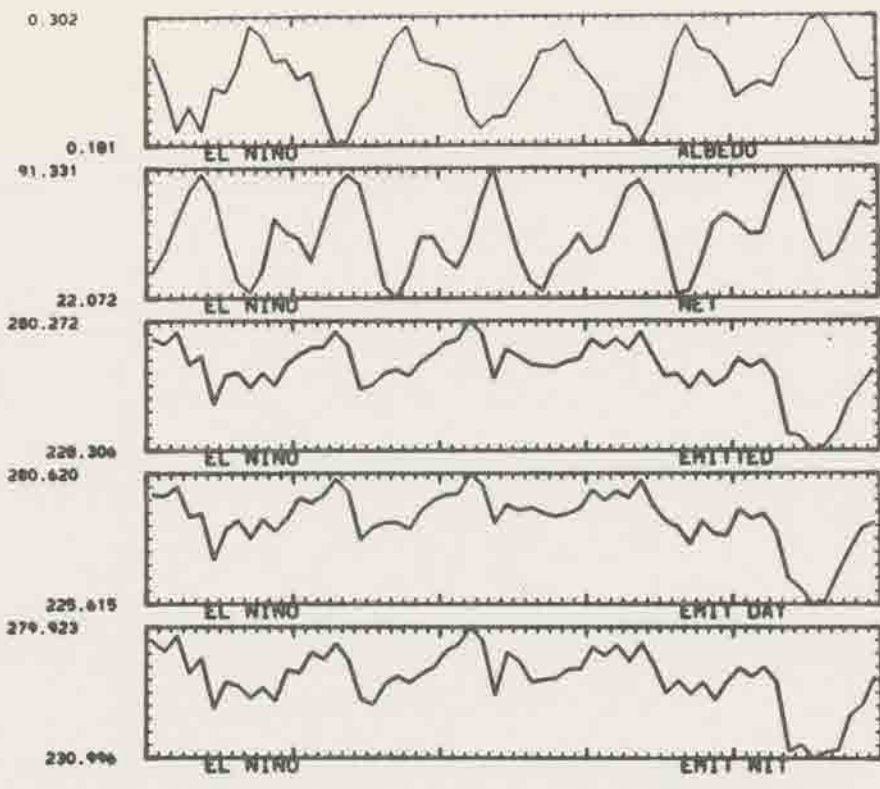
CONTOUR FROM -140.00 TO 100.00 CONTOUR INTERVAL OF 20.000 PT 13.31 -120.05

11/78-10/82 Annual Average Net Radiation

NIMBUS 7 ERB CSU  
183 M Q ENSANNET  
W/m<sup>2</sup>

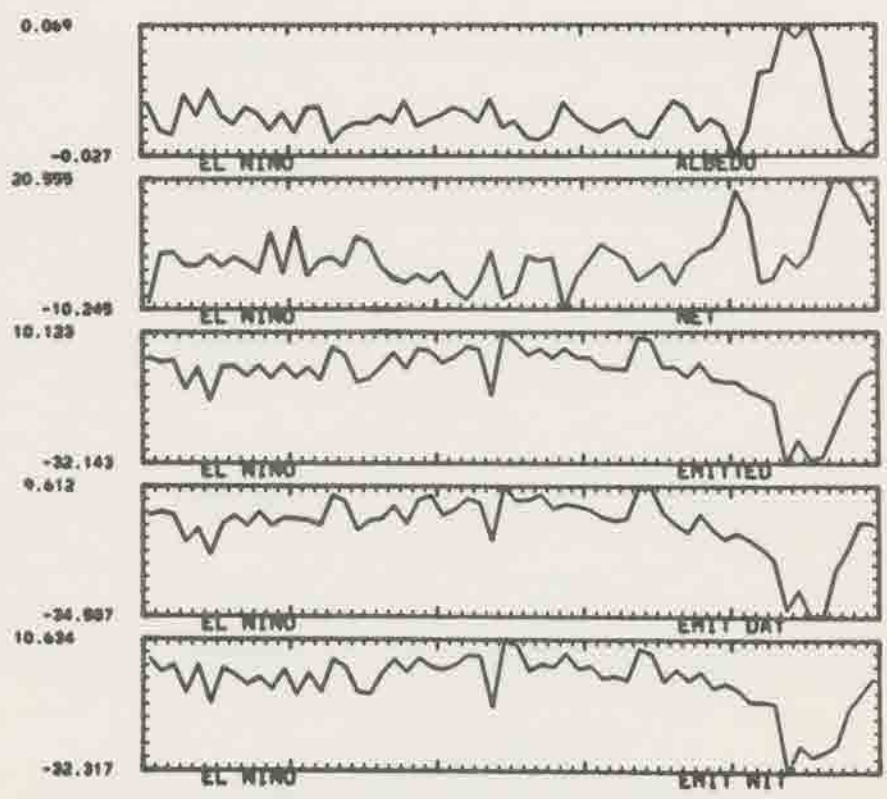


Fifth Year (11/82-10/83) Minus Four Year Average Net Radiation



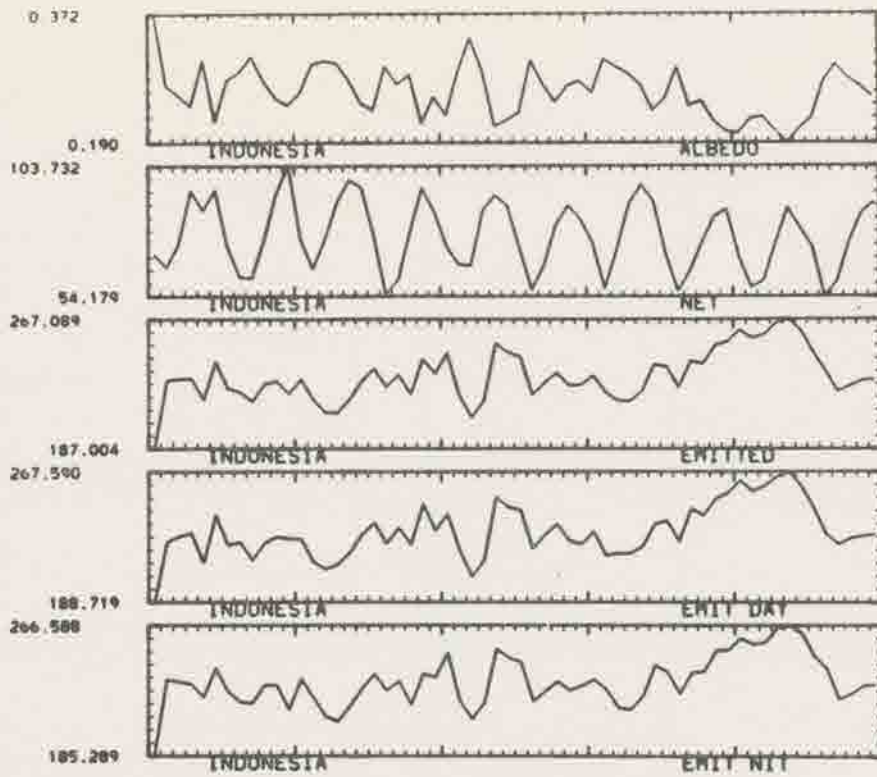
Time Series  
of El Niño  
Region

11/78 X252.0279.0 Y 4.5 -4.5 10/83

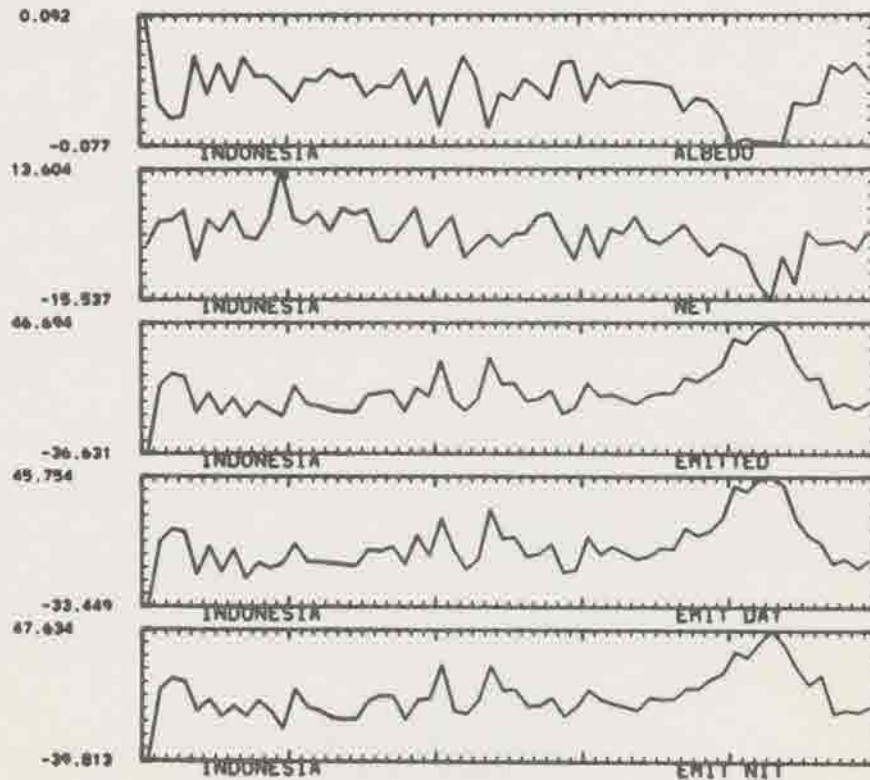


Time Series  
of Anomalies  
from Four  
Year Average

11/78 X252.0279.0 Y 4.5 -4.5 10/83



Time Series of Indonesia Region

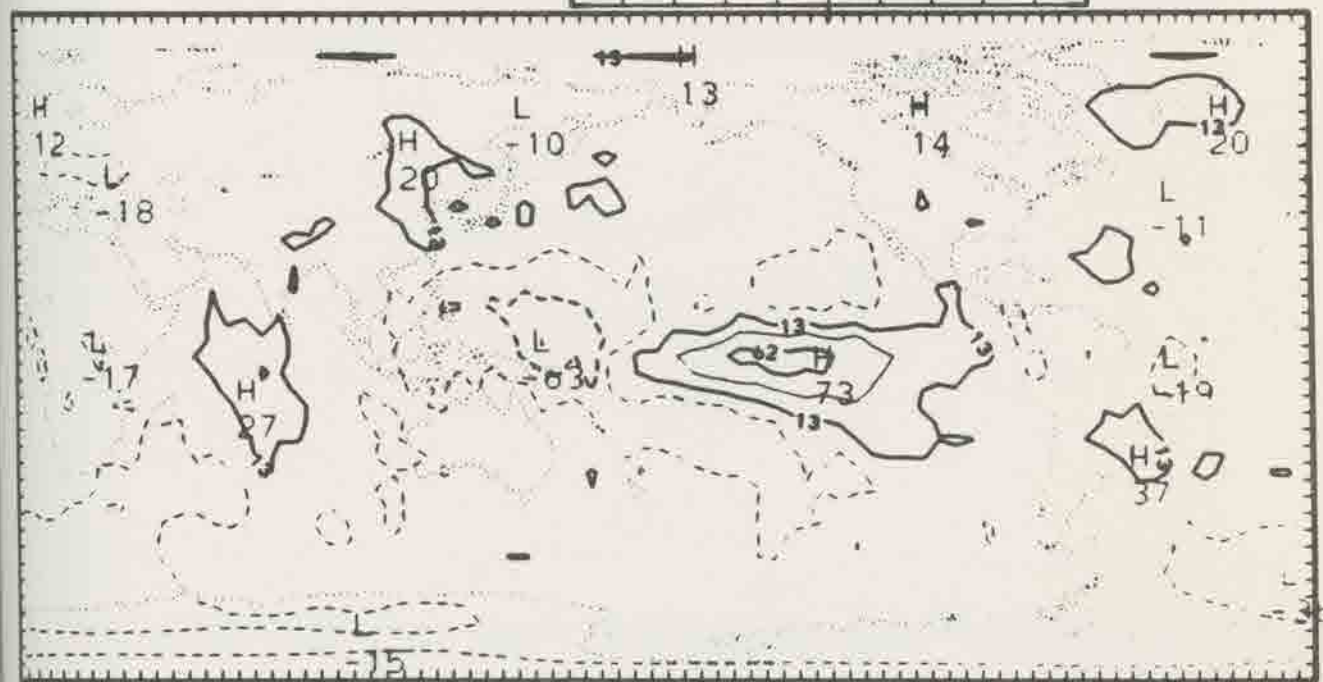
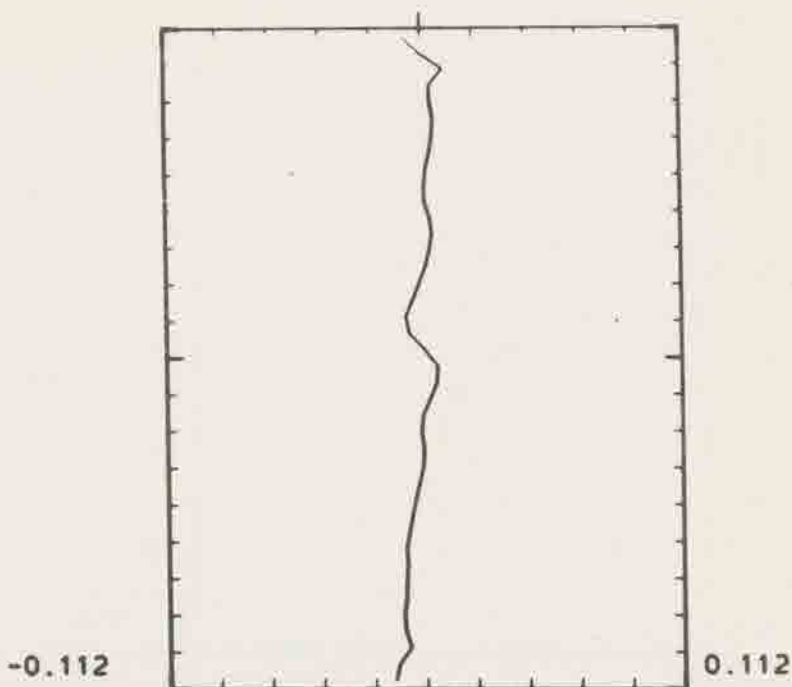


Time Series of Anomalies from Four Year Average

NIMBUS 7 ERB CSU

1983 M 0

ALB-4Y



RANGE FROM -0.11250 TO 0.87500E-01 CONTOUR INTERVAL OF 0.25000E-01 PT 13.31\* 0.73842E-02 LABELS SCALED BY 1000.0

Albedo (11/82-10/83) Minus Four Year Average

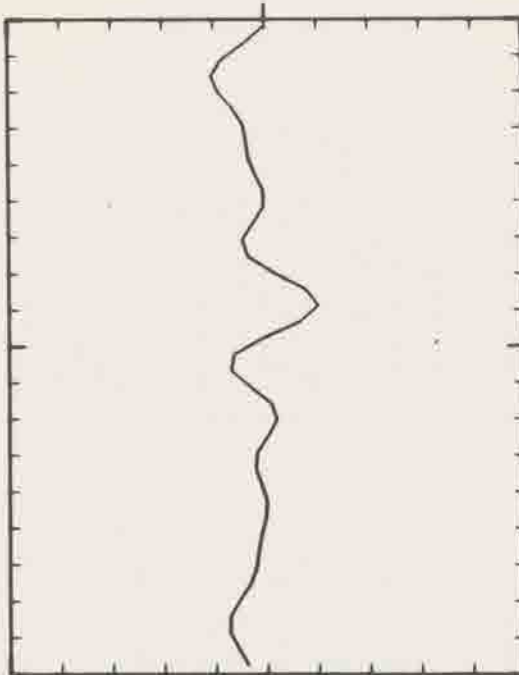
NIMBUS 7 ERB CSU

Filtered Anomaly Year = 11/82-10/83

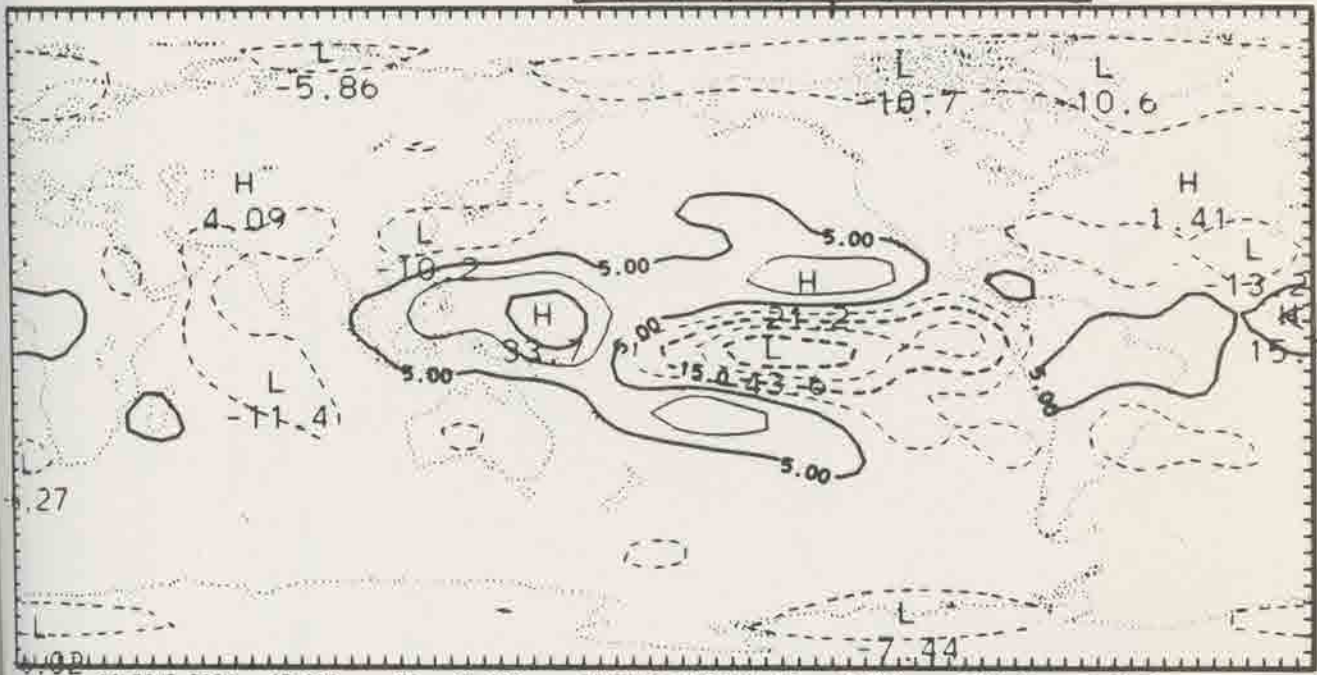
$$\Delta = 10 \text{ W/m}^2$$

Deconvoluted

-35.0



35.0



CONTOUR FROM -35.000 TO 35.000 CONTOUR INTERVAL OF 10.000 PT(3.31) = -4.6668

# Some simple solutions for heat-induced tropical circulation

By A. E. GILL  
 Department of Applied Mathematics and Theoretical Physics,  
 University of Cambridge

Down Motion

(Received 20 July 1979; revised 23 November 1979)

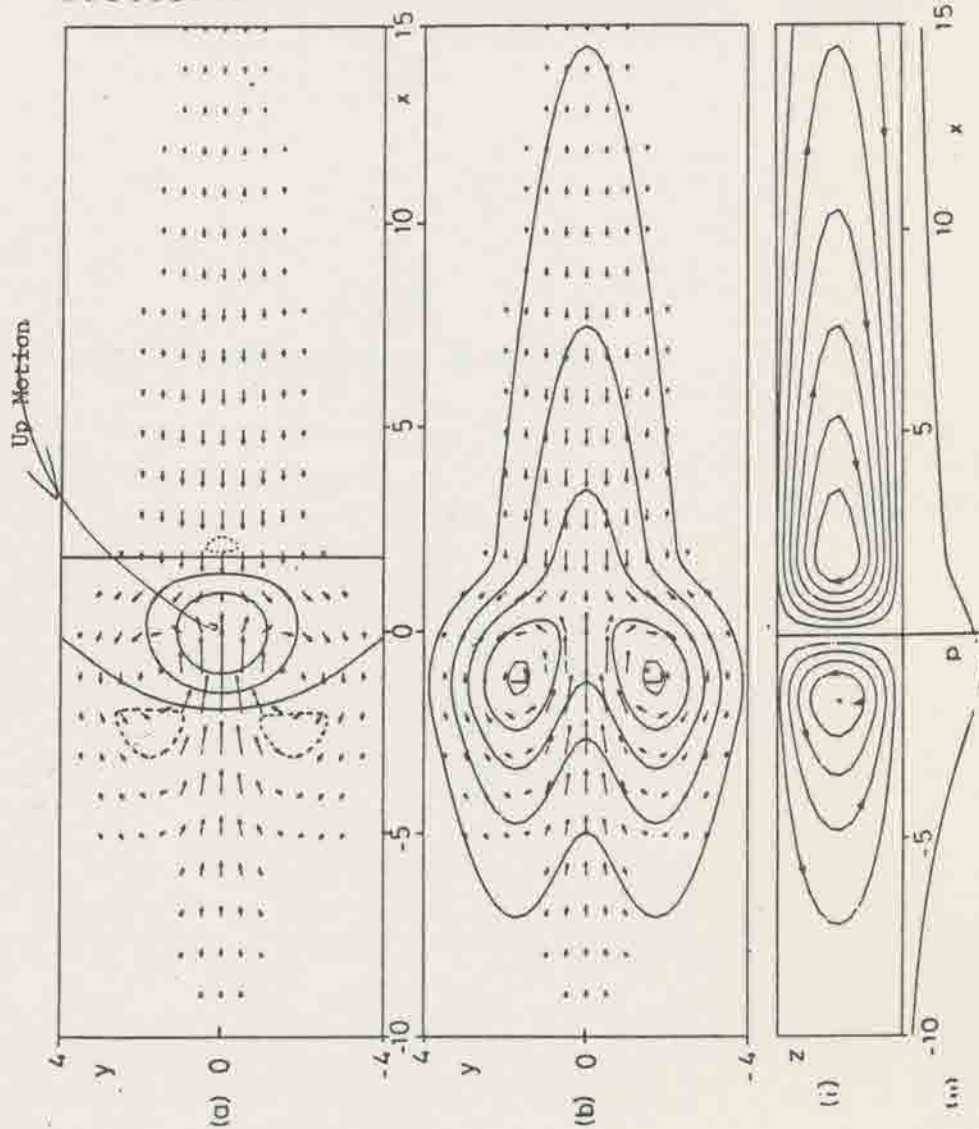


Figure 1. Solution for heating symmetric about the equator in the region  $|x| < 2$  for decay factor  $\varepsilon = 0.1$ .

(a) Contours of vertical velocity  $w$  (solid contours are 0, 0.3, 0.6, broken contour is -0.1) superimposed on the velocity field for the lower layer. The field is dominated by the upward motion in the heating region where it has approximately the same shape as the heating function. Elsewhere there is subsidence with the same pattern as the pressure field.

(b) Contours of perturbation pressure  $p$  (contour interval 0.3) which is everywhere negative. There is a trough at the equator in the easterly regime to the east of the forcing region. On the other hand, the pressure in the westerlies to the west of the forcing region, though depressed, is high relative to its value off the equator. Two cyclones are found on the north-west and south-west flanks of the forcing region.

(c) The meridionally integrated flow showing (i) stream function contours, and (ii) perturbation pressure. Note the rising motion in the heating region (where there is a trough) and subsidence elsewhere. The circulation in the right-hand (Walker) cell is five times that in each of the Hadley cells shown in (c).

D. Hillger

"Satellite Sounding Near Severe Storms"

AN ANALYSIS OF VARIOUS MESOSCALE AIR MASSES  
FOR 28 MARCH 1984 USING NOAA-7 TOVS

D.W. Hillger, J.F.W. Purdom and T.H. Vonder Haar

Cooperative Institute for Research in the Atmosphere (CIRA)  
Colorado State University  
Fort Collins, CO 80523

1.0 INTRODUCTION

The ability of satellite soundings to detect significant differences in water vapor profiles over small horizontal distances will be shown. The case study day under analysis was the Carolina tornado outbreak of 28 March 1984. This tornado outbreak case is especially significant because the air mass characteristics (water vapor and stability) were directly related to the location of developing severe weather (tornadoes and severe downbursts).

Satellite sounding radiances from the NOAA-7 TIROS Operational Vertical Sounder (TOVS) were used to retrieve water vapor and temperature profiles for single fields-of-view. Examples of vertical water vapor and temperature profiles will be shown for selected areas which were identified as having different air masses present. For each profile various water vapor and stability parameters were computed and then related to the potential for the development of severe weather. This analysis is based solely on the satellite data, without the use of surface observations or other ancillary data.

2.0 SATELLITE DATA

The TIROS Operations Vertical Sounder (TOVS) operates on board NOAA polar-orbiting satellites which normally view a region of the earth at 12-hour intervals (twice a day). Data from the infrared sensors were used in this study to derive water vapor and temperature profiles at a single-field-of-view resolution of about 35 km. The characteristics of the TOVS channels which were used are listed in Table 1. Not all channels were employed actively (used to modify the temperature or water vapor profile), only the tropospheric channels, since emphasis was placed on lower-tropospheric results. This was justified due to lack of mesoscale variations in the upper channels and for computational expediency. Of special concern were the lower tropospheric water vapor profiles. The weighting functions for the water vapor channels, which describe where the majority of the radiance contribution for these channels originates, are shown in Figure 1.

The horizontal coverage and resolution of the TOVS measurements are indicated in Figure 2, which is the channel 20 (0.7  $\mu\text{m}$ ) relative reflected radiance for approximately 21 UTC (Coordinated Universal Time - GMT) on 28 March 1984. Contours and shading are used to distinguish between cloud-free regions and those with cloud-contaminated radiances. The TOVS retrievals were performed

Table 1  
Selected TOVS Channels

TOVS Channel Number	Central Wavelength ( $\mu\text{m}$ )	Principal Absorbing Constituent	Approximate Peak Pressure (kPa)
8	11.1	window	surface
19	3.7	window	surface
10	8.3	H <sub>2</sub> O	90
11	7.3	H <sub>2</sub> O	70
12	6.7	H <sub>2</sub> O	50
4	14.2	CO <sub>2</sub>	40
5	14.0	CO <sub>2</sub>	60
6	13.7	CO <sub>2</sub> /H <sub>2</sub> O	80
7	13.4	CO <sub>2</sub> /H <sub>2</sub> O	90
13	4.57	N <sub>2</sub> O	100
14	4.52	N <sub>2</sub> O	95
15	4.26	CO <sub>2</sub> /N <sub>2</sub> O	70
16	4.40	CO <sub>2</sub> /N <sub>2</sub> O	40
20	0.7	window	reflected

only in the clear or mostly clear fields-of-view. In this case the cloudy/clear threshold was 2.0, such that values exceeding the threshold were considered cloudy and are shaded. The unshaded regions in Figure 2 compare closely with the clear regions in the Advanced Very High Resolution Radiometer (AVHRR) image in Figure 3 at 1 km resolution. This image was taken by a separate instrument on the same satellite (NOAA-7).

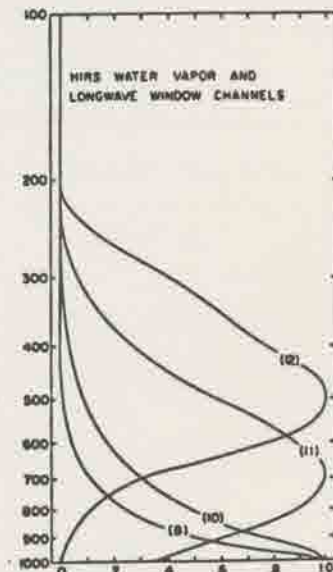


Figure 1. TOVS H<sub>2</sub>O channel weighting functions.

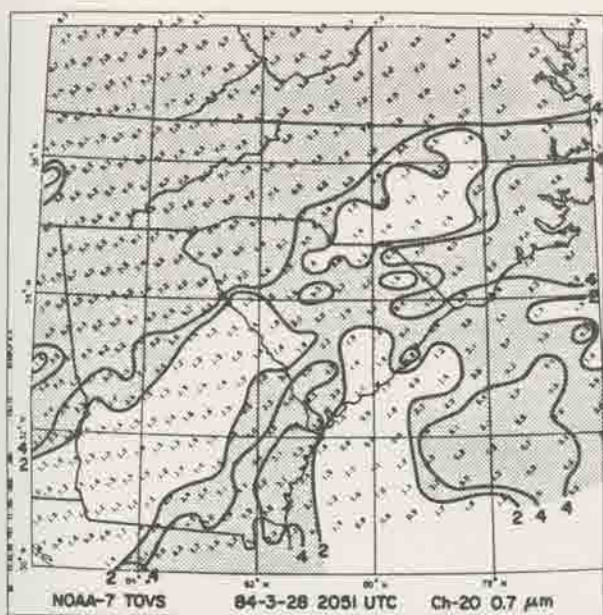


Figure 2. TOVS channel 20 ( $0.7 \mu\text{m}$ ) relative reflected radiances for approximately 21 UTC on 28 March 1984. Numbers show single-field-of-view values. Shading is used to indicate cloud-contaminated areas.

### 3.0 TOVS RETRIEVALS

The iterative retrieval method employed for the TOVS data was similar to that described by Smith (1983) and Smith and Zhou (1982) for the VISSR Atmospheric Sounder (VAS). However, before the retrievals were performed the reflected solar component of the TOVS radiances was subtracted off (Hayden, et al, 1981). Care also had to be taken to avoid cloud contaminated fields-of-view. However, oversight of cloud avoidance may be recognizable in resultant soundings as saturated or unrealistic water vapor profiles. An alternate means of cloud detection, besides a reflected



Figure 3. AVHRR 1 km resolution visible image for same area as in Figure 2. Letters A, B, C, and D denote regions where satellite retrievals were performed.

radiance threshold, is to use a threshold value of the difference in brightness temperature between the  $3.7 \mu\text{m}$  and  $11 \mu\text{m}$  window channels (Hillger, 1984). In this case a threshold of 12 K was used rather than the  $0.7 \mu\text{m}$  threshold.

In this study a single smooth composite RAOB sounding was used as the initial guess profile for all retrievals. The result is that differences between the retrievals were due to the satellite data alone and not an objectively analyzed initial guess field. Likewise, no surface observations were used in the retrieval process.

Once the retrievals were performed several water vapor and stability parameters were calculated for each sounding. Hillger and Vonder Haar (1981) showed that these parameters, as derived from satellite soundings, can be useful in the prediction of convection based on the pre-convective environment. Local maxima of low-level water vapor and instability were linked to later convective activity for several case study days.

### 4.0 RESULTS FOR 28 MARCH 1984

Figure 4 (Storm Data, 1984) shows the paths of the tornadoes and severe downbursts during this Carolina tornado outbreak. The major activity was confined to one long and nearly continuous corridor. A large storm developed in northeast Georgia and tracked east-northeast along a thunderstorm outflow boundary across South Carolina and into North Carolina. This boundary was a result of early morning convection to the northwest of this line (Purdom, 1985).

The holes between the cloudy regions allowed the use of satellite soundings to analyze the pre-storm environment surrounding this boundary. Figure 5 shows selected regions with 3 or 4 sounding locations in each. The numbers in each enclosed rectangle are the line and spot numbers for single fields-of-view. The 4 regions were selected to show the contrasting differences in the retrieved soundings, especially the water vapor profiles. The 12 K window brightness temperature difference contour is given in Figure 5 in order to distinguish between cloud-contaminated and cloud-free areas and to show where the satellite soundings are located with respect to the cloud field. The 12 K contour is nearly identical to the cloud-no cloud threshold in Figure 2 and also serves to illustrate the similarity of the two cloud detection methods.

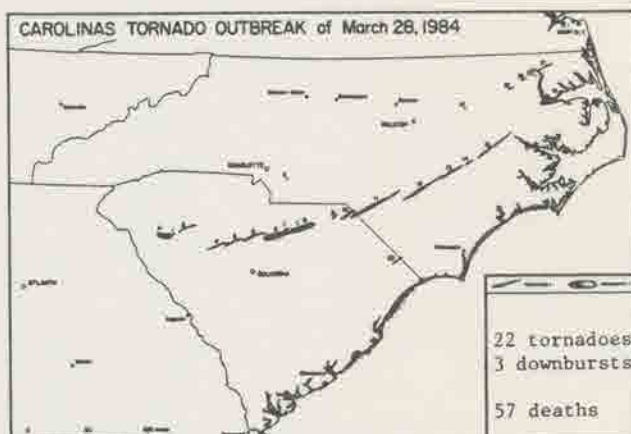


Figure 4. Line of tornadoes and severe downbursts during 28 March 1984 Carolina tornado outbreak. (Storm Data, 1984)

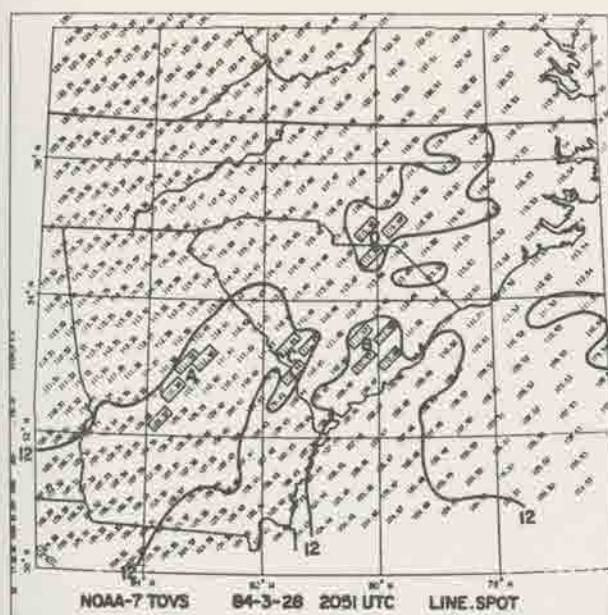


Figure 5. Locations of selected soundings in areas which have different air mass characteristics. Region letters and line and spot numbers are used for identification purposes. The 12 K window brightness temperature difference is given to distinguish between cloud-contaminated and cloud-free areas.

The 4 selected locations, chosen by examination of the visible satellite imagery and surface observations, can be categorized as:

- Region A - Dry region on the west edge of the clear tongue extending up into Georgia. This dry air is ahead of the frontal boundary stretching northeast to southwest across Georgia.
- Region B - Moist air mass over coastal south Carolina. This air is probably of oceanic origin.
- Region C - Warm sector air for the mesolow region where the tornadic storm first develops on the South Carolina-Georgia border.
- Region D - Outflow air to the north of the outflow boundary on the North Carolina-South Carolina border.

For each of these regions the selected TOVS retrievals were performed. Examples of vertical temperature and water vapor profiles in each region are given in Figures 6a through 6d. Each temperature sounding shows the radiative surface temperature as a discontinuity with the air temperature near the surface. The plots are on skew-T log-p backgrounds.

By examining the 4 sounding examples (one for each region) the contrast in the water vapor profiles is apparent. Region A (Fig. 6a) consists of a dry sounding from the surface upward. Region B (Fig. 6b) is much more moist in lower levels, as should be characteristic of maritime air. Region C (Fig. 6c) shows an even moister profile. In this case the lower levels were retrieved as saturated. However, the limited

vertical resolution of satellite soundings makes saturation in a thin layer somewhat questionable. Finally, Region D (Fig. 6d) shows a region which is again drier, but with a nearly constant dewpoint depression with height up to 60 kPa.

In contrast to the water vapor profiles, there is little difference between the temperature profiles which are shown. This is reasonable considering that water vapor varies more rapidly on small spatial scales than temperature.

Quantitative water vapor and stability information on the retrieved soundings in each region are given in Table 2. Each sounding is identified by its line and spot number as given in Figure 5. Water vapor information is given in terms of total precipitable water and the mean dewpoint temperature and mean mixing ratio in the lowest one kilometer. The contrast between the dry soundings in Region A and the more moist soundings in Regions B and C is apparent. For the dry soundings in Region A the total precipitable water is about 20 mm and the mean mixing ratio in the lowest kilometer is about  $8 \text{ g kg}^{-1}$ , compared to values of about 32 mm and  $13 \text{ g kg}^{-1}$  in Region B. Region C is likewise moist, but Region D again shows decreases in the lowest kilometer mean values.

Stability information in Table 2 is given by the Total-Totals (TT) index, the K-Index (KI), and the Lifted Index (LI). The most stable area is Region A with total-totals of about  $40^\circ\text{C}$  and positive lifted index values. The most unstable areas, according to the total-totals, are in Regions B, C and D, with values around  $50^\circ\text{C}$ . However, according to the lifted index, Regions B and especially C are more unstable, with the most negative lifted indices, with values from  $-2$  to  $-4^\circ\text{C}$ . The most humid and unstable region is therefore Region C, which is the storm genesis region for the tornado outbreak. Soundings on either side, in Region B and especially Region D, are more stable. These contrasts are striking considering the small horizontal scale involved ( $<300 \text{ km}$ ) between the analyzed regions.

## 5.0 SUMMARY AND CONCLUSIONS

Satellite sounding data were used to produce soundings at single-field-of-view locations on the 28 March 1984, the Carolina tornado outbreak. The infrared satellite measurements at high horizontal

Table 2

Region	Line and Spot Numbers	Total PW(mm)	Stability*(°C)			Lowest 1km Mean	
			TT	KI	LI	T <sub>d</sub> (°C)	w(g kg <sup>-1</sup> )
A	109 37	21	41	15	1.5	13.6	10.3
A	110 38	20	40	14	3.8	11.0	8.7
A	111 39*	19	40	15	4.6	10.1	8.2
A	111 40	16	37	11	8.5	5.3	5.9
B	110 47	32	47	29	-1.8	17.1	13.0
B	110 48	32	47	29	-2.2	17.5	13.3
B	111 47	34	48	31	-2.4	17.6	13.3
B	111 48*	31	47	28	-1.3	16.6	12.5
C	110 44*	36	50	35	-2.2	17.5	13.3
C	111 44	33	48	30	-4.3	18.8	14.4
C	111 45	37	50	34	-3.5	18.2	13.9
D	114 48	37	51	37	-1.3	16.2	12.2
D	115 48	32	47	30	-0.8	14.8	11.1
D	115 49*	32	47	30	-0.5	14.6	11.0

\*TT-Total Totals, KI- K-Index, LI- Lifted-Index

\*denotes soundings shown in Fig. 5

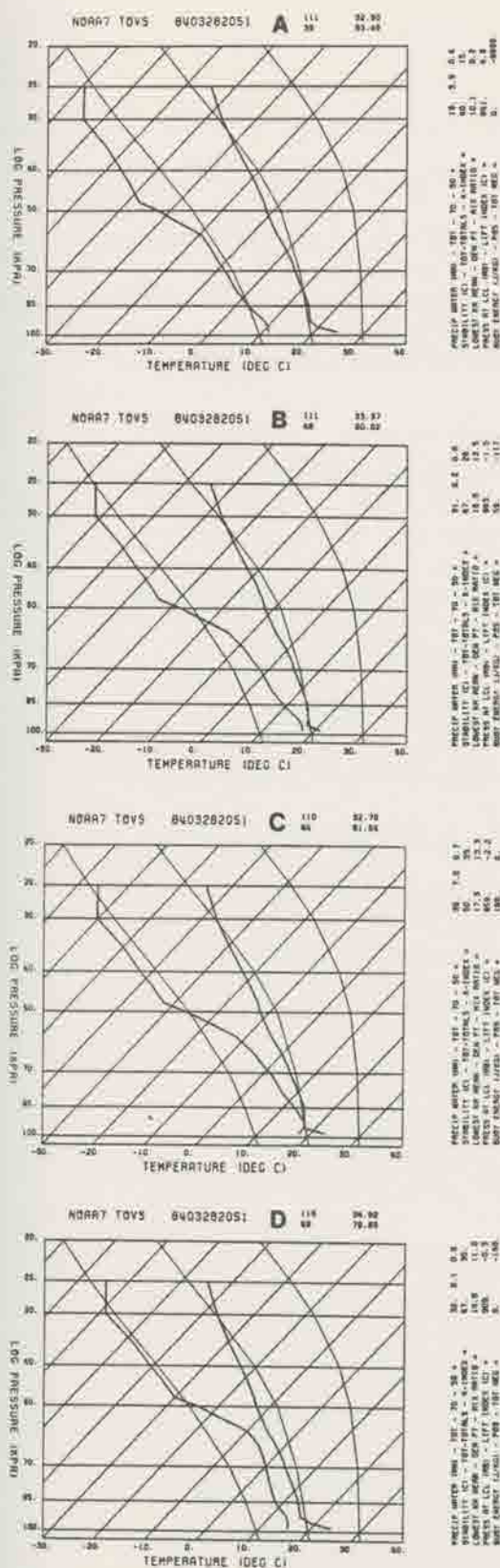


Figure 6. One TOVS retrieval for each of the 4 regions in Figure 5. (See text for details).

resolution (35 km) have the ability to detect small scale features which are undetectable by the standard radiosonde network. Only surface observations are available at a similar resolution, but they contain no information of vertical temperature and water vapor structure. The satellite soundings for this study were produced without the aid of surface observations in the retrieval process.

On this case study day, satellite soundings were examined in selected regions around the tornado genesis area. The retrieved soundings showed a wide range of water vapor profiles over a relatively small horizontal scale (<300 km). Total precipitable water and mean dewpoints and mixing ratios in the lowest one kilometer show contrasts. The primary indicator of the best region of severe weather potential is the lifted index computed from the soundings.

#### ACKNOWLEDGEMENTS

The TOVS data used in this study were obtained from the NOAA/NESDIS Development Laboratory at the University of Wisconsin. This research was supported through NOAA grants NA84AA-D-00017 and NA84AA-H-00020.

#### REFERENCES

- Hayden, C.M., W.L. Smith and H.M. Woolf, 1981: Determination of moisture from NOAA polar-orbiting satellite sounding radiances. *J. Appl. Meteor.*, 20, 450-466.
- Hillger, D.W. and T.H. Vonder Haar, 1981: Retrieval and use of high-resolution moisture and stability fields from Nimbus-6 HIRS radiances in pre-convective situations. *Mon. Wea. Rev.*, 109, 1788-1806.
- Hillger, D.W., 1984: Spatial and temporal variations in mesoscale water vapor retrieved from TOVS infrared radiances in a nocturnal inversion situation. *J. Climate Appl. Meteor.*, 23, 704-723.
- Purdom, J.F.W., 1985: The application of satellite sounding and image data to the Carolina tornado outbreak of 28 March 1984. *Proceedings, 14th Conference on Severe Local Storms*, AMS, March, 29-Oct. 1, Indianapolis, IN.
- Smith, W.L., 1983: The retrieval of atmospheric profiles from VAS geostationary radiance observations. *J. Atmos. Sci.*, 40, 2025-2035.
- Smith, W.L. and F.X. Zhou, 1982: Rapid extraction of layer relative humidity, geopotential thickness, and atmospheric stability from satellite sounding radiometer data. *Appl. Opt.*, 21, 924-928.
- Storm Data, 1984: Vol. 26, No. 3, March, NOAA/NESDIS/NCDC, 5-12.

J. Purdom

"Mesoscale Forecasting Research"

This is a summary of the first talk I gave at the 1985 CIRA Pingree Park Retreat concerning mesoscale forecasting research, both current and planned, at CIRA. The attached viewgraphs were used in the talk and are briefly summarized below:

1. Mesoscale research at CIRA, current programs with which we are involved.

This viewgraph shows the current programs with which we are involved and the various objectives of those different programs.

2. Mesoscale research planned.

This viewgraph describes various research programs with which we will be involved in the future. Some of those efforts are funded, some are not. For example, numbers 1 and 2 are funded programs, number 5 is a partially funded program for which we will be seeking additional funds. Numbers 3, 4, 6 and 7 are ones for which we need to determine our planned activity and submit proposals to the appropriate places. At the bottom of viewgraph 2 is written "satellite mesoscale initiative". This refers to a mesoscale initiative which will be spearheaded by NESDIS for FY88 submission to NOAA who may then take it to DOC. CIRA will no doubt play a major role in structuring this mesoscale initiative. Time is short, however, as there are only eight months until the time for FY88 submissions.

3. through 16. - These viewgraphs are examples of products that were made available on the CIRA IBM/PC to the PRE-STORM program which we supported from May 1 through June 30 of this year.

3. This is an example of the visible image for June 10, 1985 which was a PRE-STORM operational day. Boundaries showed up very well in the visible image. On this day, a major mesoscale convective system developed in Kansas and moved across the northern PRE-STORM network as well as through Oklahoma. This is no doubt a day that we will study in depth with the PRE-STORM experiment.
4. Once the major MCC had formed, histograms of the cloud top temperatures were taken. This is an example of the histogram output from 20 GMT to 0700 GMT for the major MCC.
5. A plot of time on the abscissa versus pixels on the ordinant. 300 pixels relates roughly to 50,000 square kilometers. This viewgraph shows the accumulated area covered by the various isotherm regions within the anvil from 2000 GMT through 0700 GMT. It is interesting to note in this histogram that almost all of the convective intensities peak at near the same time in the cirrus shield, that is, around 0300 and then begin to decay rapidly. Obviously there is some interconnection between minus -75 and -72 and so forth since the -72 area also includes the -75 area. This was a case in which dry air evolved ahead of the squall line and showed up very well in the water vapor data. This interacted with the squall line and no doubt helped it become severe with very strong winds as it moved through the Oklahoma area.
6. This is an example of a water vapor image for the water vapor sector provided for PRE-STORM. It's for June 12, 1985 at 1730 GMT. An interesting feature in this viewgraph is the short wave that shows up moving through Missouri into Arkansas and also

another short wave in Utah. This is one day after the MCC has moved through the PRE-STORM region.

7. This is a visible image for the 12th at 2100 GMT. Over the area shown by this image, satellite soundings were taken and examples follow, #'s 8-16.
8. This shows the area that is covered by the PRE-STORM sounding sector. The particular values printed out are the 0 to 1 kilometer mixing ratios at the sounding spots for the 12th of June at 1718 GMT. Each spot is for an area 75 x 75 kilometers.
9. Another sounding parameter computed on our IBM PC, in this case, total negative energy below the LCL.
10. Another sounding parameter computed by our IBM PC, in this case, positive buoyant energy available once the convective temperature for the day is reached. Notice the higher positive buoyant energies in eastern Texas and also some evidence of higher positive buoyant energy in Missouri, Arkansas and up into Iowa. Those northern higher positive buoyant energies will be available because of the trough that is moving through the area and the cold air aloft associated with it.
11. This is the convective temperature required to realize the positive energy shown in #10.
12. This is positive buoyant energy available if the parcel is forced to convection at the time of the sounding. Notice again the higher positive buoyant energies in Texas and also up through Iowa.
13. This shows by number the soundings taken, # 1 being in western South Dakota with #144 being in southern Louisiana. The

continuous line drawn on the viewgraph represents what one might envision as an instantaneous aircraft track across a very large area where we might want to look at soundings. For example, #141 compared to #137 is shown in viewgraph #14. Sounding were made for each of these spots to compare to adjacent soundings.

14. This is a comparison of soundings #141 and #137. Notice that #137 is slightly cooler than #141.
15. This is a comparison of soundings #132 and #125. Notice that #125 is cooler aloft and also shows saturation at mid-levels. This is partly because of cloud contamination. This is an area where mesoscale models may well be able to help us improve the sounding capability of the satellite.
16. Similar to 15, showing mid-level cloud effects.

Next, certain items that were spoken of by Don Hillger in his talk were reiterated concerning the Carolina tornado outbreak of March 28, 1984. The attached paper, titled "The Application of Satellite Sounding and Image Data to the Carolina Tornado Outbreak of 28 March 1984" was distributed. This paper is to appear in the preprints of the 14th Conference on Severe Local Storms. Figures 1 through 8 of that paper were used as viewgraphs in describing the outbreak and how we are trying to integrate satellite image and sounding data together to better understand mesoscale atmospheric behavior.



# Mesoscale Research (Planned)

2

1. **Mist** a/c investigations of arc cloud lines in conjunction with MEST/SPACE
2. **VDUC** Product Development for VAS data Utilization Centers (NOVA)
3. **Sat for R/M Modeling** STORM-PROFS  
Various sat obs.
4. **STORM** satellite data utilization in all phases of storm
5. **SPACE** regional & mesoscale aspects of summer precip. in S.E. USA; sat, radar, AVE
6. **Meso. Conv. Climatology** An important new area for SPACE, STORM, ..
7. **Tropical Mesoscale Systems** TBD

## Satellite Mesoscale

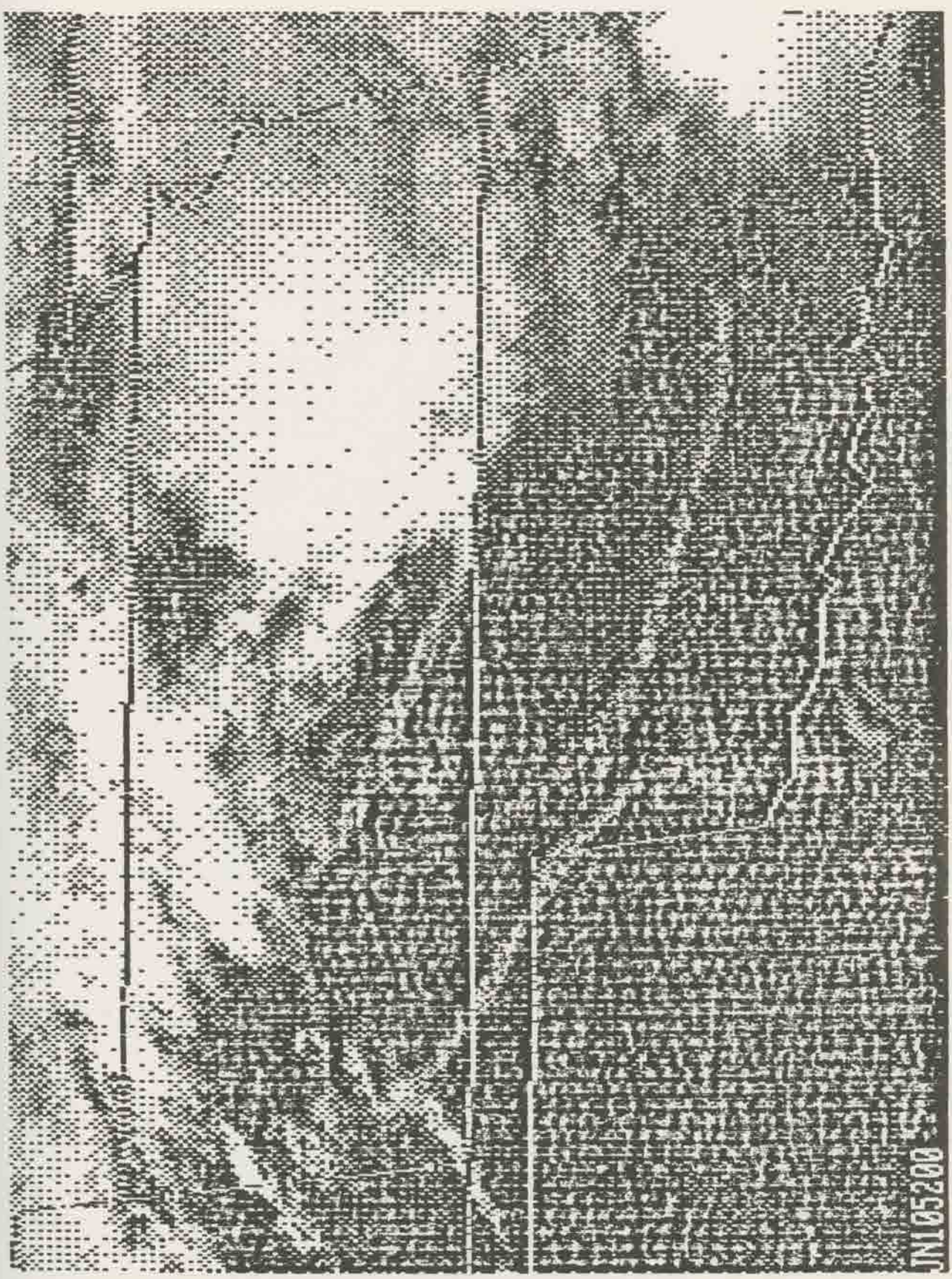
Initiative

8 mos. until

FY '88 submission.

GOES-NEXT in late '89.

What major efforts req'd:



JN105200

4

-55°C

20	21	22	23	00	01	0130	0200	0230	0300	0330	0400	0430	0500	0530	0600	0630	0700
0	0	0	0	0	0	0	0	0	0	0	0	0	0	0	0	0	0
79	38	32	19	0	0	0	0	0	0	0	0	0	0	0	0	0	0
18	167	236	258	15	0	0	0	0	0	0	0	0	0	0	0	0	0
12	204	282	339	144	0	0	0	0	0	0	0	0	0	0	0	0	0
14	941	153	383	249	859	1021	1106	1298	1851	2176	1985	2077	1649	1242	1952	2151	1243
10	169	235	238	278	143	164	170	254	375	568	514	308	572	445	471	526	427
08	85	103	116	125	71	83	113	186	242	250	266	300	389	281	225	252	244
00	105	150	168	188	103	188	183	208	283	303	291	313	415	347	388	419	467
47	145	221	253	266	174	176	206	279	325	354	385	483	496	455	735	774	590
27	162	214	285	170	196	196	249	302	300	318	493	494	422	423	604	531	460
0	44	81	91	69	113	142	185	176	218	286	277	200	263	302	274	206	174
0	9	80	103	138	132	183	194	185	270	285	195	250	259	384	191	116	109
0	0	33	56	82	194	192	173	169	175	137	171	212	252	246	74	84	88
0	0	8	35	79	209	237	230	221	158	211	224	191	317	104	76	69	32
0	0	0	1	7	70	118	155	198	168	153	195	247	24	25	20	4	2
0	0	0	0	0	18	8	34	70	152	170	104	13	14	16	0	0	0

1A  
10

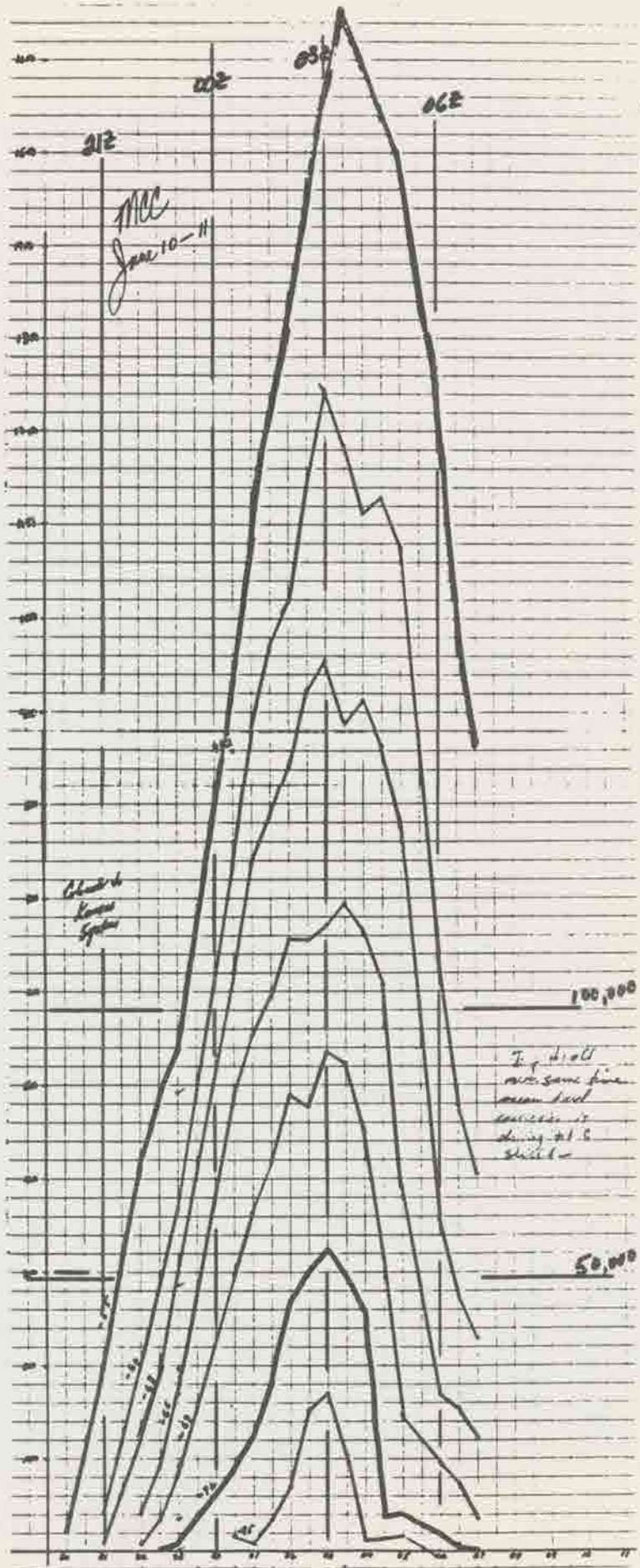
0	0	0	0	0	0	0	0	0	0	0	0	0	0	0	0	0	0
0	0	0	0	0	0	0	0	0	0	0	0	0	0	0	0	0	0
0	0	0	0	0	0	0	0	0	0	0	0	0	0	0	0	0	0
0	0	0	0	0	0	0	0	0	0	0	0	0	0	0	0	0	0
11	66	66	54	131	71	496	883	687	1003	0	0	0	0	0	0	0	0
5	17	27	25	51	76	159	190	171	178	0	0	0	0	0	0	0	0
0	3	10	8	27	51	92	71	71	80	0	0	0	0	0	0	0	0
0	7	11	11	21	113	80	71	57	48	0	0	0	0	0	0	0	0
0	10	24	32	55	184	67	56	39	11	0	0	0	0	0	0	0	0
0	19	43	58	105	103	30	16	0	0	0	0	0	0	0	0	0	0
0	7	34	58	61	0	0	0	0	0	0	0	0	0	0	0	0	0
0	4	17	21	13	0	0	0	0	0	0	0	0	0	0	0	0	0
0	0	0	0	0	0	0	0	0	0	0	0	0	0	0	0	0	0
0	0	0	0	0	0	0	0	0	0	0	0	0	0	0	0	0	0
0	0	0	0	0	0	0	0	0	0	0	0	0	0	0	0	0	0

near Clark County  
behind main system

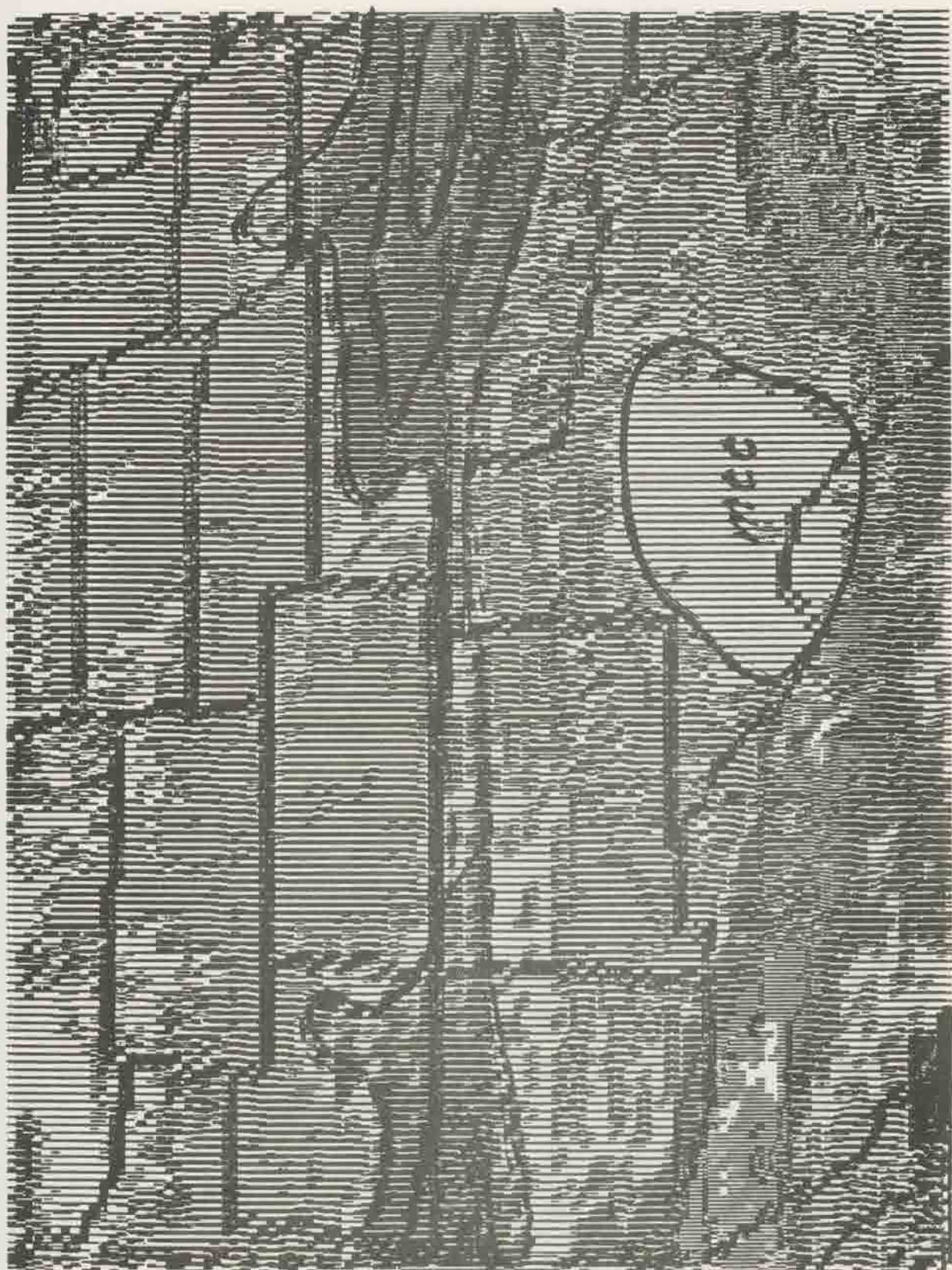
-55°C

1A  
10

151

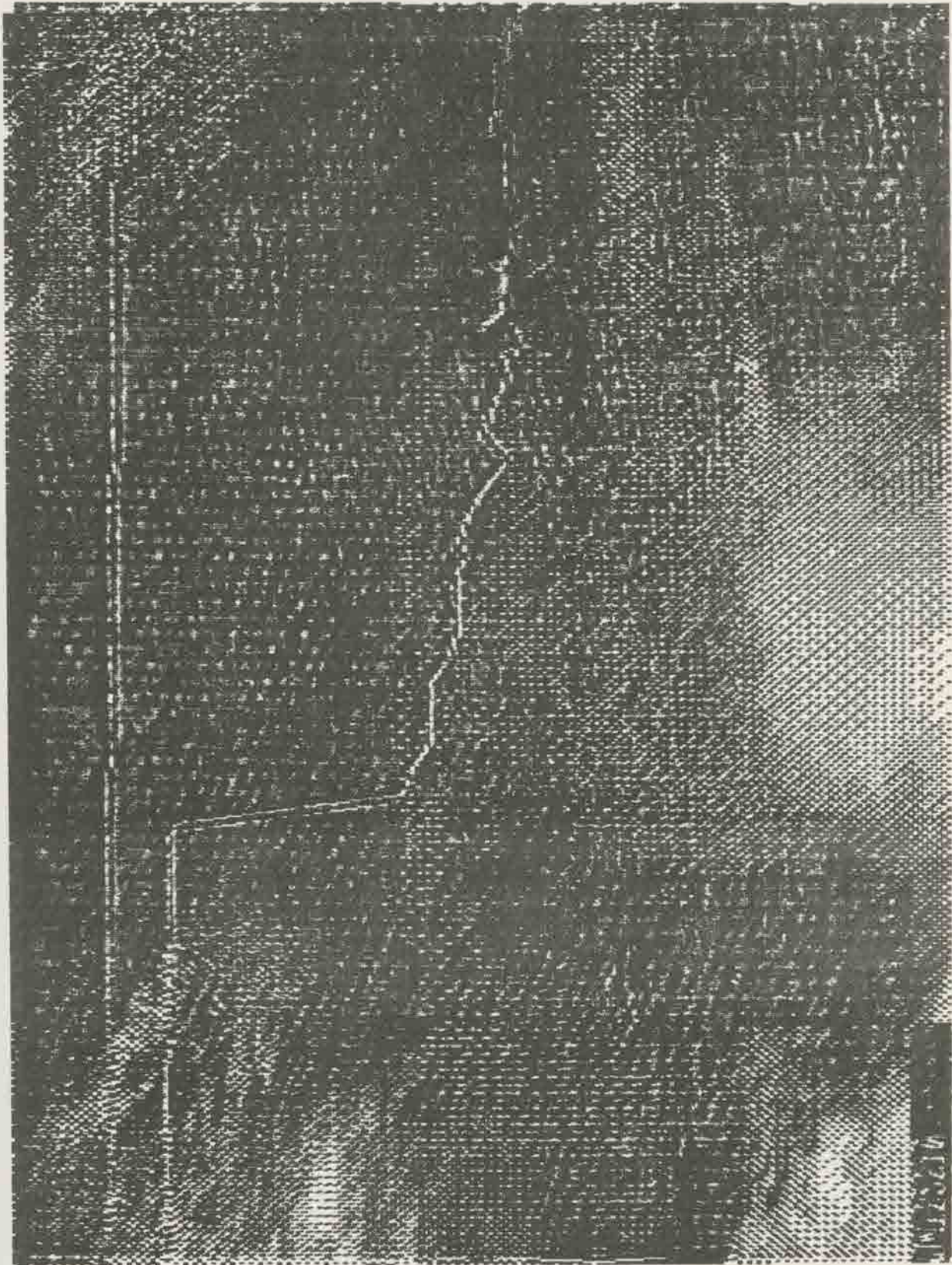


61



6.74

71

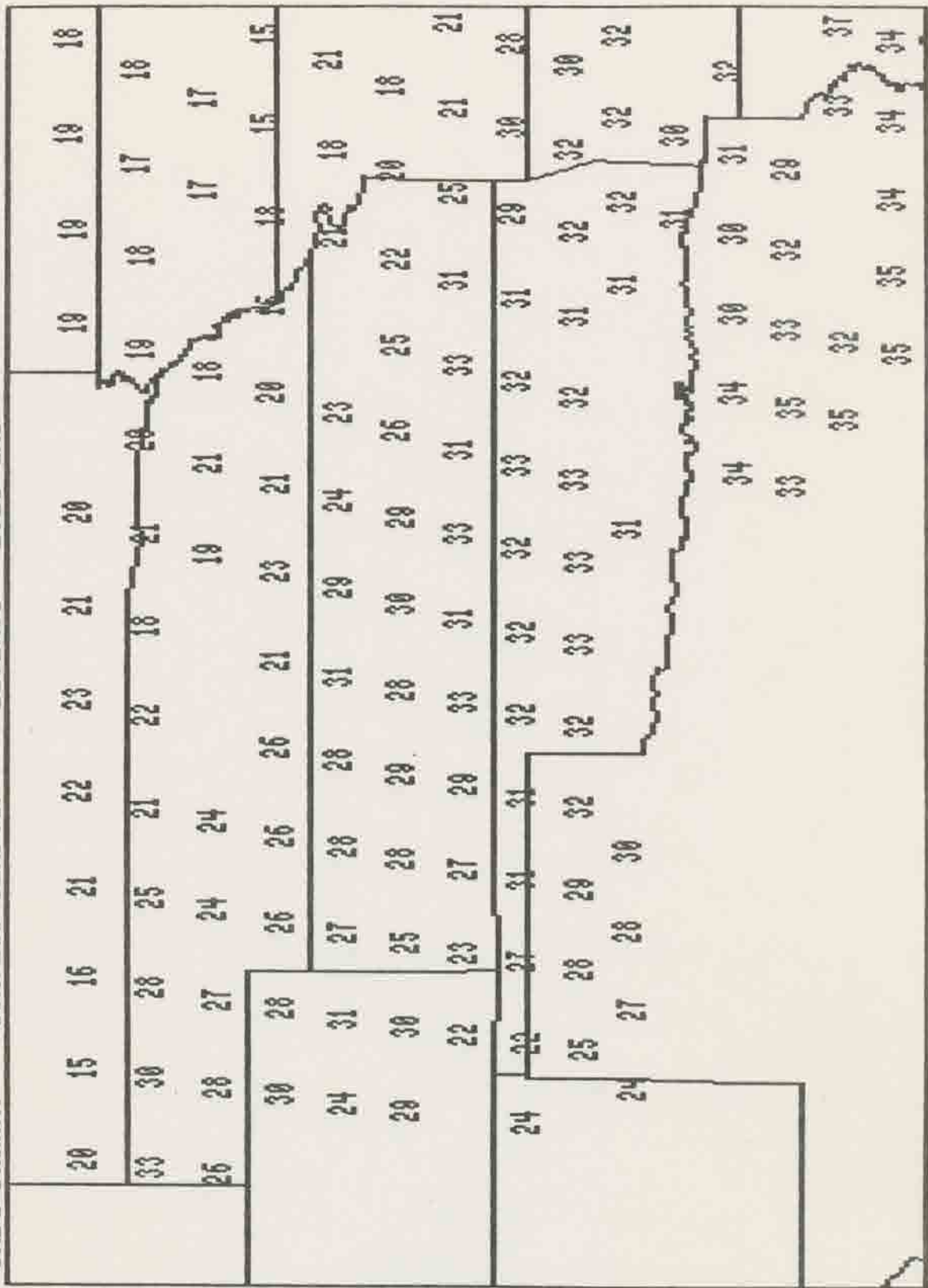




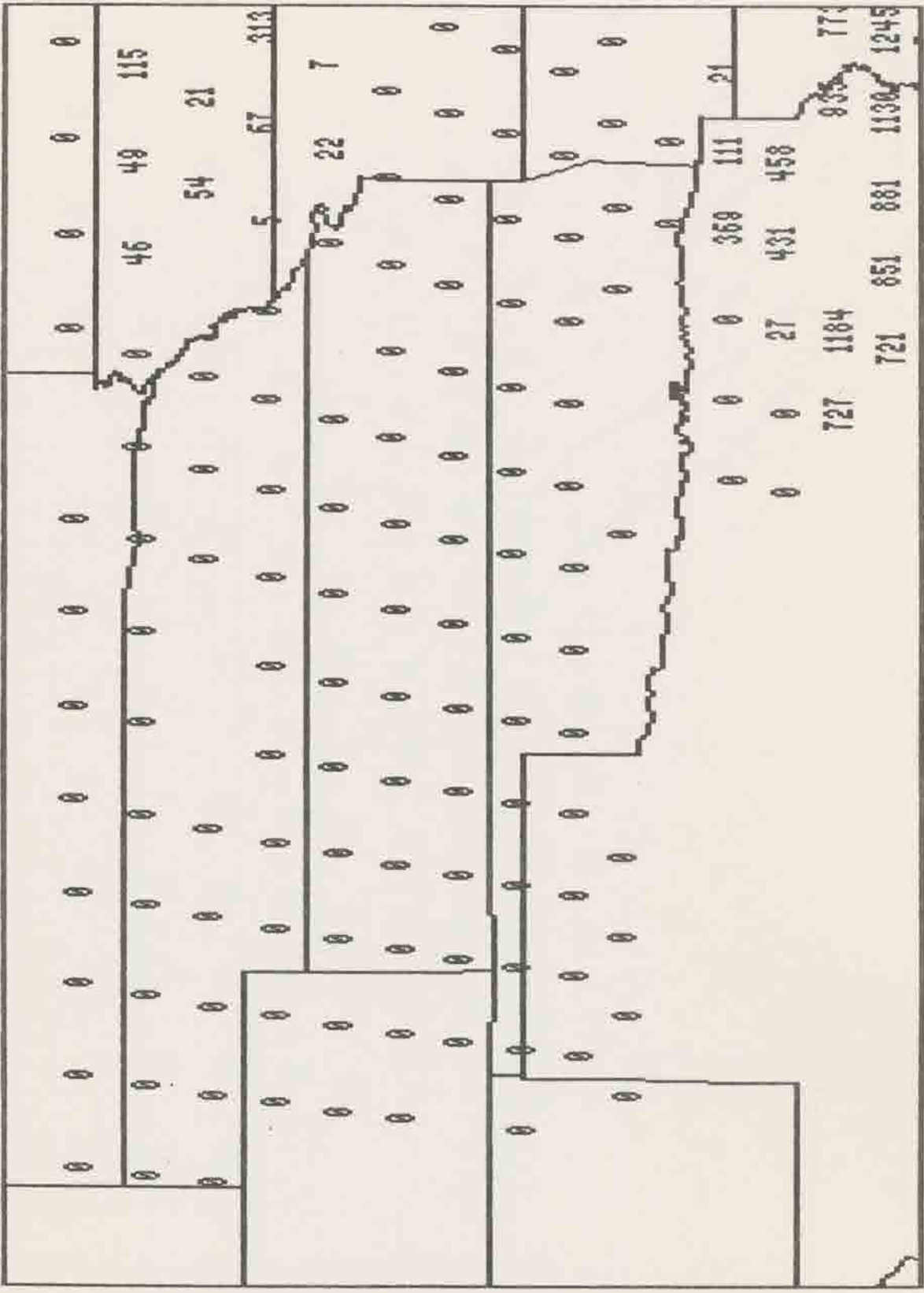




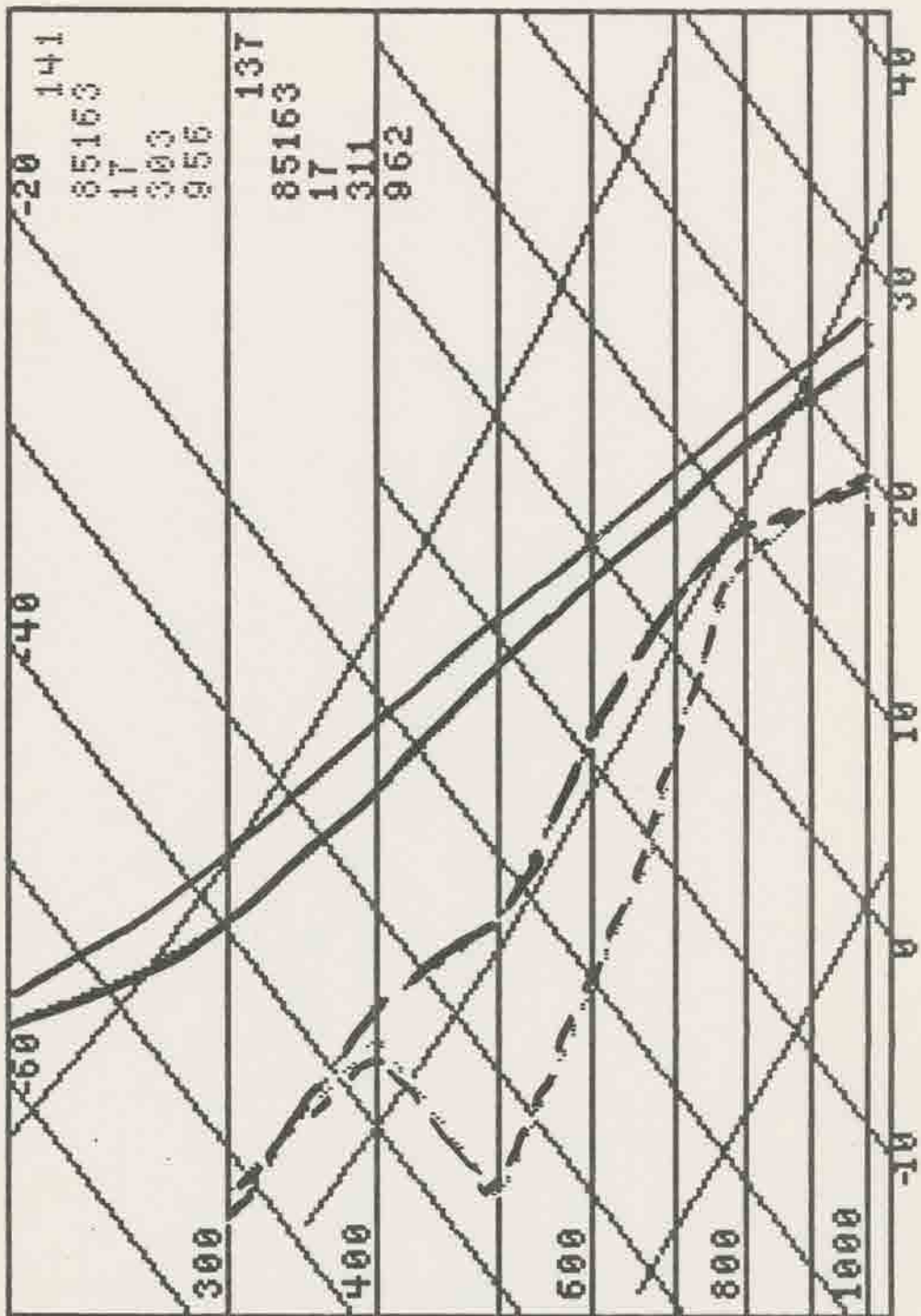
SNDG PARAM: CONVECT TEMP(C) 12JUN85 1718 GMT

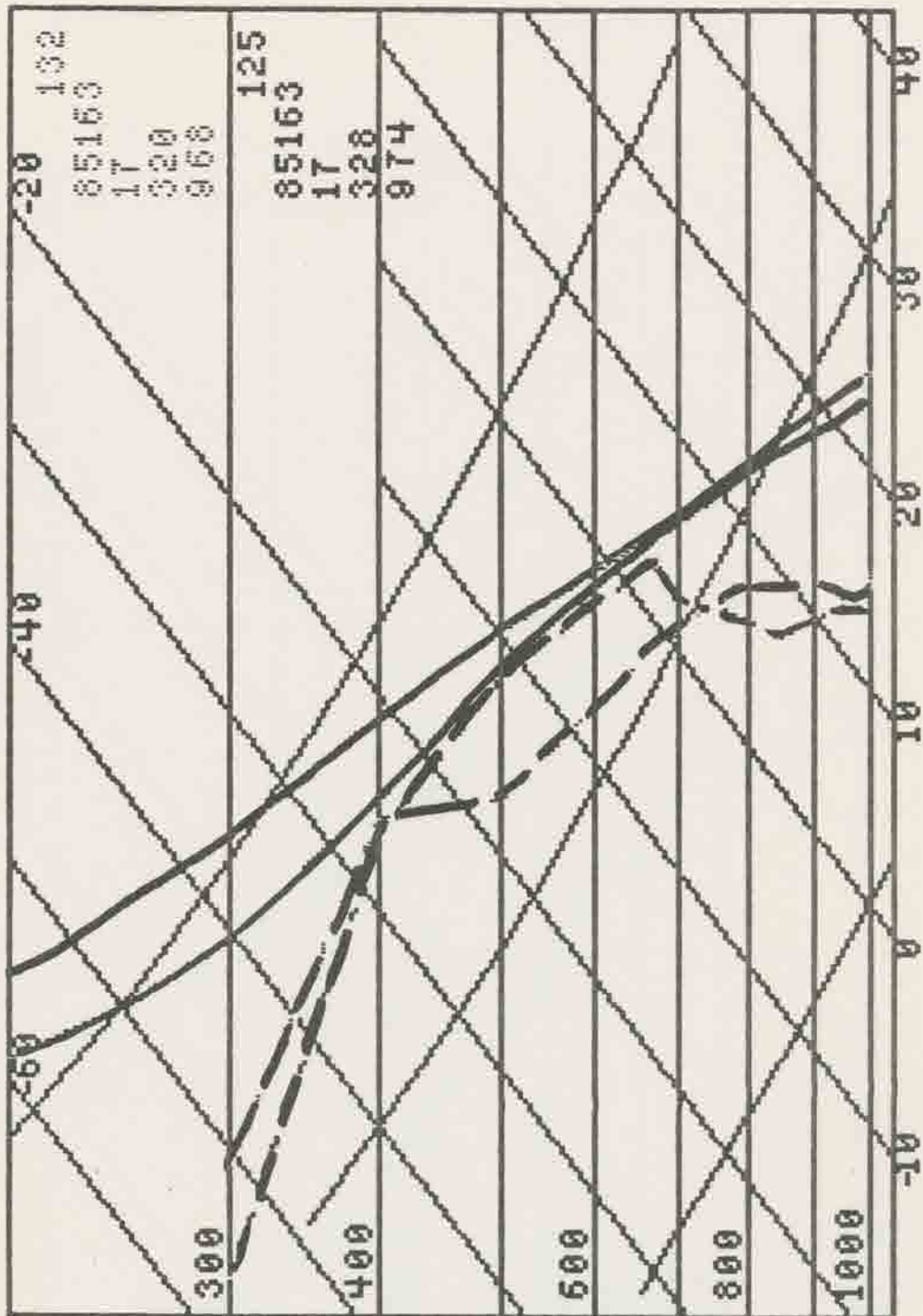


SNDG PARAM: POS BUOY (J/KG) 12JUN85 1718 GMT

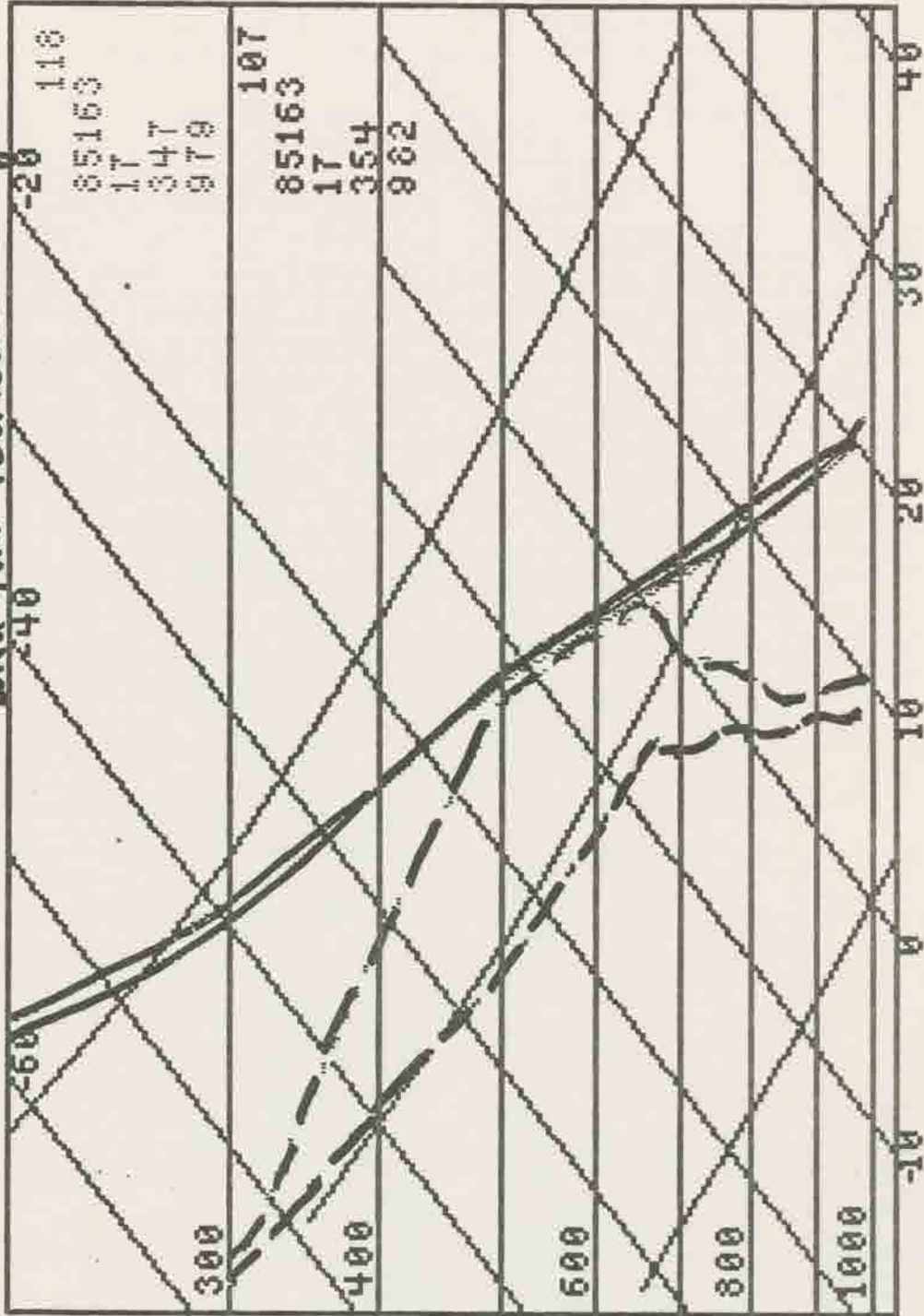








What about using a mesoscale model to help with this retrieval thing?



The Application of Satellite Sounding and Image Data  
to the Carolina Tornado Outbreak of 28 March 1984

James F.W. Purdom

Regional and Mesoscale Meteorology Branch/Development Laboratory  
NOAA/NESDIS  
and  
Cooperative Institute for Research in the Atmosphere  
Colorado State University  
Fort Collins, Colorado

### 1. Introduction

The Carolina tornado outbreak of March 28, 1984 was one of the most destructive in that area in recent history. Within a four and one-half hour period, a large supercell spawned the majority of over 20 tornadoes and downbursts that killed 59 people, injured approximately 1300 and left more than 3000 homeless. Figure 1, based on Storm Data, shows the paths covered by the major tornado activity as well as associated deaths. Notice how the major tornado activity is confined to a long and near continuous corridor.

Why did the outbreak evolve as it did? Although the supercell developed in eastern Alabama and moved through Georgia as an extremely intense thunderstorm, why did it wait until it was well into South Carolina before producing severe weather in the form of tornadoes and downburst activity? Why was the great majority of tornado and downburst activity confined to a narrow corridor out of the same supercell? Why did squall line activity south of the major supercell wait until late in the day (in South Carolina) to form along the cold front? Part of the answers to those questions will be addressed in the sections that follow. In those sections it will be shown how satellite image and sounding data may be used to better understand the Carolina tornado outbreak of March 28, 1984.

### 2. Conventional Meteorological Data (1200 GMT)

Analysis of upper air and surface data for 12Z on March 28, 1984 confirmed what had been indicated by numerical guidance: meteorological parameters were coming together to support a major severe weather outbreak over the southeast United States. A strong 850 mb jet showed significant moisture being advected across the area. Winds veered with height with dry air moving into the region at 700 mb. Between 500 mb and 300 mb, a strong jet stream was diverging over the area. A

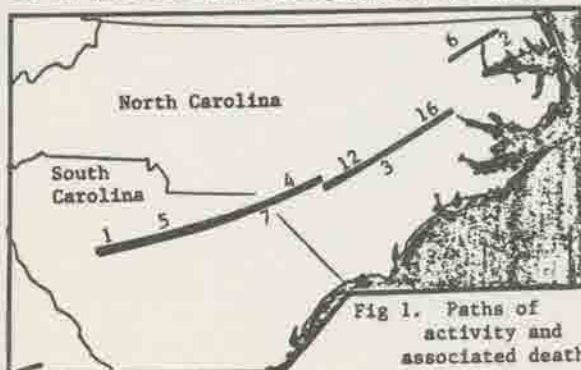


Fig 1. Paths of activity and associated deaths.

disorganized surface low in Kentucky and Tennessee had a cold front trailing southward through Mississippi. Supported by a weak short wave trough, thunderstorm activity which had moved through the southeast during the night was heading off of the Carolina coast by the early morning. This earlier thunderstorm activity was to play a major role in the events that would occur over the next 12 hours. Indications were that a strong short wave would move rapidly from Texas across the area during the day.

### 3. Satellite Data

GOES-East visible and infrared imagery were available at nominal 15 minute intervals with 6.7 micron water vapor imagery replacing the infrared imagery at 1745 and 2345 GMT. The 15 minute interval imagery from GOES precluded operating that satellite in the VISSR Atmospheric Sounder (VAS) mode, therefore VAS data were not available. However, at approximately 2100 GMT a TIROS overpass (NOAA-7) provided satellite sounding data over the storm area at a resolution of 35 km. Both GOES and TIROS data sets are used in the sections that follow.

### 4. Satellite Image Analysis

The importance of prior convection in setting a stage for tornadic storm activity has been known for many years (Miller, 1972). That satellite data can detect such boundaries has also been recognized (Purdom, 1973, 1982); this was vividly demonstrated by weather developments over the southeast United States on March 28, 1984. Thunderstorm activity that had moved through the area during the early morning hours produced a well-defined boundary which extended westward from South Carolina across Georgia and into Alabama. Surface temperatures and dewpoints in the air to the north of the boundary were several degrees cooler than in the air to its south. Figure 2 shows how that discontinuity appeared in satellite imagery early in the day. This boundary moved slowly north-eastward during the day and by mid-afternoon, new convection which formed along the boundary produced a "second generation" outflow region. This "second generation" boundary showed up strikingly in GOES imagery as a line of organized cumulus congestus clouds extending across South Carolina and into North Carolina, see Figure 3. Figure 4 is a mesoscale analysis based on conventional surface observations which confirms the observations in the satellite imagery.

The large storm in northeast Georgia (Figure 3) lies at the junction of the boundary and a



Fig 2. GOES-East 1 km visible image for 1330 GMT, 28 March 1984. Arrows point to early boundary location.

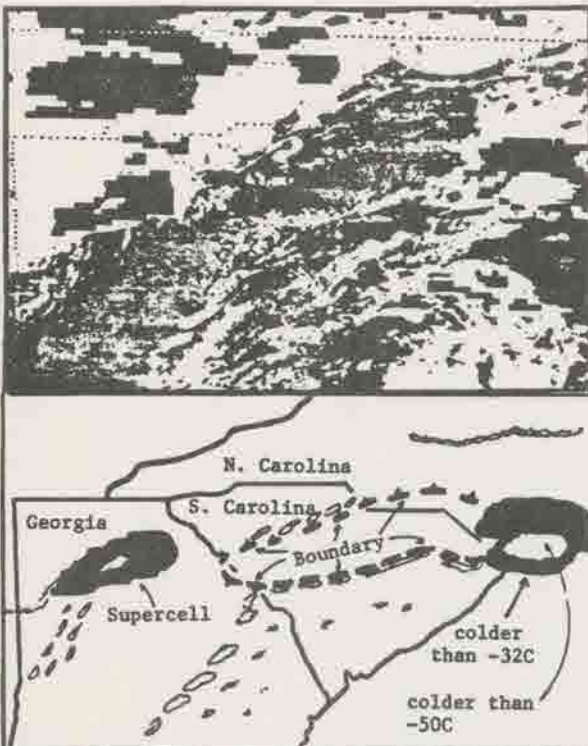


Fig 3. GOES-East 1 km visible and infrared image for 2000 GMT, 28 March 1984 (top), and analysis of significant features (bottom).

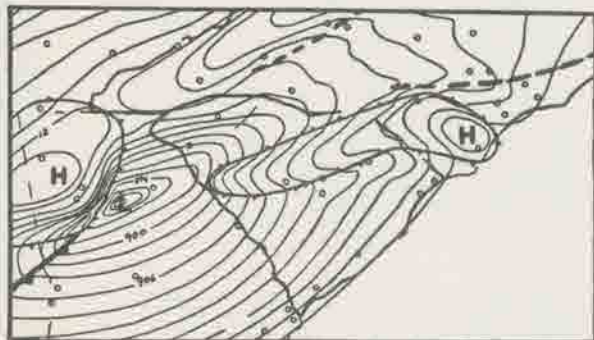


Fig 4. Mesoscale analysis for 2000 GMT, 28 March 1984 based on altimeter.

mesocyclone. That storm developed into a large supercell which tracked east-northeast along the boundary and produced most of the intense killer tornado activity during the day. It is interesting to note that strong convergence existed along the boundary. This can be seen by comparing the surface observations (below) at Columbia, SC at 2054 GMT, when that station was north of the boundary, and 2051 GMT when the boundary had moved to the north of Columbia.



#### 5. Satellite Sounding Analysis

Why did the intense supercell wait until it entered South Carolina to increase dramatically in intensity and become tornadic? Why did the squall line which formed to the south of the storm wait until the cold front had moved into South Carolina to develop? Satellite sounding data helps provide part of the answer to those questions.

At 2055 GMT the NOAA-7 polar orbiting satellite passed over the Southeast United States. Figure 5 is a visible image over the south Atlantic States from that pass. Notice that much of the area in Georgia, South Carolina and North Carolina is free of thunderstorm activity. In those areas, the TIROS Operational Vertical Sounder provided good observations for the production of soundings at a resolution of 35 km (single field of view). Forty-one soundings were selectively derived in the area with the help of Gary Wade of NESDIS Development Laboratory at the University of Wisconsin using an algorithm developed by Smith and Zhou (1982). The areas chosen for the soundings were mostly clear fields of view, microwave data were not used because of their poorer resolution. Rather than treat the satellite sounding data as if they were data with high vertical resolution, bulk quantities were derived from the data. These included information such as mean mixing ratio in the lowest kilometer, positive buoyant energy, negative buoyant energy from the surface to the lifting condensation level and negative buoyant energy from the lifting condensation level to the level of free convection.



Fig 5. NOAA-7 1 km visible image for 2055 GMT, 28 March 1984.

Selected of those parameters\* are shown in Figures 6, 7 and 8. Notice the differences shown in the TIROS soundings in three regions: 1) the clear slot extending through southwest Georgia to the South Carolina border; 2) the cumulus cloud region immediately to the clear region's east which extends through southeast Georgia and well into central South Carolina, and 3) the region in South Carolina and North Carolina to the north of the outflow boundary. In the negative buoyant energy field, notice that the highest negative buoyant energies are found in North Carolina to the north of the outflow boundary. Differences in negative buoyant energy fields are also seen between the air in Georgia versus that in the more central and southern parts of South Carolina. Taking into account that much of the air in the convective region has attained its lifting condensation level, allows replacement of the total negative buoyant energy values in the cumulus region with values of negative buoyant energy between the lifting condensation level and the level of free convection. If this is done, as in Figure 7, a marked difference between the amount of energy required to lift the air to free convection in central Georgia versus eastern Georgia and central and southern South Carolina is readily evident. Furthermore, inspection of Figure 8, positive buoyant energy, reveals that the cumulus filled air in eastern Georgia and central and southern South Carolina is much more suited for supporting intense convective activity than the air in the clear region in Georgia or that air which is to the north of the outflow boundary. Independent analyses of mesoscale air mass differences over the same area with TIROS sounding data by Hillger et al (1985) show similar results. Therefore one might surmise from information in the TIROS sounding data that: 1) the air in eastern Georgia and central and southern South Carolina is much more accessible to forcing and free convective development than air within the other parts of the image; and 2) that the air in eastern Georgia and central and southern South Carolina is much more suited to supporting intense convective activity than air in the other regions. This helps explain the intensification of the storm to tornadic and downburst proportions as it moved into South Carolina, as well as the later development of the squall line to the south of the supercell.

#### 6. Other Satellite Derived Information

It is well known that vertical wind shear plays an important role in determining the character of storms that develop in a mesoscale environment (Newton, 1963). Measurements were made in which satellite derived cloud motions were computed relative to the supercell, in a manner similar to that proposed by Purdom, et al (1984). Figure 9 shows that relative flow field. It is interesting to note how closely the relative flow field in Figure 9 compares to that proposed by Browning (1964) for severe storms which travel to the right of the wind, and tornadic storm relative proximity soundings (Maddox, 1976).

\*It is the feeling of the author that at this time the various parameters should be thought of in a relative sense rather than in terms of their absolute values.

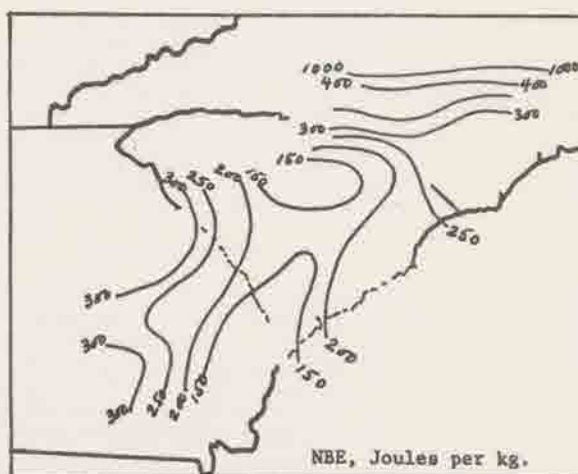


Fig 6. TIROS Negative Buoyant Energy (NBE).

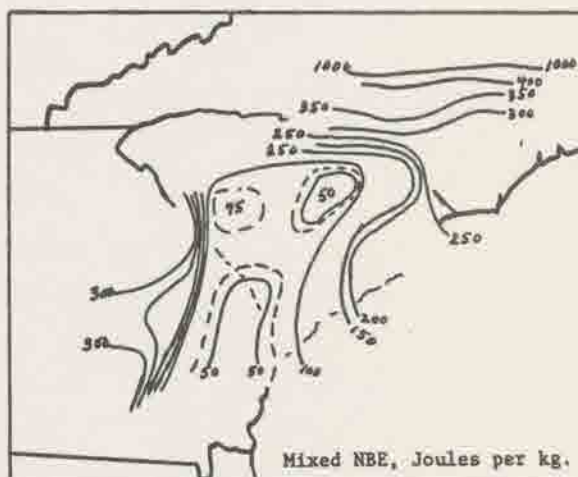


Fig 7. As Fig 6 above, but with NBE between LCL and LFC in convective regions.

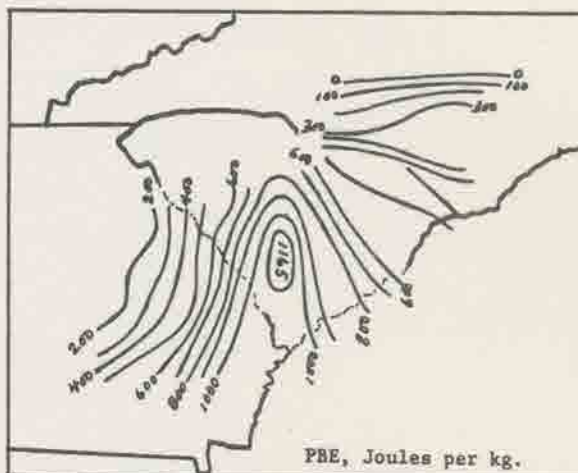


Fig 8. TIROS Positive Buoyant Energy.



Fig 9. With respect to the supercell. Low (L), Middle (M), and High (H) cloud relative flow, plus anvil expansion.

It is informative to take the information in the storm relatively flow field and combine it with the satellite sounding information from the previous section. At the low levels the air feeding the supercell was the more convectively suited air in eastern Georgia and southern and central South Carolina. Figure 10 is a 6.7 micron channel image (middle level moisture) for 2345 GMT. Note the dry region immediately to the south of the large supercell. The flow relative to the supercell would have placed dry air at middle levels in juxtaposition with the storm. The interaction of convective storms with dry air at mid-levels is important in fueling intense downdrafts and further intensifying a storm.



Fig 10. GOES-East mid-level water vapor image for 2345 GMT, 28 March 1984. Note the dark area (dry at mid-levels) adjacent to the southern side of the supercell.

#### 7. Conclusions

Both satellite image and sounding data are able to provide important information concerning the development of severe storms. This has been shown to be true for the March 28, 1984 Carolina tornado outbreak. Satellite image data is able to provide important information on trigger mechanisms such as arc cloud lines, and flows relative to the storm in question. Satellite sounding data are able to provide information concerning the required forcing and potential

storm intensity in the environment ahead of a developing storm. In the future it is hoped that VAS data and frequent interval GOES image data will be taken at the same time. If so, the energetics of the environment may be monitored at frequent intervals using the VAS data, while trigger mechanisms and flows relative to a storm may be monitored in using the satellite imagery.

#### 8. Acknowledgements

I would like to thank Sallie Varner for the preparation of the text. Gary Wade of the NESDIS Development Laboratory at SSEC, University of Wisconsin aided in the production of single field of view soundings from TIROS. Research support was provided for this work through NOAA Grants NA84AA-D-00017 and NA84AA-H-00020.

#### 9. References

- Browning, K.A., 1964: Airflow and precipitation trajectories within severe local storms which travel to the right of the winds. *J. Atmos. Sci.*, 21, 634-639.
- Hillger, D.W., J.F.W. Purdom and T.H. Vonder Haar, 1985: An analysis of various mesoscale air masses for 28 March 1984 using NOAA-7 TOVS. *Proceedings 14th Conference on Severe Local Storms*, Oct. 29 - Nov. 1, 1985, Indianapolis, IN, Amer. Meteor. Soc.
- Maddox, R.A., 1976: An evaluation of tornado proximity wind and stability data. *Mon. Wea. Rev.*, 104, 133-142.
- Miller, R.C., 1972: Notes on analysis and severe-storm forecasting procedures of the Air Force Global Weather Central. *AWS Technical Report 200 (rev)*, Air Weather Service (MAC), U.S. Air Force, 190 pp.
- National Climatic Data Center, 1984. *Storm Data*, 26, No. 3, Asheville, NC, March 1984.
- Newton, C.W., 1963: Dynamics of severe convective storms. *Meteor. Monogr.*, 5, No. 27, 33-58.
- Purdom, J.F.W., 1973: Meso-highs and satellite imagery. *Mon. Wea. Rev.*, 101, 180-181.
- Purdom, J.F.W., 1982: Subjective interpretation of geostationary satellite data for Nowcasting. *Nowcasting*, K.A. Browning (Ed.), Academic Press, 149-166.
- Purdom, J.F.W., T.H. Vonder Haar, J.K. Stewart and N.E. Leary, 1984: Diagnosing the severe thunderstorm environment by mesoscale cloud tracking - a new approach and new information. *Preprints, Conf. on Satellite Imagery/Remote Sensing and Applications*, Clearwater, Amer. Meteor. Soc.
- Smith, W.L. and F.X. Zhou, 1982: Rapid extraction of layer relative humidity, geopotential thickness, and atmospheric stability from satellite sounding radiometer data. *Appl. Opt.*, 21, 924-928.

SMALL GROUP SUMMARIES

"Computer Systems for Research"  
N. Allen, Leader

"VAS"  
A. Lipton, Leader

"Atmospheric Modeling"  
R. Pielke, Leader

"Shortrange Forecasting Including Severe Storms"  
J. Purdom, Leader

"Climate Studies"  
D. Randel, Leader

"Radiation Theory and Observations"  
M. Wetzel, Leader

Computer Systems for Research  
Working Group Summary  
N. Allen, Leader

The Computer Systems for Research Group had very good discussions of current and near future needs and uses of computer systems. The following items reflect several areas where changes or additions to our computer systems should be made or considered.

To resolve: Ingest configuration of new 11/750s when mode AAA comes up?

- a) One satellite into both systems?
- b) Multiple MDPs, small sector on 1 machine, large sector on another?
- c) Parallel system?

Recommendation: Early acquisition of 2 MVAX workstations (August) for training/familiarization.

Possible locations for MVAX workstations:

- 1. Solar House 2
- 2. CIRA
- 3. Groundstation Comtal Room
- 4. Room 301 - Main Building
- 5. Groundstation Staff Office

Questions on user organization and maintenance of these systems since they will be shared. There will be - 3/5 users.

Brubaker has a RAMTECH (umbus) system available. The system needs work. Has a color, single frame monitor. Weather lab could use?

Recommendations for next 6 months:

- a) What products will be routinely available?
- b) Scheduling of images?
- c) What will VAS collection be?
- d) Operational data flow for field projects?
- e) Realtime information/data available?

Evolution of research systems needs to be more organized. Also, publicity on accomplishments, capabilities needs to be improved.

Look into optical disk technology. Efficient mass storage/retrieval mechanism is necessary particularly with the anticipated increased computational needs.

Use existing equipment to best advantage.

- a) New students required to complete projects on OPTRONICS, Comtal, etc. to become familiar with operation?

Publications, presentations and PR work need to be increased:

NOTE: The RAMM Branch has a small expert system program running in the PC.

In addition to these items, I am recommending that a Computer Systems Advisory Group be established in CIRA to meet at least monthly for the purpose of reviewing current and future needs for computer

resources in CIRA. This will include hardware, software and training, and other items related to this very important resource to CIRA's research programs.

I would like to chair this group with representatives from NESDIS (Purdum), ISCCP (Campbell), and realtime Weather Lab (Pielke). This group would advise CIRA's director (Vonder Haar) on its findings and make formal recommendations and make assignments to those groups represented to complete action items as necessary. I believe that most action items would fall within the Earth Station and computer facility activities.

VAS  
Small Group Summary  
A. Lipton, Leader

MSI data may be useful in studying MCC development and organization. There are theories about how convection organizes into an MCC, and MSI data may provide an observational tool for evaluating the theories. Look at the theories, one by one, and consider how radiative observations could help in verification.

Dwell sounding data could be used to monitor accumulation of moisture in sea-breeze circulations. Soundings might detect the combined effects of moisture convergence and moisture flux from the surface. Results could be compared with those from models. A critical issue is whether the satellite sensors can detect the shallow features of a sea breeze.

We received the scan pattern of dwell sounding mode of VAS, and discussed retrieval resolution options.

Don Hillger needs to modify his presentation of retrieved sounding profile. Currently, people get the impression that he has retrieved the depth of the mixed layer; but, in fact, he finds some information about the mixed layer but does not get an accurate estimate of its depth. The presentations should make this point clear.

Use of VAS data from the CSU DRGS is being hampered by problems with ingest software and by delays in development of pre-processing software. Duane Whitcomb is needed full-time on this work.

Atmospheric Modeling  
Small Group Summary  
R.A. Pielke, Leader

This brief report recommends several action items related to atmospheric modeling which should be addressed by CIRA. These are:

1. CIRA needs to develop in-house mesoscale, synoptic and global circulation modeling capabilities. These tools would be used:
  - a) to promote academic research instruction
  - b) to permit more effective and accurate satellite, profiles, and data collection platform analyses
  - c) to provide more effective forecast tools on the short range and over the mesoscale
  - d) to supply more accurate interpretations of the global energy budget

Modeling and observational collection of data should be inseparable tools if the most service is to be achieved from CIRA initiatives, CIRA showed this modeling should be an intergral component in the planned NOAA/NESDIS Mesoscale Satellite initiative outlined by Jim Purdom. Approach the CSU Administration to obtain block funding for academic research access to the 205 for these modeling tools.

2. CIRA in-house computer capabilities and data access should be enhanced in two specific areas:
  - a) the actual difficulty and costs of linking the Unifax recorder to the VAX network should be explored
  - b) the NCAR plot packages should be routinely available on the VAX system.

3. CIRA should make known its activities and accomplishments through a regularly published newsletter.

$$\frac{\partial v}{\partial t} = -v \cdot \nabla_p v - z \vec{\omega} \times v - g \vec{\nabla}_p h + \frac{\partial}{\partial p} K \frac{\partial v}{\partial p}$$

$$\frac{\partial h}{\partial p} = -\frac{1}{\rho g} \Rightarrow \left[ \frac{\partial(\nabla_p h)}{\partial h_p} \right] = -\frac{r}{g} \nabla_p T \quad \begin{array}{l} \text{Need} \\ \nabla_p T; \frac{\partial}{\partial t} \nabla_p T \end{array}$$

$$\nabla_p T = \frac{\partial T}{\partial x} + \frac{\partial T}{\partial y} = \frac{\partial T}{\partial n} \approx \frac{\Delta T}{\Delta n}$$

e.g. for  $\Delta n = 10 \text{ km}$ , what is accuracy of satellite measurements of  $\Delta T$ .

$$\Delta T_{\text{obs}} = \Delta T_{\text{actual}} + \Delta E \leftarrow \text{ERROR}$$

$$\frac{\partial q}{\partial t} = -v \cdot \nabla_p q + \frac{\partial}{\partial p} K \frac{\partial q}{\partial p} + S$$

$$\nabla_p q = \frac{\partial q}{\partial n} \approx \frac{\Delta q}{\Delta n} \longrightarrow \text{How accurate can } \Delta q \text{ be measured over } \Delta n?$$

Shortrange Forecasting Including Severe Storms  
(Mesoscale and Severe Weather)  
Satellite Working Group Summary  
J. Purdom, Leader

What will be covered here is some of the current work at CIRA and also some of our future areas of interest. These two naturally tie together, especially when we look at their importance to the preparation of the 1988 NESDIS mesoscale satellite initiative that we will be participating in putting together. Concerning our present activities in mesoscale and their impacts I'd like to point out the importance of credibility. For our contracts and grants, we must stay on target and hit those targets. We must make sure that people know we come through on what we tell them we're going to do. I think we're developing an extremely good reputation in this area -- we need to keep working hard so that we keep our reputation intact. It makes getting into the future areas a lot easier when you have a good reputation behind you. In the future areas, there are three things that the working group looked at; one was technology, that is systems and software; second was science, specifically atmospheric science; and the third was something that we called a basic awareness of what's going on. Concerning this third area, you need to be in step with the community or else you'll have a lot harder time getting some of your ideas through. Staying in contact, or awareness of the scientific community, means you either know what other people are doing or you become a leader yourself so other fall in step with you. I think we want to try to become a leader so other people have an awareness and fall in step with us.

When we talk about our current work at CIRA, let's take a look at where we've had impact. Let's see how work we've done feeds into

nowcasting and mesoscale and forecasting systems and then see how they relate to future areas of interest that we'll be working in. The first thing to point to is the work we've done on the arc cloud line boundaries and how they interact with other boundaries through intersections and the mergers. We started talking about boundaries several years ago, have continued to do quite a bit of work on them at CIRA, and will continue to work on them in the MIST and the SPACE program. No doubt, these programs will have a strong impact in the STORM program. Everybody that works in the mesoscale is now talking about what we've been talking about for the last 8 or 10 years. So everybody's catching up with us. The concept is being used at the NSSFC in Kansas City, it helped pinpoint the tornado area for the March 28, 1984 outbreak, it's being used throughout PROFS and the NWS. That's one place we've had a very strong impact on mesoscale meteorology, and nowcasting or short range forecasting.

We've been interacting with PROFS for several years. We were the first people to provide satellite data to PROFS. We were the first to provide satellite data from outside of normal National Weather Service channels to the National Weather Service Forecast Office in Denver. We have continued to work with PROFS on their uses of satellite data for nowcasting and integrating satellite data with other data sets for that purpose. PROFS will no doubt have a very important role to play in defining the experimental forecast centers that go onto the national STORM Program, so we have a vested interest in that interaction.

The cloud relative flow that we're working on right now, although it's not being used widely, I would predict that in about the next three or four years people working in severe weather with satellite data will

all look at storms in a relative mode. The work that CIRA is doing in this area is the foundation that's going to lead us to being able to discern severe storm types: are we in a tornado environment according to the cumulus to cirrus level shear or are we in a heavy rain environment? Are we in an environment that is favorable for an MCC or a squall line? Just what type of storm environment are we in? There is a lot of potential here.

Cloudy versus clear areas and the various things that lead to boundary layer forcing is something that we've been talking about for several years. Other people are now working with this concept, and there's been some modeling work in this area. It's a very important concept to understand as far as environmental evolution because your cloudy area in the morning can turn around and be your most convectively unstable area in the late afternoon, depending on when the cloud goes away. We don't know when the cloud's going to go away, so it's an obvious place to use a numerical model to help us understand that and the ensuing instability.

VAS mesoscale environment, the definition of the mesoscale environment and it's evolution. Some of the work that we've been doing in this area with the PRE-STORM program, where we've actually produced VAS products on the IBM PC to help understand better where the convection will form and become more intense has been remarkable. I think the work that we're doing here will lead to how meteorologists will look at VAS data for mesoscale forecasting.

Let's jump ahead to modeling. How do you use a model? Mesoscale modeling can help us as we move into these various areas that I just talked about - boundaries, cloud relative flow, cloudy clear or the VAS

retrieval. I think sometimes we tend to be a little too esoteric and not quite practical enough. It's nice to be able to have a satellite give you all the information you need, however, there's a lot of other data and information that can help lock down some of the boundary conditions needed to derive satellite soundings. That will radically change Roger Pielke's  $\Delta t$  over  $\Delta n$ . I think we're looking at a new type of iterative procedure here where one derives the VAS mesoscale environment and then goes into the model with that mesoscale environment. The model tells us to reinitialize and do the soundings in certain areas, then we go back and forth in an iterative procedure between the model and the VAS data and improve the sounding field.

We also are doing work at CIRA using other data to better define the boundary layer, using the satellite infrared data and the various VAS channels along with SAO observations (regular surface observations) to help tie down that boundary layer temperature and moisture. When we get into the STORM program there are going to be airplanes sending back atmospheric state information as they fly through various mesoscale regions. These are other things we can use to help tie down VAS soundings and, again, get a better  $\Delta t$  over  $\Delta n$ . We should be keeping that very strongly in mind - do better soundings than anybody else has done through new ways of doing them.

The thunderstorm IR cirrus shield behavior, with PRE-STORM by making histograms of the infrared data and looking at the behavior and the various temperature ranges of the cirrus shield in the convective system. They should have different signatures when the storms behave differently, we think, and we hope to be able to use something along this line to better understand MCC's, MCS's, squall lines, regular

thunderstorms or whatever. We want to look at a whole spectrum of cloud shield behavior and I think with the new power of the computer system we'll have, that will be a fairly easy thing to do. A lot of this work is not hard and there is a wealth of information, then knowledge, to be gained.

Modeling: There are many uses for models to help us with the satellite data, or satellite data to help us with a model. First of all, the model is going to help us analyze the initial state. The model can help us interpret what we're seeing in the satellite imagery with DCP input, mesonet input, the VAS retrieval input again, going back to this iterative scheme I spoke of earlier. The idea of the mesoscale climatologies that John Weaver did over Colorado, that Jeff McQueen did over Florida, Margie Klitch did over the Dakotas - how can those fit into a model, how can we stratify the atmosphere and figure out how to better use these things in short range forecasting? This is extremely important. The idea of going back to some of the earlier CIRA/Air Force work with cloud cover and its advection and the changes in the atmosphere, again using a model should be considered. You can get into all sorts of ideas about plume dispersion, acid rain, cloud venting of materials up into the stratosphere or troposphere. This goes along with the model running with in situ observations, which I'll cover in just a minute.

What we need are composite efforts. We need to start with satellite observations and in situ observations to understand the phenomena we see in the satellite data and then we model it to get even a better understanding of that phenomena. For example, some of the things we're doing right now: "What is an arc cloud line? What drives

its circulation? What are the nowcast implications of an arc cloud line?" There are a lot of phenomena that have had some very fine guessing done about them, however, the guessers have lacked the in situ observations to prove much of what they say. For example, you may be surprised but there are not a lot of observations through comma clouds, yet an awful lot has been said about comma clouds. Severe storms and the cold V that we see in their anvil, we really don't know what causes it, or what its implications are as far as storm development. Cloudy versus clear and future convective development. We can model it, but we don't have the observations to prove that what we're modeling is exactly right. Local circulations that develop, again, in situ observations are needed, and these in situ observations can be done in a variety of ways. When I say in situ, I mean things like a Doppler Lidar pulse going out being something much closer to in situ than the satellite observation, or a Doppler radar or an aircraft flying through the area or a surface mesonet station. There are a lot of things, in situ if you think of the Lidar pulse taking that observation then coming back. It's not really in situ, but it's another type of remote sensing data.

The 6.7 micron signatures that we're seeing all the time and people are starting to claim this is a jet stream and that is something else. We need to get in and monitor those signatures directly so that we can understand what they really are.

What are some areas that CIRA needs to continue its work on that are important for future development. Obviously, boundary layer definition for VAS soundings by using the temperatures and the moisture out of the boundary layer as well as the model output to tie down that lower layer and give you a better sounding than you could get otherwise.

At CIRA, we started out looking at combinations of satellite data and Doppler radar data. We did some good work in that area, then we backed off because of a lack of manpower to continue in that area. That's a very important region that we had to slow down in. [What kind of manpower?] Somebody to actually take the data, put it together, analyze it, try to understand what it meant that he was seeing - scientific manpower. We will need a lot of scientific manpower to use all the resources we're going to have with the new system upgrade. Another area is the "short step" VAS energy field type of product where you don't go through the full retrieval, but you move more towards that first integral or whatever.

Some other things that we need to look at. With GOES-Next we expect to have 10-bit visible data. The current GOES has 6-bit visible data, but we have 10-bit visible data from the TIROS satellite. What are we going to find out when we have the 10-bit visible data? We should investigate what we will see that we don't see now, so that we'll be prepared for GOES-Next. We're going to have other multi-structural image channels that we can look at with GOES-Next. What are we going to see from them? What should we expect? We need to start looking at that right now and not wait until the satellite's up and the data's already starting to come down.

A very important area that I think we should get an answer out on very quickly is over sampling of the infrared signal. Now, that is something that started when we did our zoom and smoothing IR. We tried to replicate over sampling of an infrared signal to see if we could improve the resolution. The important thing here is that, if it is something viable to do, we may be able to impact the GOES-Next satellite

by telling them to sample the IR data at two or three times the frequency planned on now and get four or five times the information back out. So we need to look into that area.

Another thing that is extremely important, the implications of this, five research scientists are needed. Mesoscale climatologies over different areas, over dynamic systems versus terrain force systems, over systems relative to the system, etc. The opportunities in here are unlimited. [Vonder Haar - We have two new scientists coming in, Gibson and Kelley, coming this summer. So we have two, two out of five.] This area is just so exciting. We're able to go in and do mesoscale climatologies and the implications that it has for short range forecasting is beautiful. I think that we're way ahead of everybody else in something like this.

The other thing we talked about was expert systems. Their resources and how are we going to use them. In a research and nowcasting/forecasting capability they're flexible, they're adaptive to different input and to different situations, but how do you use that expert system? You can use it in your research. If you have a hypothesis, you can have an expert system make decisions based on that hypothesis, then you can go through cases and suddenly it tells you "Hey, you're 80% reliable thing is down in the 10% range." So you go back and you start changing things. It will help guide your path through research, so it won't be like a ping pong ball but be more like a snake, zig-zagging toward a final solution. So I see expert systems as being very helpful in that. Another thing when we look toward the future - what do you put into the expert system, you put information from a model output, you put data, you put a man's analysis of a

satellite image - the things that maybe the expert system has told him it needs. You put composites of these mesoscale climatologies and it gives you out a list of best alternatives, perhaps, of what you need to look at today in the forecast system. These are the three out of 130 things you better worry about. So you start worrying about those and you initialize a mesoscale model and then you reloop through the system and it tells you that you need to look at Greeley and Loveland, but Ft. Collins seems to be in the 10% area. Then you reloop as you get data and you continue to update.

The VDUC system, the IBM PC system are really forerunners to some kind of a national system. Maybe we can teach these to talk to each other. Maybe we can teach one of the PC's to talk to the VAX cluster so that it can give us the data we need and we don't need to worry about a lot of extraneous information. Maybe we can strike off one of those scientists because the expert system does the work he would have to do.

There's a lot of exciting things coming up that impact mesoscale and severe weather. Suppose all the information you use to make that forecast comes through an interactive system. Then the expert system could monitor the data you used as you went about making the decision. It may not be able to tell you what you thought when you did it, but if it watched you enough it will be able to see what data sets you used. You can then go back and analyze how you made your decision and see where you went right or wrong. Then, by doing that, help develop a better use of the expert/interactive system as a forecast tool. I think these systems have a lot of potential that I find very exciting.

The idea of an awareness, I talked at the very beginning of the future as a combination of things - of technology, science and an

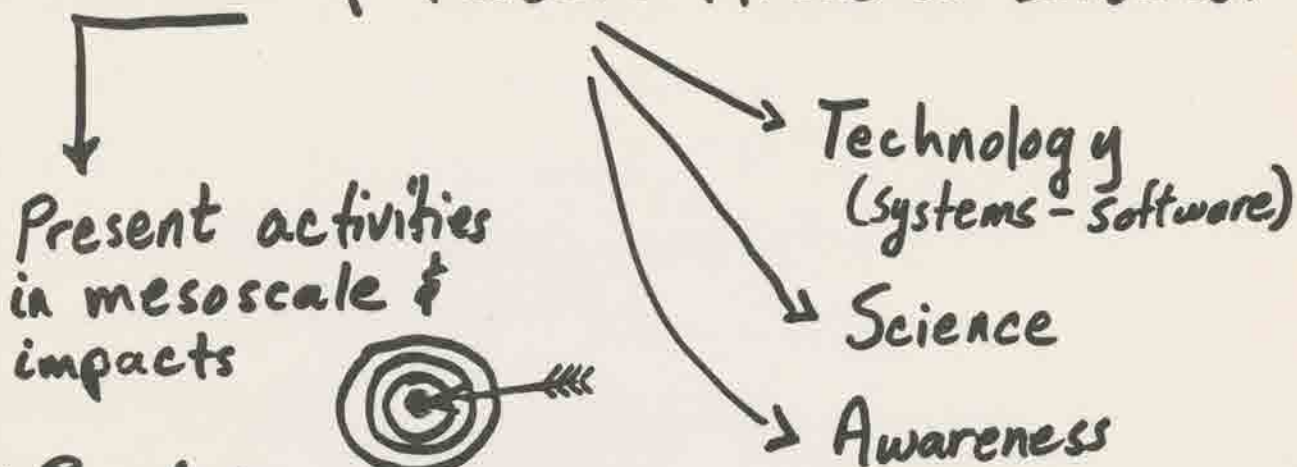
awareness. How do we maintain an awareness? You might ask yourself, how many places do we want to be the expert and how many places do we want to go out and get an expert to come in and help us for a limited amount of time. Obviously, one area of interaction is through the CIRA Visiting Scientists program. Others I know of through my work in NOAA at the NOAA labs in ERL. What are their experts like? Well, you've got the National Severe Storms Lab which has most of the doppler radar experts in the world. They have a VAX based system. You've got PROFS who are technology and forecast focusing type experts. They have a VAX based system. You have the Wave Propagation Lab which I call the new and innovative people. They're the ones that are a lot of fun to work with because they've got the Doppler Lidars and the Profilers. They've got all the new stuff, so they're a real good group to work with. How much do you want to work with them? What do you want to do with them? The Weather Research Program - they're thoughtists, that's what I call them, they kind of think about things and tell you how they think things ought to run, sometimes they're right, sometimes they're wrong. The Weather Modification Program Office is dead right now, but what's going to happen after two or three years of drought somewhere? They'll come back to life again. The STORM Program office, and I mean this seriously, we either be in or out. If we don't start being in right now and making our impacts with the people who are making the funding decisions, we can count ourselves in the out area. So we need to have a strong impact within the STORM Program office. It's to our best interest to stay in touch with other areas, National Severe Storm Forecast Center, NMC, National Hurricane Center, the NOVA Program (we work with now), the VAS Data Utilization Centers (VDUC's) (we're going

to be working with them). The VDUC's are really going to be forerunners of the interactive systems at the national centers. These are the national centers - NSSFC, NMC and NHC - all of them are going to have VDUC systems. We need to be working and telling these people how to use that data for nowcasting.

The other thing that we must have is the bi-yearly magazine, or newsletter. This has to be something we start putting out from CIRA. Something to catch the eye - it's got to say CSU in it. A lot of people have gotten us confused with our brothers down the road at CIRES.

# Satellite - Mesoscale/severe ①

## Current & Future Areas of Interest



### 1. Boundaries

Intersections/mergers → Mist/Space

2. PROFS capabilities → STORM EFC

3. Cloud relative flow → Sur. Storm types

4. Cloudy vs. Clear → Env. Evolution/model

5. VAS mesoscale env. → Env. Evolution, Definition  
use other data

6. IR, cirrus shield behavior → MCC, MCS, Q'Line

7. Modeling → Many uses

Bi-yearly mag.

"CIRA - CSU  
and NOAA's joint  
research institute  
for atmospheric  
science"

a. help analyse initial state

b. help interpret sat imagery,  
DCP input etc., VAS retrievals

c. mesoscale climatologies

d. cloud cover/model/advection  
plume dispersal, acid rain  
cloud venting into trop./strat.

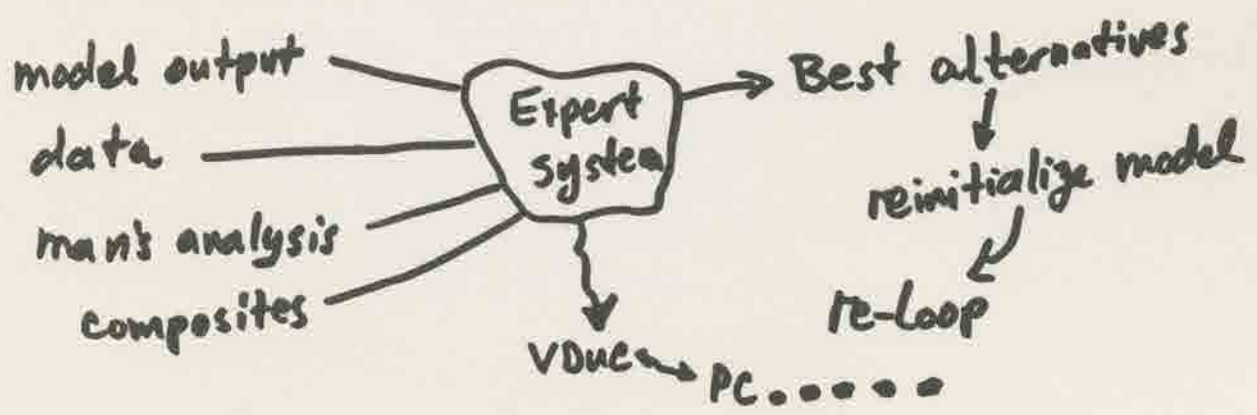
# - Composite Efforts -

Sat. Ob, "In situ" Ob, Model for better understanding -

- What is arc cloud, implications -
- What is comma cloud
- Severe storm cold "V"
- Cloudy vs clear, implications
- local circulations
- 6.74 signatures
- Boundary layer definition for VAS etc -
- Comb. Sat/Radar
- Short Step VAS nrg's
- 10 bit vis, msi GOES-NEXT
- over sampling IR

Mesoscale Climatology - over areas  
 Dynamic systems vs terrain forced  
 System Relative etc - Opportunity

Expert Systems - research & Nowcasting / forecasting  
 Flexibility - Adaptive to data sources, situations



③

Awareness -

How many places are we experts?

Interaction - CIRA visiting scientists

NOAA Labs (ERL)

→ NSSL (radar) → VAX

→ PROFS (technology / forecast focus) → VAX

→ WPL (new/innovative Lidar, Profiler...)

→ WRP (Thoughtists)

→ WMPO (dead but ???)

→ STORM Program office (be in or out)

Other

NSSFC, NMC, NHC, NOVA/VDUC

forerunner to  
National Centers

Climate Studies  
Small Group Summary  
D. Randel, Leader

- 3 subjects: 1) ISCCP  
          2) ERB-ERBE  
          3) Future Climate Studies

1. ISCCP:

- a) We have B1, B2, and B3 ISCCP data available. The usage of this set of data is not fully used yet.
- b) Since the department is redistributing the office space, the storage of ISCCP tapes is an immediate problem.
- c) Currently, the statistics of ISCCP produced includes 15-day background composite, maximum temperature albedo and minimum temperature albedo, images, 40X40 grid ( $2.5^{\circ}$  x  $2.5^{\circ}$  spatial resolution) IR, and VIS histograms.
- d) The delay of ISCCP cloudiness tape is partially caused by the difficulty in calibrating GOES instruments.
- e) We are going to order the ISCCP "C"-tape (for cloudiness) when it is available.

2. ERB-ERBE

- a) The comparison of ERB (NIMBUS-7) narrow band wide FOV of radiance, cloudiness and albedo can be done.
- b) The comparison of NIMBUS-7 cloud statistics with ISCCP cloudiness can be started when the software for reading NIMBUS-7 cloud tape arrives.
- c) Possible extension of NIMBUS-6 data could provide another El Nino coverage to compare with 1982-83 El Nino event.

3. Future Research:

a) Using satellite radiation budget only to determine

$$\frac{dF_{\text{net}}}{dA_c} \quad \frac{dx}{dA_c} \quad \frac{dIR}{dA_c}$$

- 1) Using climate models only.
  - 2) Combining satellite radiation budget and climate modelling.
  - 3) Analyzing the satellite radiation budget and satellite cloud measurements. (ISCCP+ERB+ERBE)
- b) The topic of the next generation will be related to the ocean, hydrological studies after cloud problems.

Data Sources  
(vugraph)

ISCCP CSU → A,E, C(z)  
Nimbus ERB E,A,N, [C] 7/75 →  
ERBE - E,A,N, [C] 11/84 →  
ISCCP Global Product C 7/83 →  
CCM Output

Cloud Radiation Feedback  
(vugraph)

1. Satellite Obs only  
 $\Delta N / \Delta \Delta C$  from extremes
2. Models - need better clouds
3. GCM + Obs
  - a) Check GCM for match with O
  - b) Initialize model - adj. clouds
4. Obs of radiation  
Obs of clouds

Radiation drive circulation?

1. Storage = Net-div F  
Assume  $\Delta S = 0$   
 $\Delta N = \text{div } \Delta F$
2.  $\Delta N$  impact on dynamical model
3. Diurnal

Radiation Theory and Observations

Small Group Summary

M. Wetzels, Leader

1. Proposed field observational programs

A. Marine stratocumulus.

- (i) Coincident measurements of cloud and MBL structure that controls extinction in spectral bands narrowly centered at 0.53, 0.75, 0.83, 0.91, 1.05, 1.25, 1.6, and 2.1  $\mu\text{m}$ .
- (ii) Input and comparison of above data to cloud radiation models which allow representation of horizontal and vertical inhomogeneties.
- (iii) Evaluate sensitivity of SCU cloud dynamics model of fine resolution to the parameterization of radiative flux (e.g. LWP, VP).
- (iv) Interpret available satellite imagery in near-infrared channels (CZCS, DMSP).

B. Surface emissivity at 3.7 vs. 11 $\mu\text{m}$ .

- (i) Characterize emissivity for a variety of surface conditions.
- (ii) Improve method of using 3.7 and 11 $\mu\text{m}$  "windows".

2. Satellite sounding above clouds.

- A. Current statistical procedure does not use physical cloud information.
- B. Better estimates of cloud-top pressure and optical depth/emissivity at various (sounding) wavelengths could contribute to sounding accuracy

3. Effects of pressure broadening on transmittance in the gaseous absorption channels used for satellite sounding.
4. Future of satellite radiometry.
  - A. Lidar (DMSP).
  - B. Microwave scatterometer (NASA).
  - C. Millimeter receiving antenna (Shuttle).

